EFFECT OF STONE COLUMN SOIL IMPROVEMENT ON LIQUEFACTION RESISTANCE: FIELD AND NUMERICAL STUDY

A Thesis Submitted to
the Graduate School of
İzmir Institute of Technology
in Partial Fulfillment of the Requirements for Degree of

MASTER OF SCIENCE

in Civil Engineering

by
Merve BUDAK

June 2023
İZMİR

We approve the thesis of **Merve BUDAK**

Examining Committee Members:

Prof. Dr. Nurhan ECEMİŞ
Department of Civil Engineering, İzmir Institute of Technology

Prof. Dr. Alper SEZER
Department of Civil Engineering, Ege University

Asst. Prof. Volkan İŞBUĞA
Department of Civil Engineering, İzmir Institute of Technology

22 June 2023

Prof. Dr. Nurhan ECEMİŞ
Supervisor, Department of Civil Engineering, İzmir Institute of Technology

Prof. Dr. Cemalettin DÖNMEZ
Head of the Department of Civil Engineering

Prof. Dr. Mehtap EANES
Dean of the Graduate School

ACKNOWLEDGMENTS

This thesis study is dedicated to those who lost their lives in the Kahramanmaraş Earthquakes in February 2023 and their relatives.

First, I would like to present my deepest gratitude to my thesis advisor Prof. Dr. Nurhan Ecemiş for her patience and support in the completion of this thesis.

I would like to thank my thesis examining committee members, Prof. Dr. Alper Sezer and Asst. Prof. Volkan İşbuğa for their valuable comments and vision on my thesis.

Also, I would like to give my endless gratitude to Dr. Mustafa Koç, who provided the necessary data for the thesis and supported this study. I would like to thank Başak Karsavuran for always supporting me during my business life.

I sincerely want to thank my dear friend Aybüke Karaoğlu, with whom I shared the same feelings throughout the thesis study and who at all times gave me power.

Finally, I would like to thank my parents, Hatice and Yıldırım, and my brother Mert, who have always supported and loved me throughout my entire life.

ABSTRACT

EFFECT OF STONE COLUMN SOIL IMPROVEMENT ON LIQUEFACTION RESISTANCE: FIELD AND NUMERICAL STUDY

This study aims to understand how effective the group of stone columns is in the liquefaction mitigation of loose silty sands. Stone columns have drainage properties that help dissipate pore water pressure under cyclic loading, so the technique is used to improve the behavior of the soil under cyclic loadings, such as earthquake loading. Several analytical, experimental, and numerical studies on the liquefaction mitigation of soils by stone columns are available in the literature. Analytical methods are usually directly or indirectly based on the results of field tests that reveal the effects of stone columns. More research is needed to identify the reduction of liquefaction by stone columns, as several variables control the percentage of soil liquefaction improvement in the field. In this study, the behavior of the group of stone columns is modeled by the finite difference method (FDM), where the field test data is used as an input. The pre and post-improvement soil data used in the analyses were obtained from cone penetration tests (CPT) performed in the field before and after the construction of the stone columns using the vibroflotation (wet bottom-feed) method. Then, the earthquake loading has been applied to the unimproved and improved soil models by the stone columns. Finally, under the earthquake loading, the percentage of the liquefaction resistance increase and the settlement of the loose silty sand under structural load after stone column construction is investigated.

ÖZET

TAŞ KOLON İLE ZEMİN İYİLEŞTİRMESİNİN SIVILAŞMA DİRENCİ ÜZERİNDEKİ ETKİSİ: SAHA VE NÜMERİK ÇALIŞMALAR

Bu çalışma, taş kolon grubunun gevşek siltli kumların sıvılaşmasının azaltılmasında ne kadar etkili olduğunu sonlu farklar yöntemini kullanarak anlamayı amaçlamaktadır. Taş kolonlar, boşluk suyu basıncını dağıtmaya yardımcı olan drenaj özelliklerine sahiptir, bu nedenle deprem yüklemesi altında zeminin davranışını iyileştirmek için kullanılırlar. Analitik yöntemler genellikle doğrudan veya dolaylı olarak taş kolonların etkilerini ortaya koyan saha testlerinin sonuçlarına dayanmaktadır. Sahada zemin sıvılaşmasının iyileşme yüzdesini çeşitli değişkenler kontrol ettiğinden, taş kolonlarla sıvılaşmanın azaltılmasını belirlemek için daha fazla araştırmaya ihtiyaç vardır. Bu vaka çalışmasında, taş kolon grubunun davranışı sonlu farklar yöntemi ile modellenmiştir. Analizlerde kullanılan iyileştirme öncesi ve sonrası zemin verileri, vibroflotasyon (ıslak dip beslemeli) yöntemi kullanılarak taş kolonların inşasından önce ve sonra sahada gerçekleştirilen koni penetrasyon deneylerinden (CPT) elde edilmiştir. Daha sonra, taş kolonlarla iyileştirme öncesi ve sonrası durum nümerik olarak modellenerek deprem yüklemesi uygulanmıştır. Son olarak, deprem etkisi altında gevşek siltli kum üzerinde taş kolon yapımından sonra sıvılaşma direncinin artış yüzdesi ve yapı yükü altında zeminin oturmaları araştırılmıştır.

TABLE OF CONTENTS

LIST OF FIGURES viii

LIST OF TABLES xiv

CHAPTER 1. INTRODUCTION 1

1.1. Introduction and Scope of Study 1
1.2. Organization of the Thesis 2

CHAPTER 2. LITERATURE REVIEW OF STONE COLUMNS 3

2.1. Introduction 3
2.2. Liquefaction 3
2.3. Stone Columns 6
2.3.1. Stone Column Construction Methods 9
2.3.2. Stone Column Material 14
2.3.3. Stone Column Design 15
2.3.4. Bearing Capacity 19
2.3.5. Failure Mechanism on Stone Columns 22
2.3.6. Dynamic Behavior of Stone Columns 23
2.4. Conclusion 43

CHAPTER 3. SITE STUDY / SOIL SURVEY 45

3.1. Site Properties 45
3.2. Geotechnical Evaluation of the Field 46
3.3. Field Tests 47
3.3.1. Standard Penetration Test (SPT) 47
3.3.2. Geophysical Studies 52
3.3.3. Cone Penetration Test (CPT) 54
3.4. Laboratory Tests 57
3.5. Idealized Soil Profile 60
3.6. Seismicity of the Site 61
3.6.1. Cone Penetration Test Based Liquefaction Assessment 61
3.6.2. Standard Penetration Test Based Liquefaction Assessment 65
3.7. Conclusion 66

CHAPTER 4. NUMERICAL MODELING OF STONE COLUMNS BY THE FDM.. 67

4.1. Introduction 67
4.2. Explicit and Implicit Solution 67
4.3. FLAC 3D Software 68
4.3.1. Mesh and time discretization 68
4.3.2. Rayleigh Damping 70
4.3.3. Dynamic Boundary Conditions 71
4.3.4. Finn Soil Model 73
4.3.5. Model Geometry 77
4.3.6. Dynamic Loading 78
4.4. Conclusion 78

CHAPTER 5. ANALYSIS OF IMPROVEMENT OF LIQUEFACTION BY STONE COLUMN 79

5.1. Introduction 79
5.2. Investigation Area by Pre-Post Survey Test Values 79
5.3. Modeling of Stone Columns 84
5.3.1. Meshing and Boundary Conditions 85
5.3.2. Geometry 85
5.3.3. Mesh Convergence 87
5.3.4. Constitutive Model and Material Properties 87
5.3.5. Interface 88
5.4. Dynamic Loading 89
5.5. Results and Discussions 90
5.5.1. Excess Pore Water Pressure (EPWP) 90
5.5.2. Settlement Analysis 97
5.6. Conclusion 101

CHAPTER 6. CONCLUSION 103

6.1. Recommendation for Future Research 105

REFERENCES 106

LIST OF FIGURES

Figure **Page**

Figure 2.1 Sand behavior criteria proposed by Boulanger & Idriss, 2008 4

Figure 2.2 Diagram of liquefaction by Benjamin Schlue, Ph.D., Marine Engineering. (Schlue) 5

Figure 2.3 Deep vibratory techniques grain size range (Source: Bohn & Lambert, 2013) 7

Figure 2.4 Wet–top–feed method process schematic (Source: Taube G. Martin, 2022) 10

Figure 2.5 Dry–top–feed method process schematic (Source: Taube G. Martin, 2022) 10

Figure 2.6 Dry–bottom–feed method process schematic (Source: Taube G. Martin, 2022)..... 10

Figure 2.7 Wet–bottom–feed method rig and constructed stone column (Georgia, 2023) 11

Figure 2.8 Variation in relative density according to the probe area used in stone column construction (Source: FHWA-RD-83-026)..... 13

Figure 2.9 CPT tip resistances obtained before and after construction (Source: Kirsch & Kirsch, 2010)..... 13

Figure 2.10 Load sharing diagram for rigid foundation loading (Source: Bergado et al., 1996)..... 17

Figure 2.11 (a) Change in compressibility in the disturbed area; (b) Change in permeability in the disturbed area (Source: Deb & Behera, 2017) 18

Figure 2.12 Design chart for Improvement Factor (Source: Priebe, 1995) 19

Figure 2.13 Vesic's cylindrical cavity expansion factors (Source: FHWA-RD-83-026) 20

Figure 2.14 Equivalent diameter for (a) triangular layout, (b) square layout and (c) hexagonal layout (Source: Demir, 2011) 21

Figure **Page**

Figure 2.15 Failure mechanism of single stone column (a) Bulging Failure, (b) Shear Failure (c) Punching Failure (Source: Barksdale & Bachus, 1983) 22

Figure 2.16 Stone column group failure mechanism (a) Lateral Spreading, (b) General Circular Failure, (c) Bulging Failure, (d) Punching Failure (Source: Barksdale & Bachus, 1983) 23

Figure 2.17 (a) Cross-sectional view and (b) Plan view of geotechnical centrifuge models tested to evaluate the liquefaction reduction efficiency of stone columns in non-plastic silty deposits (Source: Adalier et al., 2003) 25

Figure 2.18 Pore water distribution and settlement results for Model 1 (left side) and Model 2 (right side) (Source: Adalier et al., 2003) 26

Figure 2.19 Pore water distribution and settlement results for Model 3 (left side) and Model 4 (right) (Source: Adalier et al., 2003) 27

Figure 2.20 Finite element model with stone columns (a) unit cell, (b) plan view, (c) stone columns arrangement (Source: Tang et al., 2016) 28

Figure 2.21 Excess Pore Pressure Time Histories of the Silty Sand for Cases SC(with stone column) and SS (without stone column) (the initial effective vertical stresses at depths of 2.0, 3.4, 4.3, and 6.7 m are 14.0, 23.8, 30.1 and 46.9 kPa, respectively) (Source: Tang et al., 2016) 29

Figure 2.22 The pore pressure of 1.25 m in depth and from the center of columns (a) 1.0 m distance, (b) 1.5 m distance, (c) 2.0 m distance, (d) 2.5 m distance (Source: Esmaeili & Hakimpour, 2015) 30

Figure 2.23 The pore pressure of 2.5 m in depth and from the center of columns (a) 1.0 m distance, (b) 1.5 m distance, (c) 2.0 m distance, (d) 2.5 m distance, (e) 3.0 m distance (Source: Esmaeili & Hakimpour, 2015) 31

Figure 2.24 The finished difference mesh for the group of stone columns with a diameter of 150 cm and a center-to-center spacing of 4.5 m (Source: Esmaeili & Hakimpour, 2015) 32

Figure **Page**

Figure 2.25 The excess pore pressure for a group of stone columns of s / d = 2 to 5. (a) 1.2 m diameter, (b) 1.5 m diameter, (c) 0.9 m diameter at 1.25m depth (Source: Esmaeili & Hakimpour, 2015) 33

Figure 2.26 The excess pore pressure change comparison with VELACS project Model 1; with the depth (a)1.5m, (b)2.5m, (c) 5.0m, and (d) 7.5m (Source: Meshkinghalam et al., 2017)..... 34

Figure 2.27 The excess pore pressure change s/d ratio with individual column diameter 1.0 m at a depth of (a) 1.5m, (b) 2.5m, and (c) 5.0m (Source: Meshkinghalam et al., 2017)..... 35

Figure 2.28 The flow vectors with radial drainage (Source: Meshkinghalam et al. 2017) 36

Figure 2.29 Finite difference mesh for the column group (Source: Meshkinghalam et al., 2017) 37

Figure 2.30 Variation of excess pore water pressure for stone columns that have s/d ratios = 2, 3, 4 with (a)d=0.6 m, (b) d= 1.0 m, (c) d= 1.2 m (Source:Meshkinghalam et al., 2017) 38

Figure 2.31 Changes in soil surface settlement for the group of columns with different s/d values. (a) diameter 0.6 m, (b) diameter 1.0 m, (c) diameter 1.2 m (Source:Meshkinghalam et al., 2017) 39

Figure 2.32 Schematic view of the (a) Shake Table Model (b) Cone Penetration System; (Source: Ecemiş, 2013)..... 41

Figure 2.33 Measured and computed with numerical analysis excess pore pressure time histories during (a) first shake; (b) second shake; (c) third shake; and (d) fourth shake (Source: Ecemiş, 2013)..... 42

Figure 3.1 Çanakkale province location in Türkiye Map 45

Figure 3.2 Plan view of investigation area (Source: https://parselsorgu.tkgm.gov.tr) ... 46

Figure 3.3 CPT and SPT field test locations..... 46

Figure 3.4 Variation of corrected SPT N ((N1)60) values with depth 52

Figure 3.5 Geophysical surveys directions..... 53

Figure **Page**

Figure 3.6 Variation of cone tip resistance with depth 55

Figure 3.7 Variation of normalized cone tip resistance with depth 56

Figure 3.8 Türkiye Earthquake Hazard Map, determination of PGA (Source: https://tdth.afad.gov.tr, 2023)..... 61

Figure 3.9 Scheme of liquefaction assessment (Source: Boulanger and Idriss, 2014) ... 63

Figure 3.10 F.S and liquefaction potential according to CPT results 64

Figure 4.1 Solution procedure of FLAC 3D (Source: Billaux et Cundall, 1993)..... 69

Figure 4.2 Variation of damping with frequency (Source: Itasca's FLAC 3D Documentation, 2019)..... 71

Figure 4.3 Rigid base boundary conditions (Source: Itasca's FLAC 3D Documentation, 2019) 72

Figure 4.4 Flexible base boundary conditions (Source: Itasca's FLAC 3D Documentation, 2019)..... 72

Figure 4.5 Modelling layout methods (a) whole layout, (b) unit cell, (c) longitudinal gravel trenches, (d) cylindrical rings of gravel, (f) small groups of stone columns (Source: Castro, 2017)..... 77

Figure 5.1 Illustrative locations of Pre and Post CPT..... 80

Figure 5.2 Pre and Post values of CPT (Test-1 for 1.6m spacing) 81

Figure 5.3 Pre and Post values of CPT (Test-2 for 1.6m spacing) 82

Figure 5.4 Dr values from CPT Test-1 cone tip resistance values 83

Figure 5.5 Dr values from CPT Test-2 cone tip resistance values 84

Figure 5.6 Soil and stone columns model and mesh system 86

Figure 5.7 Analysis model section view..... 86

Figure 5.8 Time-dependent- acceleration-velocity and displacement graph of Düzce earthquake in Flac 3D dynamic input wizard 90

Figure 5.9 Excess pore water pressure ratio values concerning depth unimproved soil 91

Figure **Page**

Figure 5.10 Sudden increment of pore water pressure ratio values in first 3 second concerning depth unimproved area for first 3 seconds 92

Figure 5.11 Change in excess porewater pressure by time at a depth of 1.0 m 93

Figure 5.12 Change in excess porewater pressure by time at a depth of 1.5 m 93

Figure 5.13 Change in excess porewater pressure by time at a depth of 2.0 m 93

Figure 5.14 Change in excess porewater pressure by time at a depth of 5.0 m 94

Figure 5.15 Change in excess porewater pressure by time at a depth of 10.0 m 94

Figure 5.16 Change in excess porewater pressure by time at a depth of 15.0 m 95

Figure 5.17 Change in excess porewater pressure by time at a depth of 20.0 m 95

Figure 5.18 Percentage of EPWP increment before and after improvement by the depth at the end of earthquake loading 96

Figure 5.19 Displacement by time from the soil surface under earthquake loading and stress of 100 kPa 97

Figure 5.20 Displacement by time from 1.0 m depth under earthquake loading and stress of 100 kPa 97

Figure 5.21 Displacement by time from 1.5 m depth under earthquake loading and stress of 100 kPa 98

Figure 5.22 Displacement by time from 2.0 m depth under earthquake loading and stress of 100 kPa 98

Figure 5.23 Displacement by time from 5.0 m depth under earthquake loading and stress of 100 kPa 98

Figure 5.24 Displacement by time from 10.0 m depth under earthquake loading and stress of 100 kPa 99

Figure 5.25 Displacement by time from 15.0 m depth under earthquake loading and stress of 100 kPa 99

Figure 5.26 Displacement by time from 20.0 m depth under earthquake loading and stress of 100 kPa 99

Figure **Page**

Figure 5.27 Percentage of settlement improvement by the depth at the end of earthquake loading..... 101

LIST OF TABLES

Table **Page**

Table 2.1 Grain-size distributions for various stone column manufacturing methods given in source TS EN 14731 11

Table 2.2 Construction characteristics for stone columns using vibroflotation (Source: FHWA-RD-83-026-Stone Column Design & Construction)..... 12

Table 2.3 Commonly used gradations for stone columns (Barksdale & Bachus, 1983) 15

Table 2.4 Some data obtained from the CSST liquefaction test of sand with a relative density (Dr) 40% and 70% (Source: Beyaz et al., 2021) 40

Table 2.5 Relation of Excess Pore Pressure Ratio (ru) and Relative Density (Dr) (Source: Ecemiş, 2016) 43

Table 3.1 α and β values corresponding to IDI percentages (Source: TDBY, 2018) 48

Table 3.2 SPT correction factors (Source: TDBY, 2018)..... 48

Table 3.3 SPT-N values obtained from the SPT..... 49

Table 3.4 Soil class (TDBY, 2018)..... 54

Table 3.5 Physical properties of the soil in the investigation area..... 57

Table 3.6 Mechanical properties of the soil in the investigation area 59

Table 3.7 Mechanical and physical properties of soil 60

Table 3.8 SPT based liquefaction analysis 66

Table 4.1 Comparison between explicit and implicit methods (Source: Cundall, 1980) 67

Table 5.1 Values representing the physical properties of fully saturated sands (Source: Kirsch & Kirsch, 2010) 84

Table 5.2 Properties of soil and stone columns 88

Table 5.3 Finn Model parameters 88

Table 5.4 EPWP increment values varying depth under earthquake loading..... 96

Table 5.5 Settlement values under surcharge and earthquake loading 100

CHAPTER 1

INTRODUCTION

1.1. Introduction and Scope of Study

Stone columns are considered a practical way to improve the behavior of soils in seismic zones due to their drainage characteristic; the main idea beyond is to dissipate water, decrease the pore water pressure, and the effective stresses increase, and as a result stone columns reduce the phenomenon of soil liquefaction.

The dynamic behavior of stone columns or the mitigation of liquefaction by improvement method presents a fascinating area of research because of the several variables that control liquefaction. Several analytical, experimental, and numerical studies have been conducted on the liquefaction mitigation of stone columns' improved soils. The analytical methods are generally based on the results of in situ tests, mostly Standard Penetration Test (SPT), Cone Penetration Test (CPT), or other approaches introducing the effect of stone columns. Numerical models had usually been made to remodel the laboratory studies. After verifying laboratory works with numerical models, focuses on finding the optimum stone column spacing, rearrangement of columns, and diameter for mitigating liquefaction potential using stone columns.

The objective of this thesis is to understand the role of soils improved with stone columns in reducing excess pore water pressure and liquefaction potential under earthquake loading In this context, the cone tip resistance values obtained from CPT data before and after the stone column construction in the field were compared, and the relative density changes of the silty sand soil between the columns were evaluated depending on the construction method of vibroflotation. Then, using the obtained field data, three-dimensional numerical modeling of a group of stone columns under earthquake loads in loose silty sand improved with stone columns is performed with ITASCA software FLAC 3D (Fast Lagrangian Analysis of Continua in 3 Dimensions). Finn Soil Model is used to simulate the liquefaction phenomenon. In addition to earthquake loading, structural loads were also included in the model to investigate the settlement of the soil.

In the literature, some studies investigated the changes in excess pore water pressure and liquefaction resistance by numerically modeling the data obtained from shaking table tests and centrifuge tests in the laboratory. In addition, some studies examined the improvement of soil before and after the stone column construction based on the construction method used. However, no study uses the Finn Soil Model to numerically model the CPT data obtained before and after the stone column construction.

1.2. Organization of the Thesis

This thesis consists of six chapters. The first section (CHAPTER 1) is an introduction chapter summarizing the thesis studies.

The dynamic soil liquefaction mechanism is discussed in the second section of this thesis (CHAPTER 2). Then, the available stone column design methodologies, the construction phase of stone columns, the behavior of the soil after improvement with stone columns, and the behavior of stone columns under cyclic loadings are summarized.

The third part of the thesis (CHAPTER 3) is mainly reserved for presenting the field investigations performed in Çanakkale, Türkiye. In this section, the liquefaction potential of the site is determined by empirical methods using data obtained from field tests.

In the fourth section of this study (CHAPTER 4), the FLAC 3D is introduced, and critical issues such as meshing, dynamic boundary conditions, model geometry, and dynamic loading to be considered in the analysis are explained. In addition, the Finn Soil Model, which is the material model used during the analysis, and the way of obtaining its parameters are mentioned.

The fifth part of the thesis (CHAPTER 5) includes the determination of the dynamic parameters to be used in the analyses using field tests, the results of liquefaction and settlement analyses under earthquake loads, and the evaluation of the results.

The final part of the thesis (CHAPTER 6) is the conclusion part. This section summarizes all the studies and obtained results.

CHAPTER 2

LITERATURE REVIEW OF STONE COLUMNS

2.1. Introduction

This literature review chapter is basically organized into two parts. The first section presents an overview of the soil liquefaction mechanism, while the second part examines the review of the existing methodologies of stone column design, the construction phase of stone columns, the behavior of the soil after improvement, and the behavior of stone columns in dynamic loading conditions. Finally, in this chapter, some studies on the dissipation of excess pore water from the soil to the columns, the increase in the relative stiffness of the soil based on the construction method, and the decrease in the amount of settlement in the soils after the improvement of the soil with stone columns under earthquake loading are presented.

2.2. Liquefaction

The first usage of the word liquefaction was by Hazen in 1918 to explain the Calaveras dam break. Hazen explained the liquefaction phenomenon as a concentration of pressures induced by a movement or a deformation in the material. When this occurs rapidly, the water contained between the pores is pressurized. The continuous increase of this pore pressure leads to a decrease of the intergranular forces in the soil (physical explanation), and the material loses all its strength when the pore pressure becomes equal to the initial effective stress (Hazen, 1918).

Soil liquefaction is a case in which the strength and stiffness of the soil is reduced by earthquake shaking or similar cyclic loadings. This has become an issue of great importance recently due to sudden and catastrophic failures, often resulting in fatalities and enormous financial consequences. Saturated, low cohesion soil or cohesionless loose soils contract under earthquake-induced cyclic shear stresses, increasing excess pore water pressure. High pore water pressure created by cyclic loadings relieves effective stresses, and the upward flow reduces the interparticle binding forces to zero and triggers

liquefaction. After a sudden increase in pore pressure and with it, stress transfer occurs, and the resulting effective stress controls the shear strength. Liquefaction takes place if this stress transfer is completed to pore water pressure (Boulanger and Idriss, 2014, Youth et al., 2001).

$$\sigma = \sigma' + u \tag{2.1}$$

$$\lim(\sigma - u) \rightarrow 0 \tag{2.2}$$

Liquefaction basically occurs in water-saturated fine-grained, sandy, and silty soils (cohesionless soils) when the effective vertical stress is zero due to increased pore water pressure during an earthquake. Thus, the soil layer behaves like a liquid, cannot support the superstructure, and the structures tilt over, yield, collapse, overturn or rotate. After the earthquake that happened in Türkiye in 1999 (Adapazarı, North Anatolian Fault), which has a magnitude of 7.6, investigations in and around Adapazarı showed that non-plastic fine particles passing the #200 sieve could also liquefy. The studies showed that it is appropriate to use the relations developed for sands and silty clayey sands for clay and silty clay units with a plasticity index of less than 7 (Boulanger & Idriss, 2008). As shown in Figure 2.1, soils with a plasticity index less than 2 show cohesionless soil behavior, while units with a plasticity index between 2 and 7 show a transition between cohesionless and cohesive behavior. Therefore, it is recommended to consider cohesionless behavior for units with PI values less than 7.0.

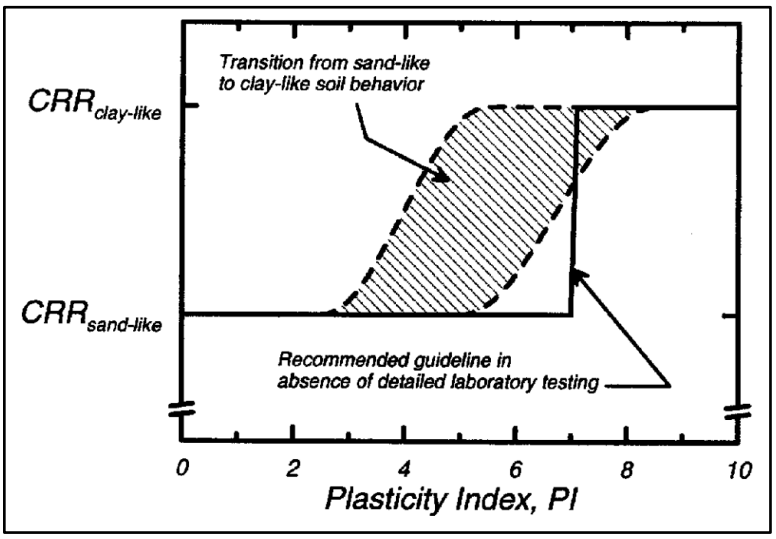

Figure 2.1 Sand behavior criteria proposed by Boulanger & Idriss, 2008

Soil behavior must be well-defined before any sudden increase in loading conditions, such as earthquakes (Figure 2.2). The most characteristic feature of all liquefaction events is the excess pore water pressure under undrained loading conditions.

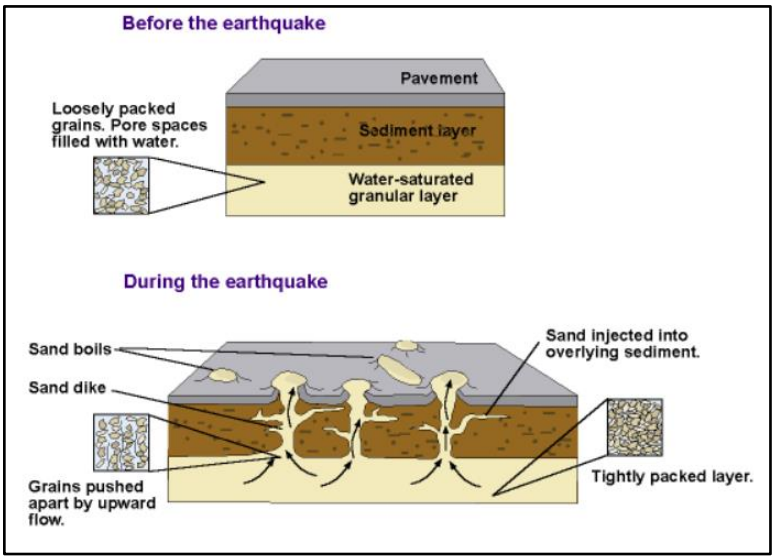

Figure 2.2 Diagram of liquefaction by Benjamin Schlue, Ph.D., Marine Engineering. (Schlue)

Theoretically, there are two ways to prevent liquefaction: increasing effective stress (bonding force between particles) and/or decreasing pore water pressure (Marcuson, 1978).

The factor of safety (F.S.) is calculated by comparing the repetitive shear stress ratio (CSR) and the repetitive shear strength ratio (CRR), which defines the liquefaction resistance of the soil to the earthquake-induced ground motion (NCEER, 1997).

The effect of the earthquake on the soil is calculated by the following relation developed by Seed et al. (1985):

$$CSR = 0.65 * \left(\frac{a_{max}}{g}\right) * \left(\frac{\sigma_v}{\sigma'_v}\right) * r_d \quad (2.3)$$

$$for\ z \leq 9.15m \quad r_d = 1.0 - 0.00765 * z \quad (2.4)$$

$$for\ 9.15 \leq z \leq 23m \quad r_d = 1.174 - 0.0267 * z \quad (2.5)$$

$$for\ 23 \leq z \leq 30m \quad r_d = 0.774 - 0.008 * z \quad (2.6)$$

$$for\ z > 30m \quad r_d = 0.5 \quad (2.7)$$

The F.S for the liquefaction potential is defined as:

$$F.S. = \frac{CRR_{7.5}}{CSR} * MSF \quad (2.8)$$

$CRR_{7.5}$: liquefaction resistance for a magnitude of 7.5 earthquake;

CSR: cyclic stress applied on the ground;

MSF: Magnitude Scaling Factor.

When the F.S exceeds 1.0, the soil would theoretically be stable under an M magnitude of an earthquake; in practice, a safety factor greater than 1.0 is recommended. According to Turkish Building Earthquake Code (Türkiye Bina Deprem Yönetmeliği (TBDY), 2018) the F.S number against liquefaction is 1.1. If the F.S is not achieved, it is proposed to evaluate the reduction in strength and stiffness properties of the layers expected to be liquefied, possible bearing capacity problems, slope stability problems, settlement problems and lateral spreading type failures (TBDY, 2018).

2.3. Stone Columns

Stone columns were first constructed in France in the 1830s in natural soils. The first stone columns application was developed in 1835 by French army engineers as a heavy weapons factory, and an ammunition depot was built to improve the structure's ground (Barksdale and Bachus, 1983). Since the last decade, it has been used worldwide, especially in dynamic loading conditions (earthquakes, machine foundations, etc.), to pre-compact possible voids, reduce the void volume, and create a drainage path with the replaced qualified material. It was developed to improve soils by using drainage when subjected to vibration, particularly cohesive, stratified, and mixed soils that are not easy to compact. Today, construction methods have been diversified using different techniques and equipment in the manufacturing stages of stone columns for various kinds of soil.

Stone columns improve weak soils under lightweight structures such as railway and highway embankments and non-multi-story buildings (Cimentada & Costa, 2009). However, this method was widely used in Europe after 1950 and in the USA after 1972.

The most effective use of the stone column method is observed in soils with an undrained shear strength of 7-50 kPa (Barksdale & Bachus, 1983). Studies have shown that stone columns successfully work in soft clay, silt, and silty sand soils.

In the seismic areas, there are many techniques for improving liquefiable soil: Vibro-compaction of dynamic compaction, soil reinforcement methods like stone columns or rigid inclusions, jet grout, and deep soil mixing techniques.

The stone column method's main advantage is that it can be applied to all soil types, as shown in Figure 2.3. Due to the granular structure of the stone columns, they can maintain their integrity without the risk of internal collapse (Bohn & Lambert, 2013).

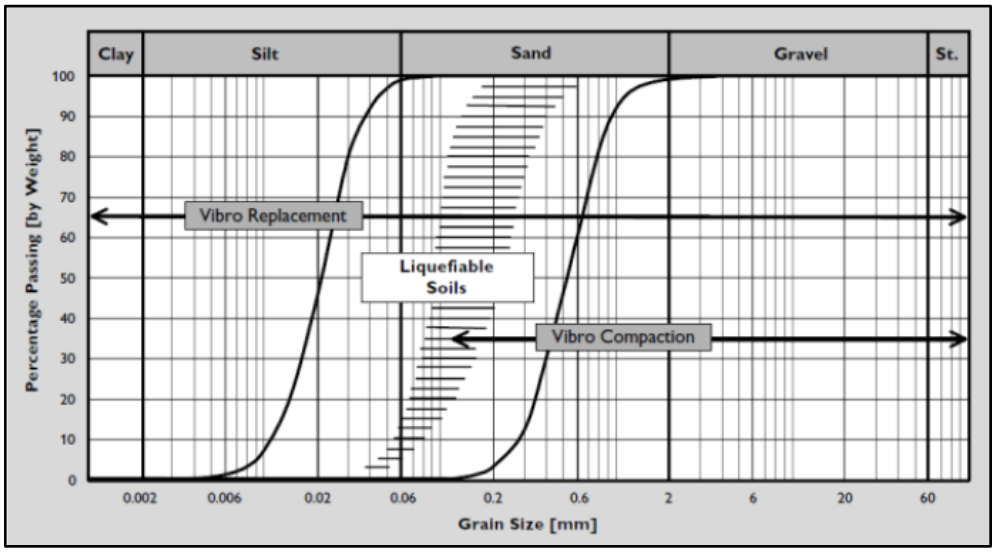

Figure 2.3 Deep vibratory techniques grain size range (Source: Bohn & Lambert, 2013)

The effect of decreasing liquefaction risk using stone columns has been widely emphasized in the literature, and many studies have been done, such as Pestana, (1998); Adalier et al., (2003); Sivakumar et al., (2004); Adalier & Elmagal, (2004); Bouassida & Frikha, (2015) and Tang et al., (2016). The primary purposes of stone columns are to increase bearing capacities, reduce the liquefaction potential by lowering the pore water pressure with drainage, and decrease the total and differential settlement.

Stone column application on soil that has liquefaction potential should be expected to gain the following properties (Demir, 2011):

- During the construction of stone columns, the relative density of the surrounding soil increases due to vibration and displacement.

- Stone columns increase the bearing capacity of the soil with their high strength and density.

- Stone columns reduce excess pore water pressure by drainage.

- Lateral stress increases in the soil around the column where the stone column is applied.

Stone columns are similar to drainage systems since they take charge of the drainage path. However, unlike drainage systems, stone columns increase the bearing capacity of the system since they are elements with high stiffness modulus. In addition, with the application of the stone columns, consolidation, and total settlements of the soil are reduced.

Stone columns have more rigid coarse grains than the soil in which they are located. During the construction of stone columns, drilling holes are formed in soft fine-grained soils as the steel pipe connected to the vibrator penetrates the soil. Depending on the method used, stone columns are manufactured within the fine-grained soil by gradually filling and compacting the gravel/crushed stone material from the top or bottom. As a result of stone column application, a new composite unit consisting of fine-grained, soft, medium-dense, and rigid crushed stone columns is obtained. The load transfer platform of sufficient thickness between the stone columns and the structure's foundation ensures the transfer of loads uniformly to this improved area.

With the development of deep vibration systems, the application of vibro-stone columns has been widely extended from cohesionless soils to cohesive soils. The load-carrying capacity of the improved soil depends on the interaction between the stone column and the surrounding soil. Stone columns are supported by the soil they replace, so the soil must have a specific minimum strength (Kirsch and Kirsch, 2010).

The degree of soil improvement with stone columns can be determined by the area replacement ratio method used to improve soil (Balaam & Booker, 1985; Priebe, 1995; Sivakumar et al., 2004). Despite this, when the bottom feed method is used for placing stone columns, the confining stress on the column by expanding it and increasing the soil's stiffness results from heightened stress in the surrounding soil. Contrary to the area replacement ratio assumed to be improved with stone columns (Priebe, 1995), Kirsch, (2006) showed that the improvement continues between 4 and 8 times the column diameter. Ammari & Clarke, (2018) showed that the stiffness of the soil increased with the extension of the column during the stone column construction, and the settlement values decreased by 55%. After the excess pore water pressure generated during construction is distributed to the stone columns, the soil around the columns is reformed and shows a permanent increase in stiffness. For this reason, when designing stone columns, it should be considered that the soil will improve during the installation phase, and these improvements should be considered in the models to be created (Kirsch, 2006). By using 3D Coupled Eulerian-Lagrangian analyses, the stone column installation effect

has been examined. This analysis was performed with groups of one, two, and nine columns. It showed that the soil improved during construction by recreating the surrounding soil change with increases in horizontal stresses and pore pressures (Geramian et al., 2022).

2.3.1. Stone Column Construction Methods

Stone columns are formed by placing and compressing crushed stone material after boring with compression with a heavy and vibrating tip. It is based on the compaction method of the surrounding ground by the lateral displacement of the crushed stone placed in the cylindrical cavity opened in the environment with the help of an eccentric mass using the probe's vibration.

The volume required to manufacture stone columns is provided by laterally compressed soil (displacement) rather than removing the natural soil deposits (replacement). For this reason, drilling-extracting the natural soil deposit process is not used in stone column formation.

Stone columns formed with compressed high-strength aggregate material strengthen the weak natural soil. In this way, the aggregate column with higher stiffness takes more stress and reduces the stresses and strains on the lower-strength soil.

The area where the stone column will be manufactured should be leveled, and a stable working platform for the machine to move shall be established. The application points of stone columns should be precisely marked on the working platform. The column manufacturing process is performed after the appropriate area has been provided. There are various methods for manufacturing stone columns. The most commonly used are the Vibro-replacement method (Wet, Top Feed method) and the Vibro-displacement method (Dry, Top, and Bottom Feed Method). The vibro-displacement method combines gravel backfill, resulting in stone columns that increase the density and provide a degree of reinforcement and a potentially effective means of drainage. The methods of stone column construction are shown in Figure 2.4, Figure 2.5, and Figure 2.6, respectively. The main processes in stone column manufacturing are first drilling with a vibrating vertical probe, simultaneously filling the cavity formed by pulling the probe up a little with crushed stone by feeding from the bottom or top, depending on the ground conditions, and compacting it with the probe and repeat the filling and compaction processes until the entire probe comes to the surface.

A fixed frequency vibrator operating at a frequency of approximately 1800 or 3000 rpm is used during the construction of columns. In the wet method, the vibrator sprays a hole using large quantities of water under high-pressure body vibration at the tip caused by eccentric weights rotating inside the probe body. The eccentric end, rotated using electric or hydraulic power, allows it to move along the soil.

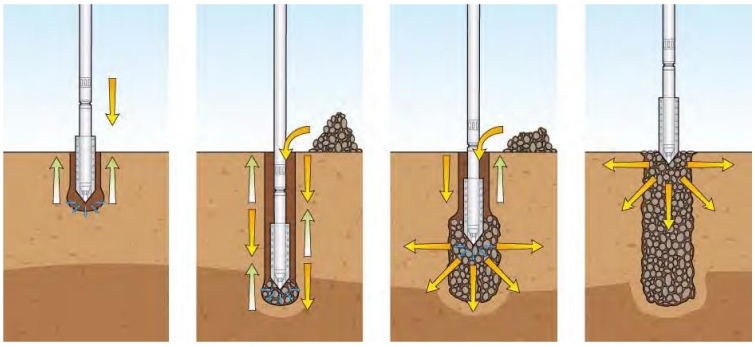

Figure 2.4 Wet–top–feed method process schematic (Source: Taube G. Martin, 2022)

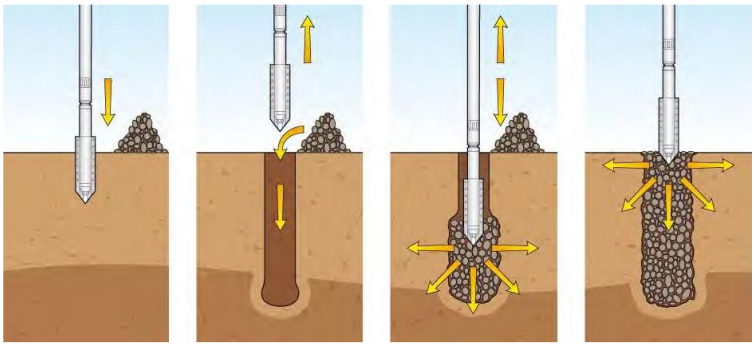

Figure 2.5 Dry–top–feed method process schematic (Source: Taube G. Martin, 2022)

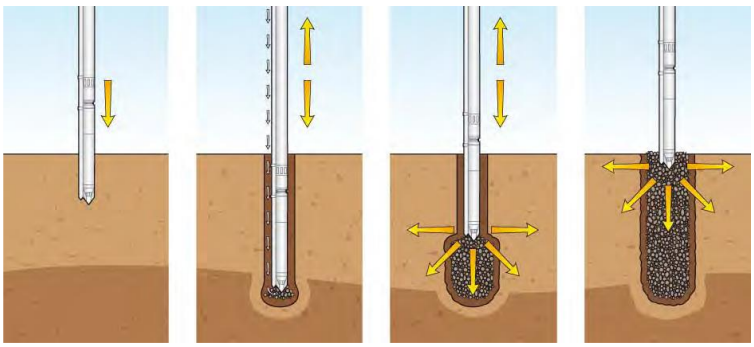

Figure 2.6 Dry–bottom–feed method process schematic (Source: Taube G. Martin, 2022)

The photograph shown in Figure 2.7 demonstrates the stone column rig used in the bottom-feed wet method and the stone column under construction. The author took this photograph in Batumi Georgia, in May 2023.

Figure 2.7 Wet–bottom–feed method rig and constructed stone column (Georgia, 2023)

Table 2.1 Grain-size distributions for various stone column manufacturing methods given in source TS EN 14731

Construction Process	Particle Size (mm)
Dry Top-Feed	40-75
Wet Top Feed	25-75
Dry Bottom Feed	8-50

Vibroflotation (sometimes called Vibro-compaction) method is used to densify loose sandy soils. The principle of this technique is based on the vibrations of a vibrator (Figure 2.7). This vibrator descends to the desired depth under the effect of its weight, as well as air or water jetting (Figure 2.7), which helps transport the sand to the compaction zone at the base of the vibrator.

The vibrations generate a temporary phenomenon of liquefaction of the soil under the effect of interstitial overpressures; then, the grains are rearranged in a denser state, presenting better mechanical characteristics. This technique is reserved for pulverulent soils which contain a percentage of fine particles less than 10 to 15%; beyond these percentages, the fines decrease the phenomenon of liquefaction and thus the densification.

According to FHWA-RD-83-026, the rig characteristics of stone columns to be constructed by the vibroflotation method should satisfy the limits given below.

Table 2.2 Construction characteristics for stone columns using vibroflotation (Source: FHWA-RD-83-026-Stone Column Design & Construction)

Construction Method	Column Diameter (m)	Column Install Rate	Jetting
Vibrofloatation Method	<1.2 typically	12.2 m/hr.	Water at 690 kPa cool electric vibrator

It is noted that when designing stone columns, in sandy soils, depending on the vibroflotation construction method and the probe area used, the relative density of the soil will increase (FHWA-RD-83-026-Stone Column Design & Construction). Figure 2.8 below shows the variation of probe area used in the vibroflotation method and the relative densities to be reached after improvement in sandy and silty soils.

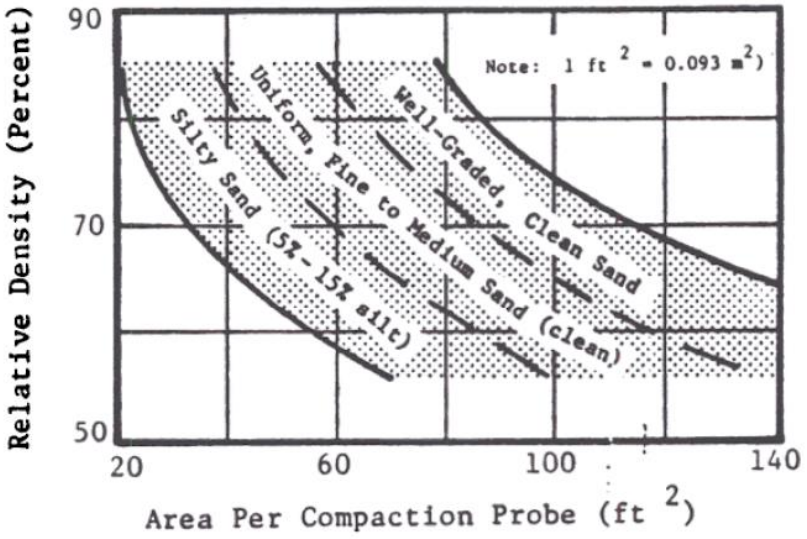

Figure 2.8 Variation in relative density according to the probe area used in stone column construction (Source: FHWA-RD-83-026)

The improvement in the ground during the construction of stone columns has been the subject of many studies. The increases in a typical CPT cone tip resistance obtained before and after the construction of stone columns with vibro methods are shown in Figure 2.9 (Kirsch & Kirsch, 2010).

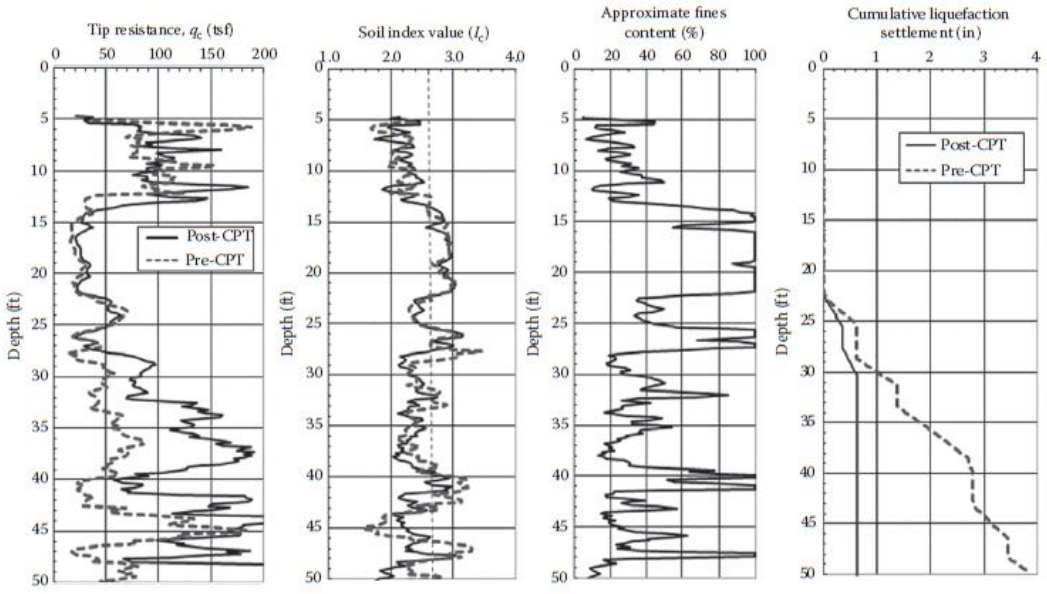

Figure 2.9 CPT tip resistances obtained before and after construction (Source: Kirsch & Kirsch, 2010)

The soil profile of the area shown in the CPT graph above includes the first 3.96 m from the surface as dense sand, the next 3.0 as medium stiff clay, and the next 7.62 m medium dense sand. Especially in the sand units, an increase in the cone tip resistances is observed after the stone column construction.

2.3.2. Stone Column Material

The material that passes through the 2 mm sieve will be considered fine-grained for stone column manufacturing. The fines content of the material must not exceed 5%.

In addition to the grain size distribution given above, a suitability number S_N is defined as follows (Brown, 1977):

$$S_N = 1.7 * \sqrt{\frac{3}{(D_{50})^2} + \frac{3}{(D_{20})^2} + \frac{3}{(D_{10})^2}} \quad (2.9)$$

D_{50}, D_{20}, and D_{10} are the diameters in mm through which 50, 20, and 10% of the material passes. The suitability number to be determined according to the above equation for the aggregate use should be at most 5.

Stone column materials must be chemically unaffected by groundwater and not be crushed/crumbled by the abrasive vibrations of the vibrator. The gradation of the material should allow the column to be compressed and not prevent it from having a high degree of permeability. European norms EN 14731: vibrating deep compaction methods, EN 1097-2 and EN 13450: physical properties of crushed stone materials give the necessary properties for selecting durable stone column materials.

The grain size distribution commonly used in stone column application is given in the table below (Barksdale & Bachus, 1983). Using gradations 1 and 2 in the table below Table 2.3 is recommended.

Table 2.3 Commonly used gradations for stone columns (Barksdale & Bachus, 1983)

Nominal Maximum Size Square Openings. mm	Sieve Number	Alternative 1 Percentage of Passing the Sieve	Alternative 2 Percentage of Passing the Sieve	Alternative 3 Percentage of Passing the Sieve	Alternative 4 Percentage of Passing the Sieve
100.00	4.00	-	-	100	-
90.00	3.50	-	-	90-100	-
75.00	3.00	90-100	-	-	-
63.00	2.50	-	-	25-100	100
50.00	2.00	40-90	100	-	65-100
37.50	1.50	-	-	0-60	-
25.00	1.00	-	2	-	20-100
19.00	0.75	0-10	-	0-10	10-55
12.50	0.50	0-5	-	0-5	0-5

2.3.3. Stone Column Design

Analytical studies of stone columns are generally based on a composite foundation system and a unit-cell approach (Priebe, 1995). Stone column design parameters such as column material, layout model, diameter, area replacement ratio, bearing capacity, and settlement are defined in the following sections below.

The appropriate design should first verify the permissible bearing capacity of the improved soil and, secondly, verify the acceptable settlement for any foundation. However, methods are also based on an isolated column or an infinite network of columns for another purpose.

The dimensioning of stone columns is based on the calculation of the following three parameters;

- the area replacement ratio (a)
- stress concentration ratio (n)
- the settlement reduction factor (β)

a) Area Replacement Ratio (a)

The performance of the improved soil by stone columns is significantly affected by the volume of soil replaced. The Area Replacement Ratio can be defined as the ratio of the compacted stone column (A_c) area to the total area within the unit cell (A).

Increasing the area ratio can enhance the overall response of the reinforced ground by granular piles (Shahu et al., 2000). A minimum area replacement ratio of 0.25 or greater is required to improve bearing capacity for ground treated with stone columns significantly (Wood et al. 2000). If the area replacement ratio is < 0.25, a granular bed layer can be used for the increasing bearing capacity (Shahu et al., 2000).

$$a_s = \frac{A_c}{A} \tag{2.10}$$

b) Stress Concentration Factor (n)

The stress concentration factor of a stone column refers to the ratio of the maximum stress at the point of contact between the column and the surrounding soil to the average pressure applied to the column. The stress concentration factor depends on various factors, such as the diameter and length of the column, the soil properties, and the applied load. A higher stress concentration factor implies a higher risk of failure at the interface between the stone column and the surrounding soil. Therefore, it is crucial to consider the stress concentration factor in the design of stone column systems to ensure their safe and effective performance.

The average vertical load applied to the soil surface, σ or σ_0, is distributed over the surface of the cylindrical domain between the stone columns (σ_c) and the surrounding soil (σ_s) in a manner that is proportional to their surface areas.

The correlation between the average stress σ_0 or σ applied to the whole area, the stress sc transferred to the area of the stone column A_c, and the stress σ_s carried by the soil on the soil area A_s is stated as (Bergado et al., 1996):

$$A * \sigma = A_c * \sigma_c + A_s * \sigma_s \tag{2.11}$$

Load sharing by the stone columns is illustrated in Figure 2.10 below:

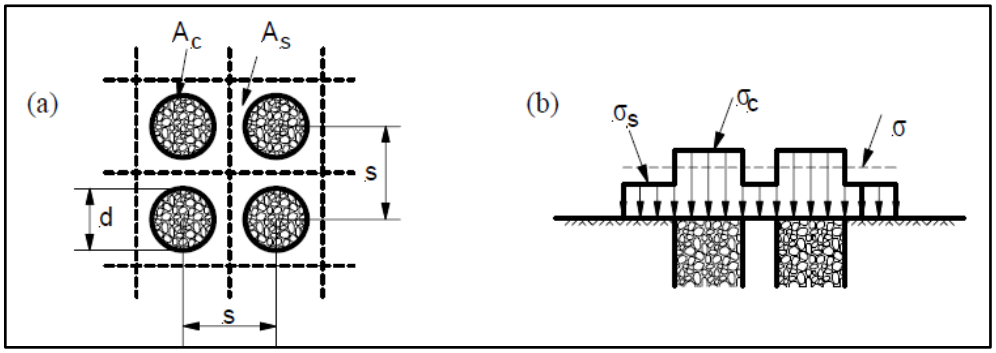

Figure 2.10 Load sharing diagram for rigid foundation loading (Source: Bergado et al., 1996)

The strength parameters of the stone columns are greater than the improved soil. As a result, a load transfer mechanism σ_0 develops, causing an accumulation of vertical stress on the stone columns σ_c and a decrease in the stress of the soil σ_s.

The stone columns have higher strengths and modulus than the treated soil. For this reason, a load transfer mechanism σ_0 develops, leading to a concentration of the vertical stress on the columns σ_c and a reduction of the load on the soil σ_s. By definition, the vertical stress concentration ratio is the ratio of the stress contributed by the column σ_c to that contributed by the soil after treatment σ_s.

$$n = \frac{\sigma_c}{\sigma_s} \tag{2.12}$$

Rigid foundations and elastic soils where the soil settlements between columns are uniform, the stress concentration factor can be calculated as the ratio of the deformation modulus of the stone columns (E_c) to the surrounding soil (E_s):

$$n = \frac{E_c}{E_s} \tag{2.13}$$

For exceptionally soft and heterogeneous soils, the value of n could reach very high values of 50 Vautrein, 1980; for Dhouib, 2005, the value of n varies between 4 and 10.

c) Settlement Reduction Factor (β)

The load σ_0 applied by the foundation to the subgrade would cause an initial settlement S_i before the soil treatment. After the treatment, the settlement values decrease overall. The settlement reduction factor β can be defined as the ratio of the settlement s_i of the soil before treatment to the settlement s_f of the composite medium obtained after treatment, which is:

$$\beta = \frac{s_i}{s_f} \tag{2.14}$$

Due to the construction of stone columns in soft soils, the properties of the surrounding soil change in such a way that the permeability and compressibility in the disturbed zone (smear) decrease and increase towards the column. There are three possibilities for the variation of horizontal permeability and volume compressibility in the disturbed zone (Figure 2.11):

- reduced constant permeability with reduced constant compressibility,
- linear variation for permeability and compressibility,
- parabolic variation for permeability and compressibility.

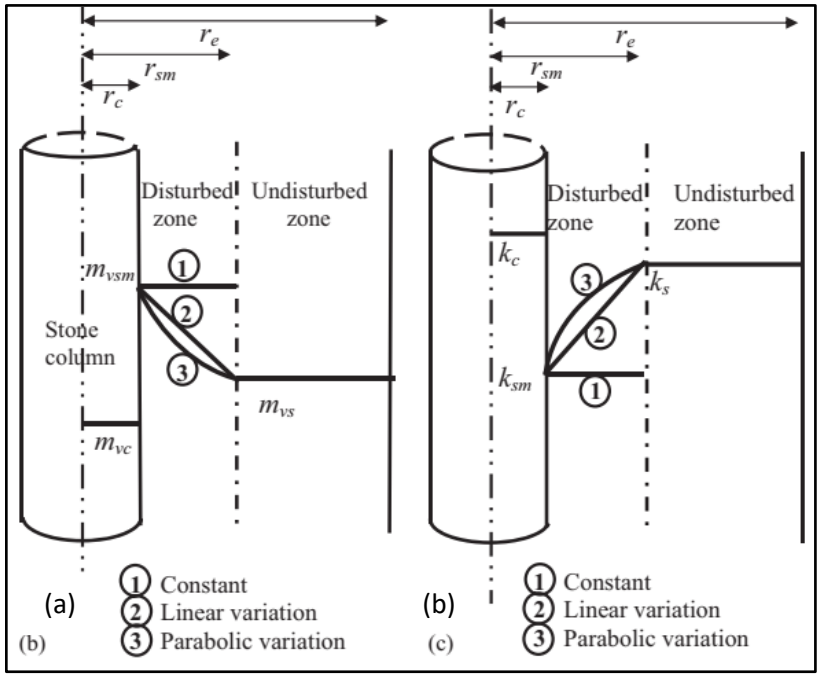

Figure 2.11 (a) Change in compressibility in the disturbed area; (b) Change in permeability in the disturbed area (Source: Deb & Behera, 2017)

Priebe (1995) used the unit cell method to estimate the settlement values of the soil with stone column improvement. In this method, the column is supposed to be incompressible; also bulk density of the soil and column is ignored. It is also assumed that the soil around the stone columns is displaced until the initial resistance of the soil reaches the liquid state when the stone columns are constructed (vibro-replacement method). This means that the earth's pressure coefficient, K, equals 1.0. Then, the improvement factor, the settlement ratio before and after the stone column installation, is given as a function of the area improvement (1/ area replacement ratio). The internal friction angle ϕ' was chosen between 35^o and 45^o for a Poisson's ratio μ_s of 1/3. The design scheme proposed by Priebe (1995) is given in Figure 2.12. It shows that the n coefficient change by area ratio (A/A_c) at constant μ_s and varying ϕ'.

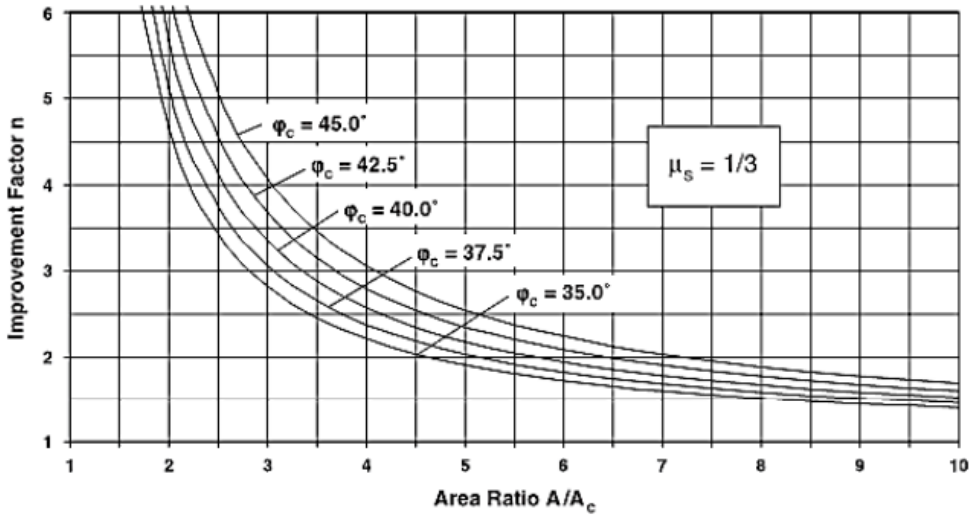

Figure 2.12 Design chart for Improvement Factor (Source: Priebe, 1995)

2.3.4. Bearing Capacity

Bearing capacity calculations after the soil improvement by stone columns is adjusted generally according to Vesic's cavity expansion theory recommended by FHWA-RD-83-026-Stone Column Design & Construction.

The bearing capacity formula according to Vesic's expansion theory is given below:

$$q_{stone\ column} = (c \times F_c + q \times F_q) \times \left(\frac{1+sin\emptyset_s}{1-sin\emptyset_s}\right) \qquad (2.15)$$

q_u: stone column bearing capacity, kPa

c: cohesion, kPa

q: failure depth (FHWA: 2D)

$\emptyset_s$: internal friction angle of stone column=43˚

F_c, F_q: bearing capacity coefficients

F_q and F_c coefficients were chosen according to (FHWA-RD-83-026, 1983), which is prepared according to the rigidity index; these graphs are shown in Figure 2.13.

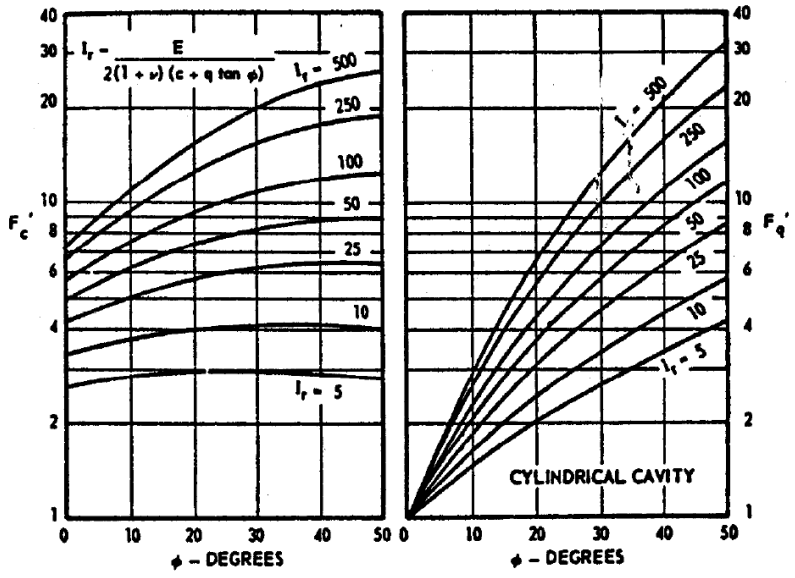

Figure 2.13 Vesic's cylindrical cavity expansion factors (Source: FHWA-RD-83-026)

The rigidity index can be calculated according to the formula below,

$$I_r = \frac{E}{2\times(1+\mu)\times(c+q\times tan\emptyset)} \tag{2.16}$$

E: Elasticity modulus of soil

μ: Poisson’s ratio of soil

ϕ: Internal friction angle of soil

Due to the difference in stiffness between the soil and the stone column, their bearing capacities also have differences. Using the area replacement ratio given in Section 2.3.3.a) , the bearing capacity of the soil improved with stone columns can be calculated as given in equation below.

$$q_{imp-soil} = A_r * q_{stone\ column} + q_{soil} * (1 - A_r) \quad (2.17)$$

2.3.4.1. Equivalent Diameter

For settlement and stability analysis, the soil surrounding each column should be considered together with the column. Accordingly, a single column of equivalent diameter D_e and the surrounding soil is called a unit cell. The centers of the stone column and the unit cell are common. Figure 2.14a-c shows the equivalent diameter calculation according to the stone column layout.

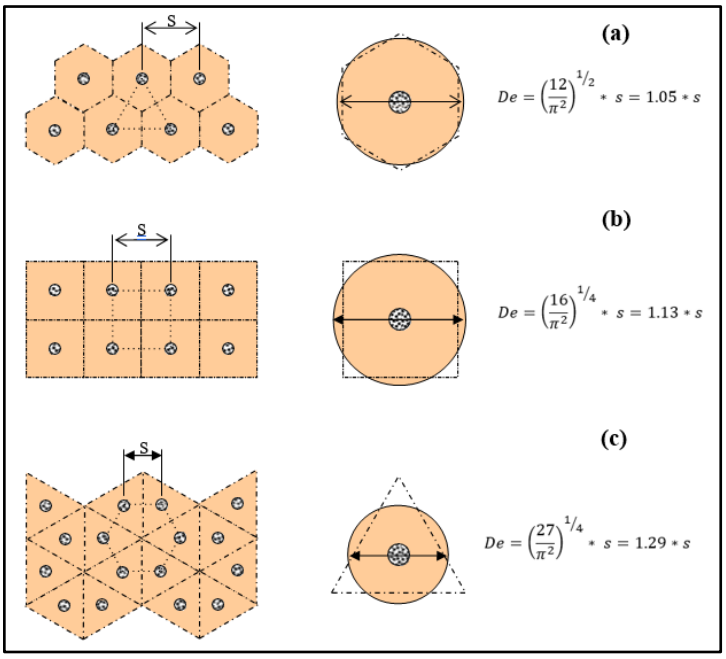

Figure 2.14 Equivalent diameter for (a) triangular layout, (b) square layout and (c) hexagonal layout (Source: Demir, 2011)

According to the equivalent diameter, the area calculations:

$$A = \frac{\pi * D_e^2}{4} \quad (2.18)$$

$$A_c = \frac{\pi * D_c^2}{4} \quad (2.19)$$

$$A_s = A - A_c \quad (2.20)$$

Where A is the total area of the unit cell, A_c represents the area of the stone column area, and A_s represents the area of the soil which is surrounding the stone column.

2.3.5. Failure Mechanism on Stone Columns

a) Single Stone Column Failure Mechanism

The types of failure that will happen when single columns are loaded can be classified in three different ways. Figure 2.15a shows that bulging failure may occur if the column is more than 3-4 times longer than its diameter. As seen in Figure 2.15b, if a stone column is constructed short length, a shear failure may occur. Figure 2.15c demonstrates that if the stone column length is smaller than 2-3 times its diameter, the failure may occur at the tip of the column because of exceeding the bearing capacity.

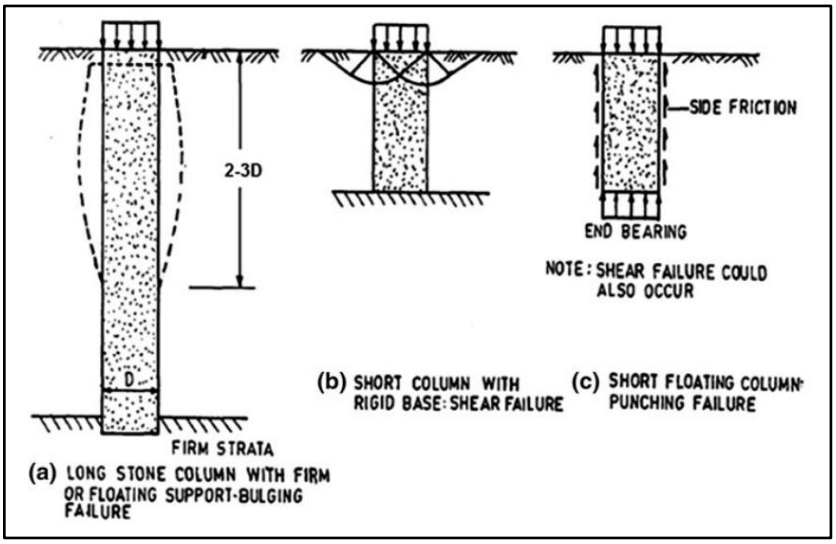

Figure 2.15 Failure mechanism of single stone column (a) Bulging Failure, (b) Shear Failure (c) Punching Failure (Source: Barksdale & Bachus, 1983)

b) Group of Stone Columns Failure Mechanism

Stone column groups are formed by placing individual stone columns in specific spacing next to each other. An individual stone column within a group has higher ultimate bearing capacity than that of a single stone column. During the construction of a group of stone columns, when stone columns are constructed around an individual stone column, the soil between the stone columns will be compacted, limiting the movement of the inner column. Therefore, the ultimate bearing capacity of each column is slightly increased. Suppose sufficient compaction cannot be supplied in stone columns constructed in weak

soils. In that case, it will cause lateral movement of the improved soil under the foundation due to the loads from the structures constructed in the improved area. This situation, called lateral spreading, reduces the lateral support between the soil and the stone column. Groups of stone columns constructed in soft soils may also collapse due to lateral spreading (Figure 2.16a) or beated the bearing capacity at the tip (Figure 2.16c), as in the case of individual stone columns. Also, stone column groups constructed in the soft ground may be damaged by bulging failure, as in single columns, or by exceeding the bearing capacity at the tip (Figure 2.16c and Figure 2.16d).

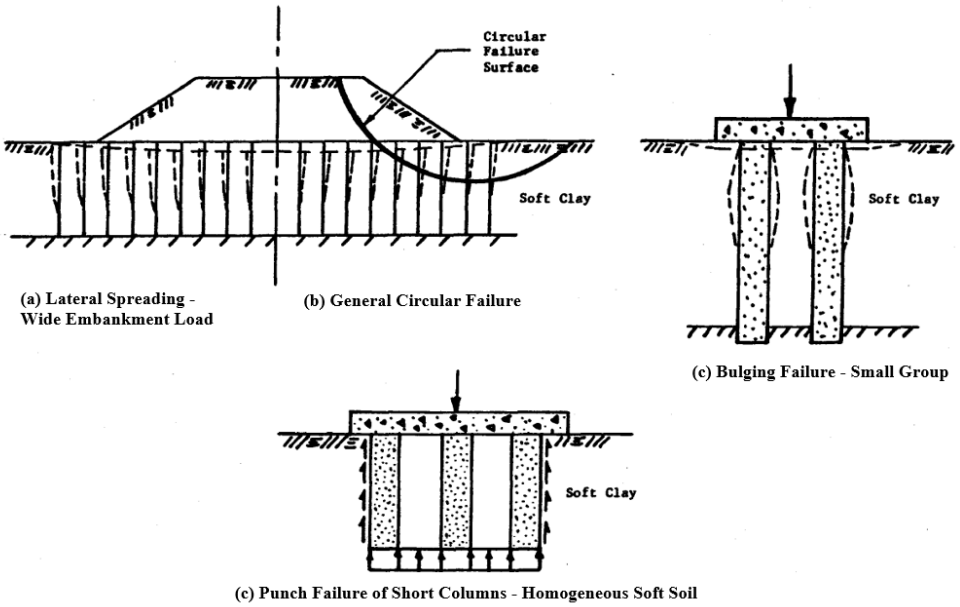

Figure 2.16 Stone column group failure mechanism (a) Lateral Spreading, (b) General Circular Failure, (c) Bulging Failure, (d) Punching Failure (Source: Barksdale & Bachus, 1983)

2.3.6. Dynamic Behavior of Stone Columns

Research on the dynamic behavior of stone columns needs to be sufficiently developed methods to study the behavior of stone columns in seismic zones. Various approaches have been recommended to analyze seismic liquefaction mitigation by stone columns, ranging from physical modeling with the simplified analysis method to complex numerical analyses.

The following research was done by Selçuk & Kayabalı, (2015); they developed software to monitor the change in the pore water pressure of liquefiable soils under

earthquake loading. This software assumes that the permeability of stone columns is infinite and that no excess pore water pressure occurs at the boundary (Seed & Booker, 1977). During the analyses, it was aimed to find the optimum stone column diameter and spacing by examining the undrained condition before the construction of the stone columns and the drained state after the construction of the stone columns. As a result of the analysis, it was founded that the excess pore water pressure ratio enlarged as the distance between the stone columns increased. However, it is concluded that the pore water pressure reaches its maximum value when the radius of action of the stone columns and the radial distance between them is equal.

The calculation of the excess pore water pressure in the soil under dynamic loads is essential to determine the soil liquefaction potential (Meshkinghalam et al., 2017). Stone columns increase the stiffness of the soil and dissipate the pore water pressure through drainage (Priebe, 1998). Therefore, stone columns have been used as a improvement method for potentially liquefiable soils (loose sand with a fines content of less than 35%) (Dhouib, 2004).

The study was done by Adalier et al. (2003), and four centrifuge tests (Figure 2.17) on silty soil were performed to simulate the dynamic response of the different conditions under the sinusoidal wave. Figure 2.17a and Figure 2.17b shows the section view and plan view of the geotechnical centrifuge model.

The first two tests are focused on the free field case (without surcharge), with (Model 2) or without (Model 1) stone columns. Model 3 and Model 4 have the same special as Model 1 and Model 2, respectively, except for having a foundation-loaded field with a surcharge. The soil response was analyzed under dynamic excitation conditions at the base, and settlement, acceleration, and pore pressure change were examined (Adalier et al., 2003).

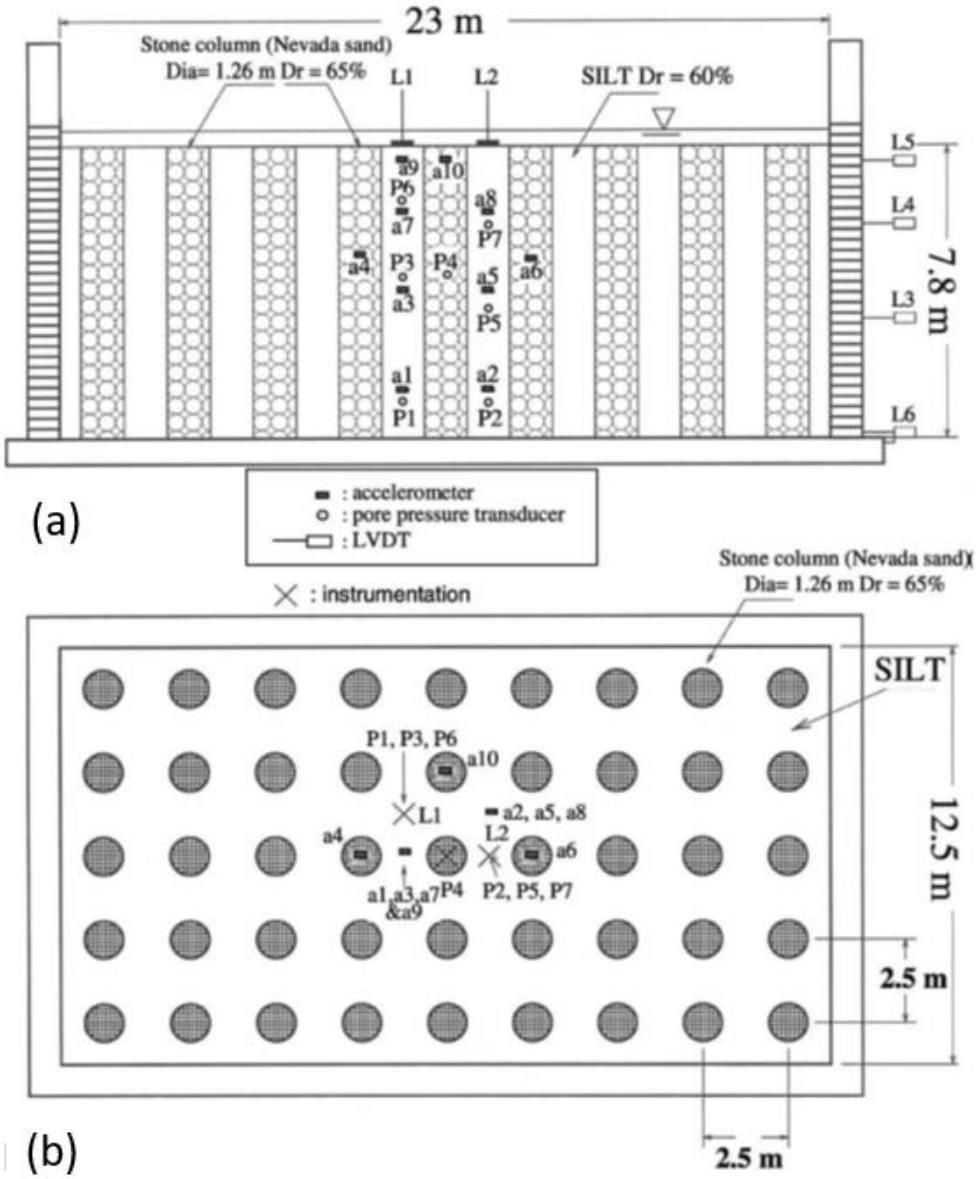

Figure 2.17 (a) Cross-sectional view and (b) Plan view of geotechnical centrifuge models tested to evaluate the liquefaction reduction efficiency of stone columns in non-plastic silty deposits (Source: Adalier et al., 2003)

Comparing the results of Model 1 and Model 2, although both models' pore water pressure increases, their dynamic behavior is markedly different. The decrease in accelerations (i.e., loss of strength) in Model 1 was significantly faster than in Model 2. The silt layer showed a significant strength reduction in Model 2 compared to Model 1, i.e., it took approximately two to three times more shaking cycles for the soil to liquefy. Therefore, although the stone columns did not prevent liquefaction (Model 2), the composite soil (with stone columns) had a significantly higher liquefaction resistance than the uniform silt soil.

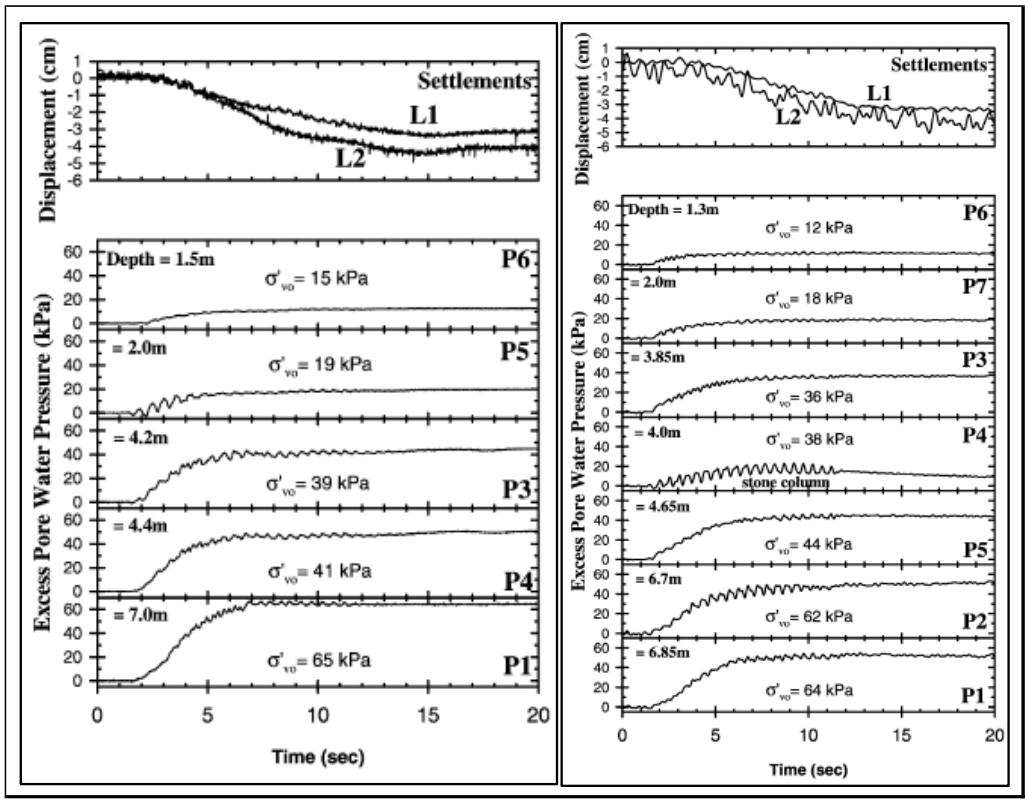

Figure 2.18 Pore water distribution and settlement results for Model 1 (left side) and Model 2 (right side) (Source: Adalier et al., 2003)

In two other works by Adalier et al. (2003), Model 3 and Model 4, the foundation settlement developed more or less linearly with time, the settlements being much less in the case of stone columns (Model 4). Although the pore water pressure appears to be very low due to the improvement provided by the stone columns, the stone column elements prevented excessive settlements by providing higher overall foundation shear strength and bearing capacity. However, the composite structure also allowed for more effective transmission (and even amplification) of foundation accelerations propagating to the foundation superstructure.

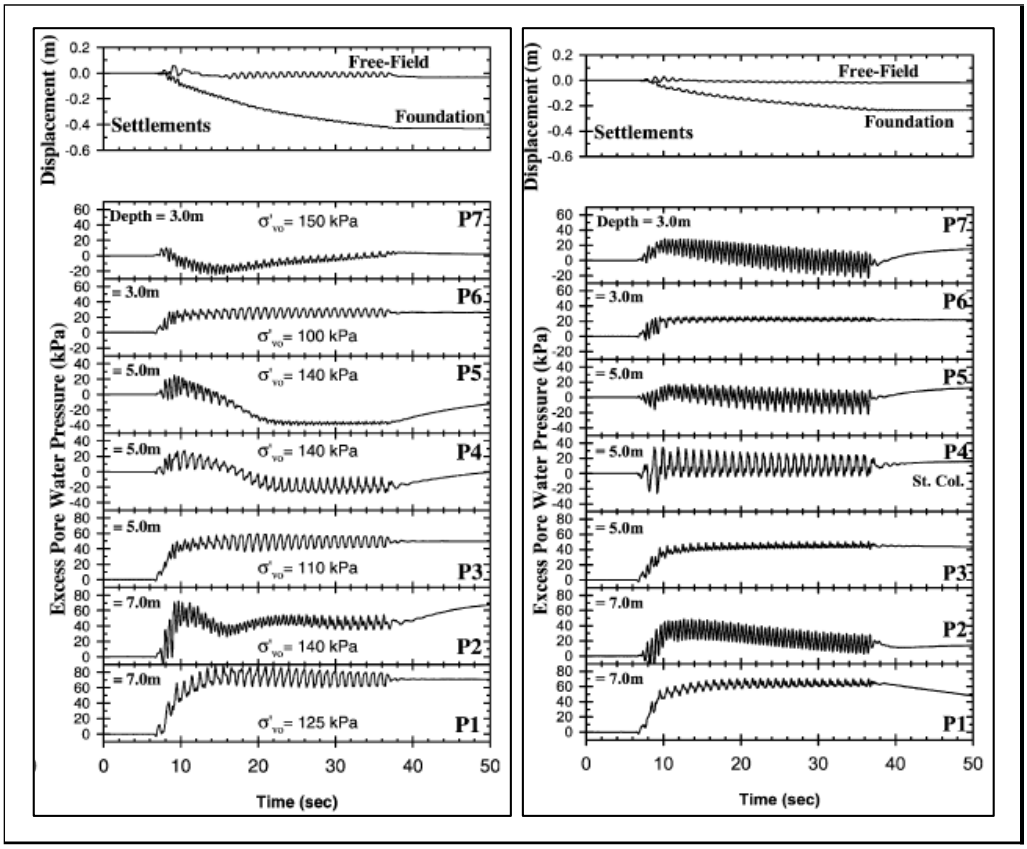

Figure 2.19 Pore water distribution and settlement results for Model 3 (left side) and Model 4 (right) (Source: Adalier et al., 2003)

Another study was done by Tang et al. (2016) shows a unit cell with periodic boundary conditions; for symmetrical considerations, a half-mesh configuration was used to simulate the test. The plan and section view of the configuration is given in the Figure 2.20 below.

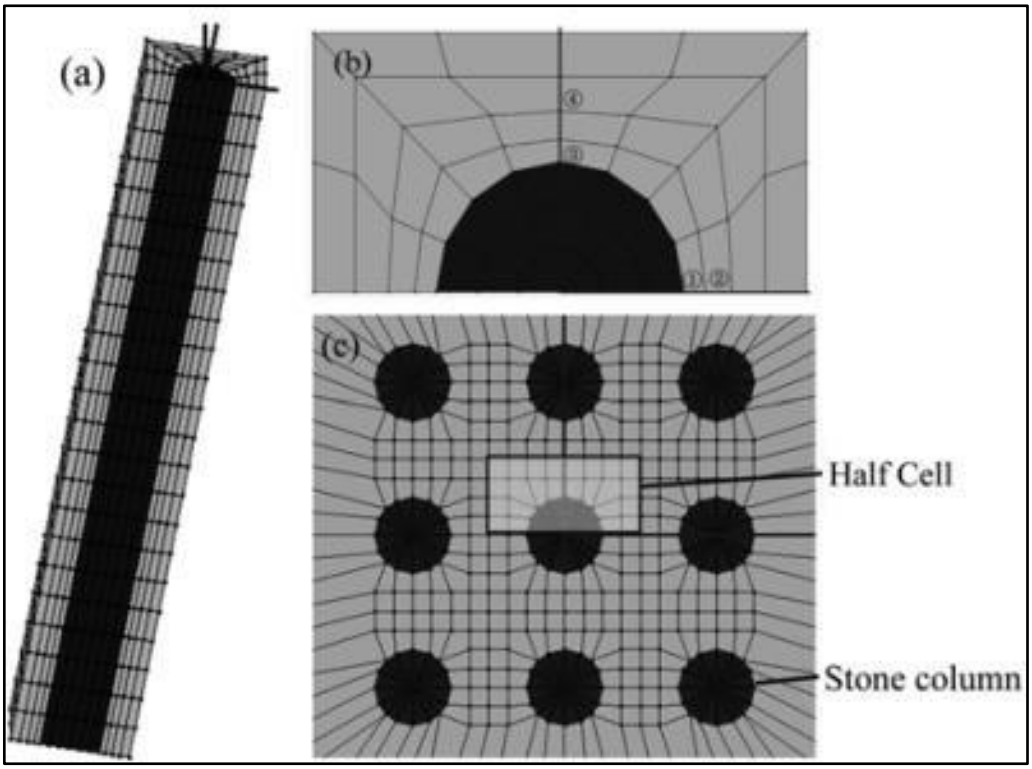

Figure 2.20 Finite element model with stone columns (a) unit cell, (b) plan view, (c) stone columns arrangement (Source: Tang et al., 2016)

The results of the analyses by Tang et al., 2016 agreed reasonably well with the experimental measurements (Figure 2.21). In general, it was observed that the soil improved, and liquefaction was prevented for the silty layer enhanced with stone columns compared to the unimproved layer. However, the upper half silt layer could not prevent complete liquefaction. After the agreement with the experimental results, the analyses were continued by changing the permeability of the stone columns. High permeability stone columns were able to significantly retard the formation of pore water pressure along the silty layer and significantly reduce the effective stress reduction of the soil. Similarly, low permeability stone columns could not effectively prevent the increase of pore water pressure, especially in the silty sand close to the ground surface, and thus did not reduce the liquefaction probability (Figure 2.21).

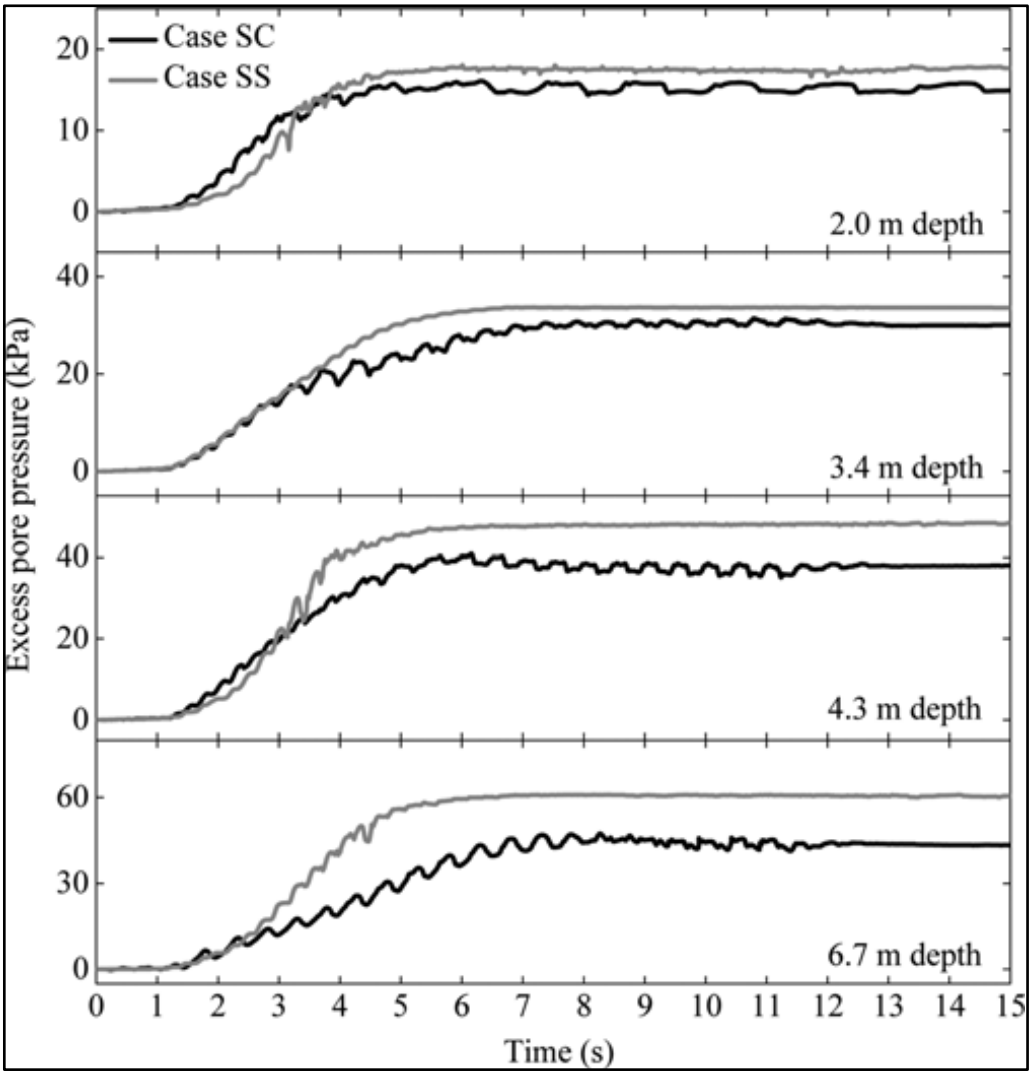

Figure 2.21 Excess Pore Pressure Time Histories of the Silty Sand for Cases SC(with stone column) and SS (without stone column) (the initial effective vertical stresses at depths of 2.0, 3.4, 4.3, and 6.7 m are 14.0, 23.8, 30.1 and 46.9 kPa, respectively) (Source: Tang et al., 2016)

Another numerical model using stone columns to mitigate earthquake-induced liquefaction in cohesionless soils was developed by Esmaeili and Hakimpour, (2015) using FLAC 3D software. In this model, liquefaction analysis was performed using Finn Soil Model. The model was first validated with the results of Model No. (1) of the VELACS project (Adalier et al., 2003). Then, the effects of several parameters such as the diameter of the stone columns, the distance between the columns, the performance of the stone columns at different depths of the soil, the effective radius and the sufficient depth were investigated.

The first case was modeled as an individual stone column. In the analyses, the diameter of the column was changed and the effect of this change on the reduction of the excess pore water pressure was investigated. Figure 2.22 shows the excess pore pressure for a depth of 1.25 m in different distances, 1.0m (Figure 2.22a), 1.5 m (Figure 2.22b), 2.0 m (Figure 2.22c), and 2.5 m (Figure 2.22d), from the column centered. Figure 2.23 shows the excess pore water pressure at 1.0, 2.0, 2.5 and 3.0 m distance from the center of stone columns of different diameters for a depth of 2.5 m. The analyses result for individual column show that the single column with diameters 0.90, 1.20, and 1.50 m can prevent liquefaction (Esmaeli & Hakimpour, 2015). The stone column increases the excess pore pressure reduction with increasing depth (Figure 2.22 and Figure 2.23). On the other hand, the area of influence of the single stone column is 3 and 4 times larger than the diameter of the individual column in the 1.25 m and 2.5 m depths, respectively.

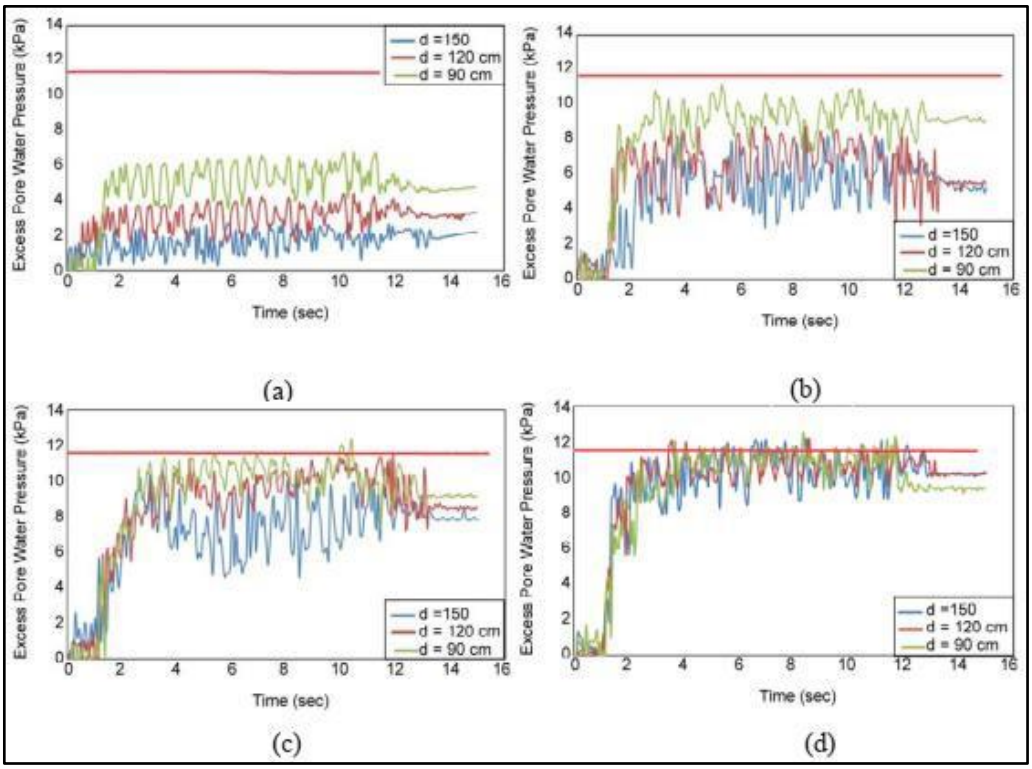

Figure 2.22 The pore pressure of 1.25 m in depth and from the center of columns (a) 1.0 m distance, (b) 1.5 m distance, (c) 2.0 m distance, (d) 2.5 m distance (Source: Esmaeili & Hakimpour, 2015)

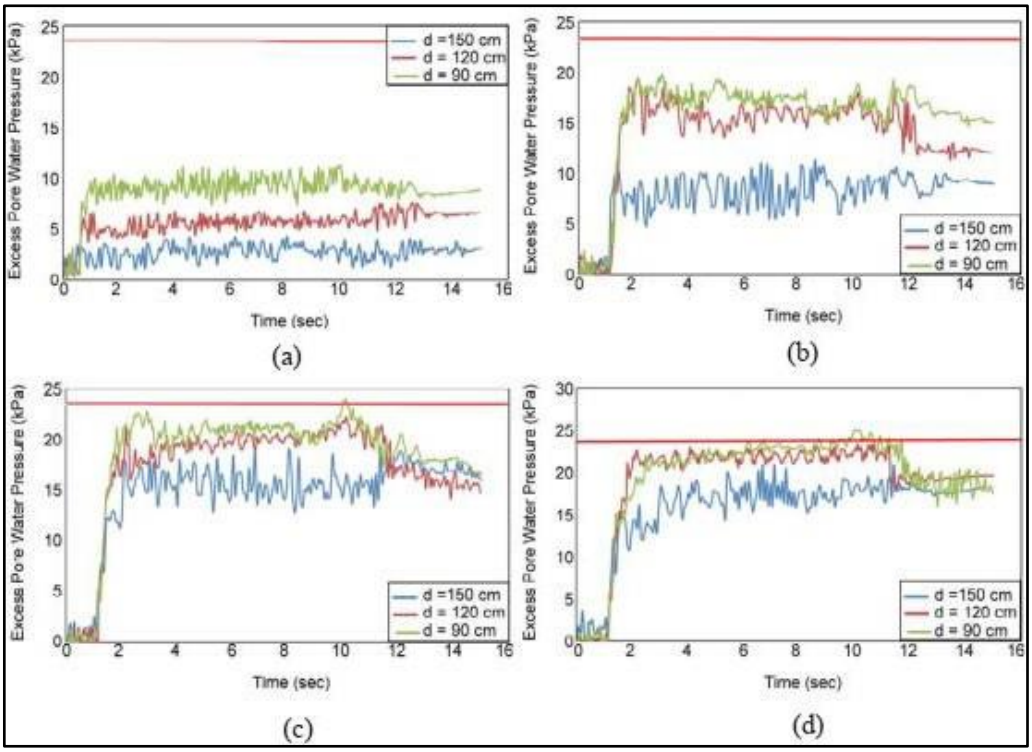

Figure 2.23 The pore pressure of 2.5 m in depth and from the center of columns (a) 1.0 m distance, (b) 1.5 m distance, (c) 2.0 m distance, (d) 2.5 m distance, (e) 3.0 m distance (Source: Esmaeili & Hakimpour, 2015)

Esmaeli & Hakimpour (2015) modeled a group of stone columns spaced 4.5 meters from center to center as the second case (Figure 2.28). It is investigated by changing the stone columns' diameters and the effect of the s/d ratio on the excess pore water pressure (Figure 2.25).

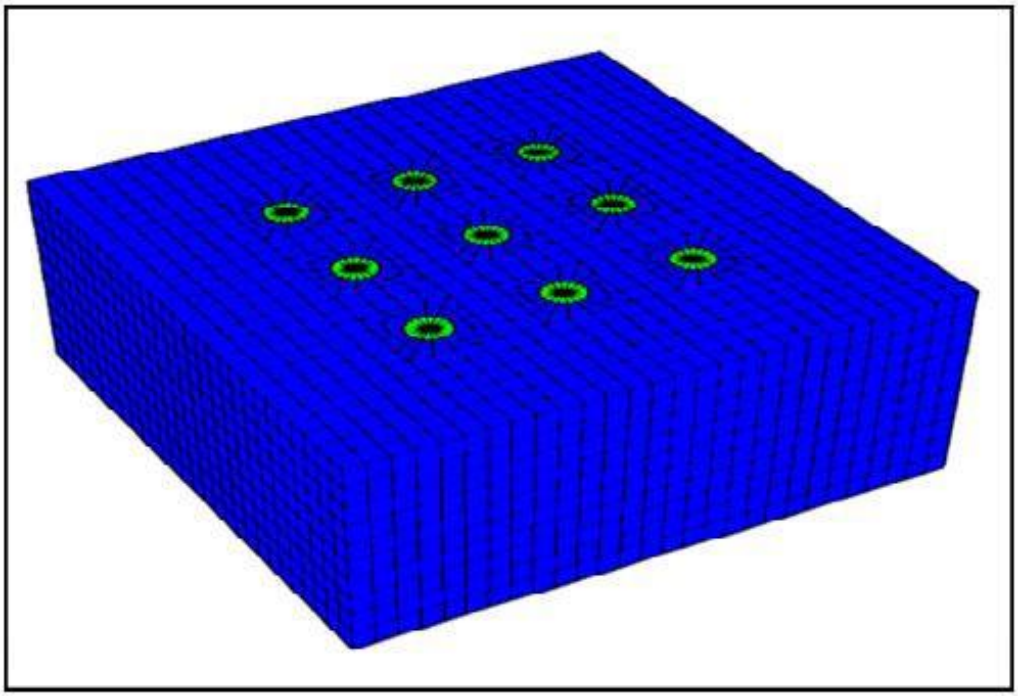

Figure 2.24 The finished difference mesh for the group of stone columns with a diameter of 150 cm and a center-to-center spacing of 4.5 m (Source: Esmaeili & Hakimpour, 2015)

According to the analysis results of the stone columns designed as a group, stone columns with diameters of 0.90 (Figure 2.25c), 1.20 (Figure 2.25a), and 1.50 m (Figure 2.25b) reduced the excess pore water pressure and consequently the liquefaction potential. When the spacing/diameter ratio was 2 and 3, the side columns contributed to reducing the pore excess pore water pressure and drainage of the central column. In the case of spacing/diameter ratios (s/d) of 4 and 5, they did not show group behavior, so there was no significant reduction in the excess pore water pressure and liquefaction potential. As a result, when all the studies are evaluated together, stone columns designed as the group were more effective than single stone columns in increasing drainage and reducing the mitigation liquefaction (Esmaeili & Hakimpour, 2015).

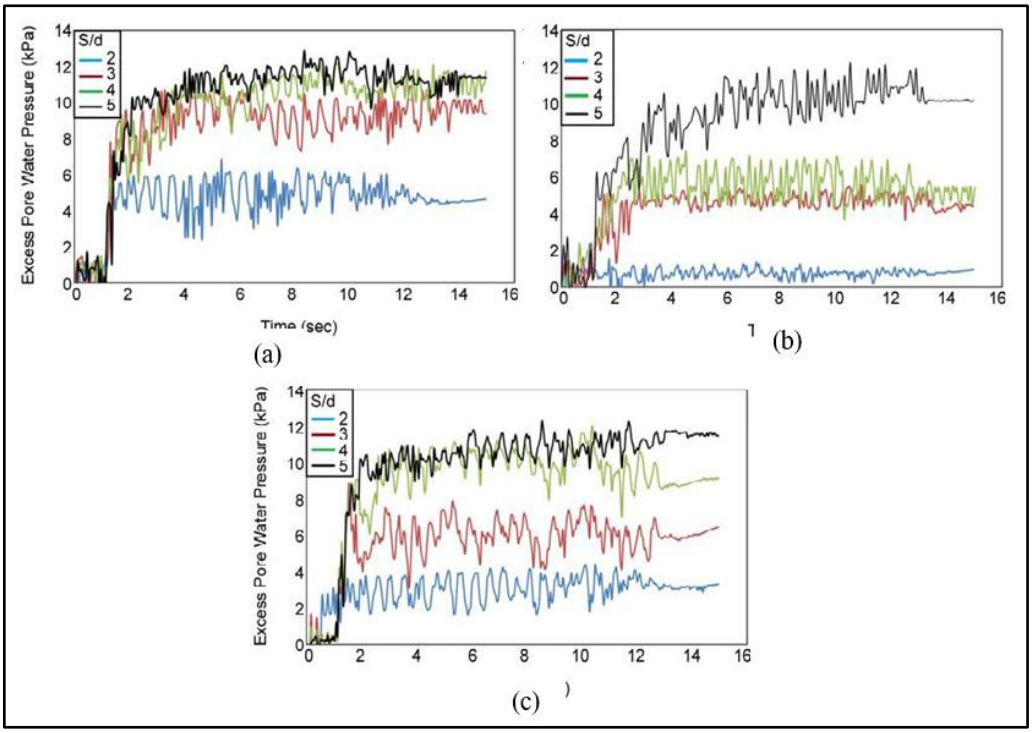

Figure 2.25 The excess pore pressure for a group of stone columns of s / d = 2 to 5. (a) 1.2 m diameter, (b) 1.5 m diameter, (c) 0.9 m diameter at 1.25m depth (Source: Esmaeili & Hakimpour, 2015)

Another study using FLAC 3D investigated the effect of the stone column on liquefaction potential and soil settlement by varying the individual stone column diameter and group column diameters and spacing (Meshkinghalam et al., 2017). The study was verified by the results of the VELACS international project, Model 1 by Adalier et al. (2003) as seen in Figure 2.26. At depths of 1.0 m (Figure 2.26a), 1.5 m (Figure 2.26b), and 2.5 m (Figure 2.26c), the excess pore water pressure values obtained from the experiments and the numerical model are consistent. At 1.5 m and 2.5 m depths, the excess pore water pressure ratio is above 1.0. At 7.5 m depth (Figure 2.26d), experiments and numerical model results are incompatible.

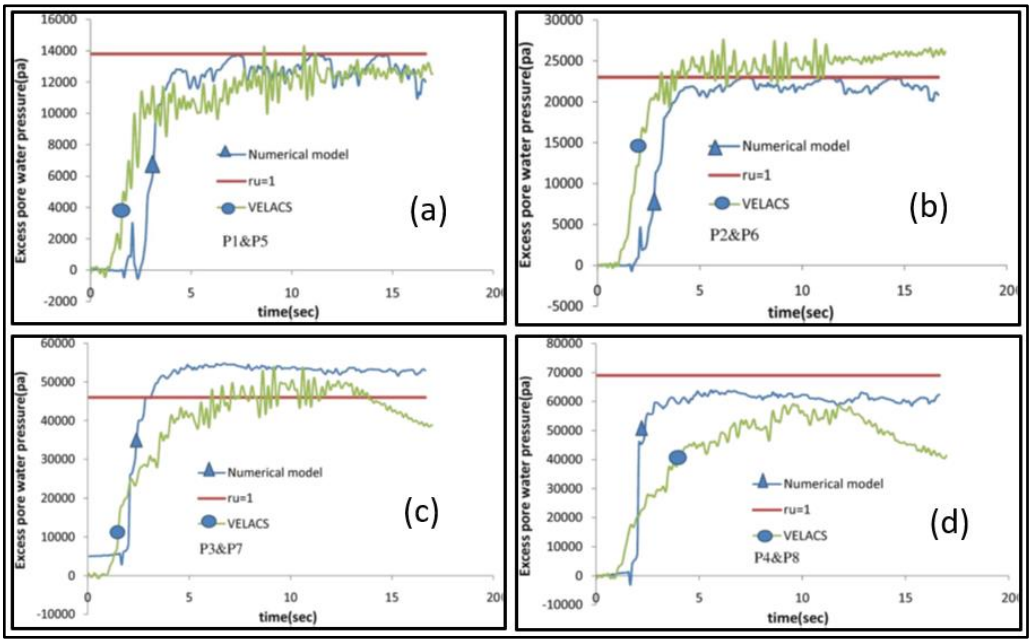

Figure 2.26 The excess pore pressure change comparison with VELACS project Model 1; with the depth (a)1.5m, (b)2.5m, (c) 5.0m, and (d) 7.5m (Source: Meshkinghalam et al., 2017)

Excess pore water pressures in the case without stone columns were reduced by the drainage effect of the stone column with different spacing(s)/diameter(d) ratio values at a depth of 1.0m, 1.5m, 2.5m and 5.0 (Figure 2.27a,b,c,d). The drainage characteristic of the stone column is shown in Figure 2.28 below as flow vectors.

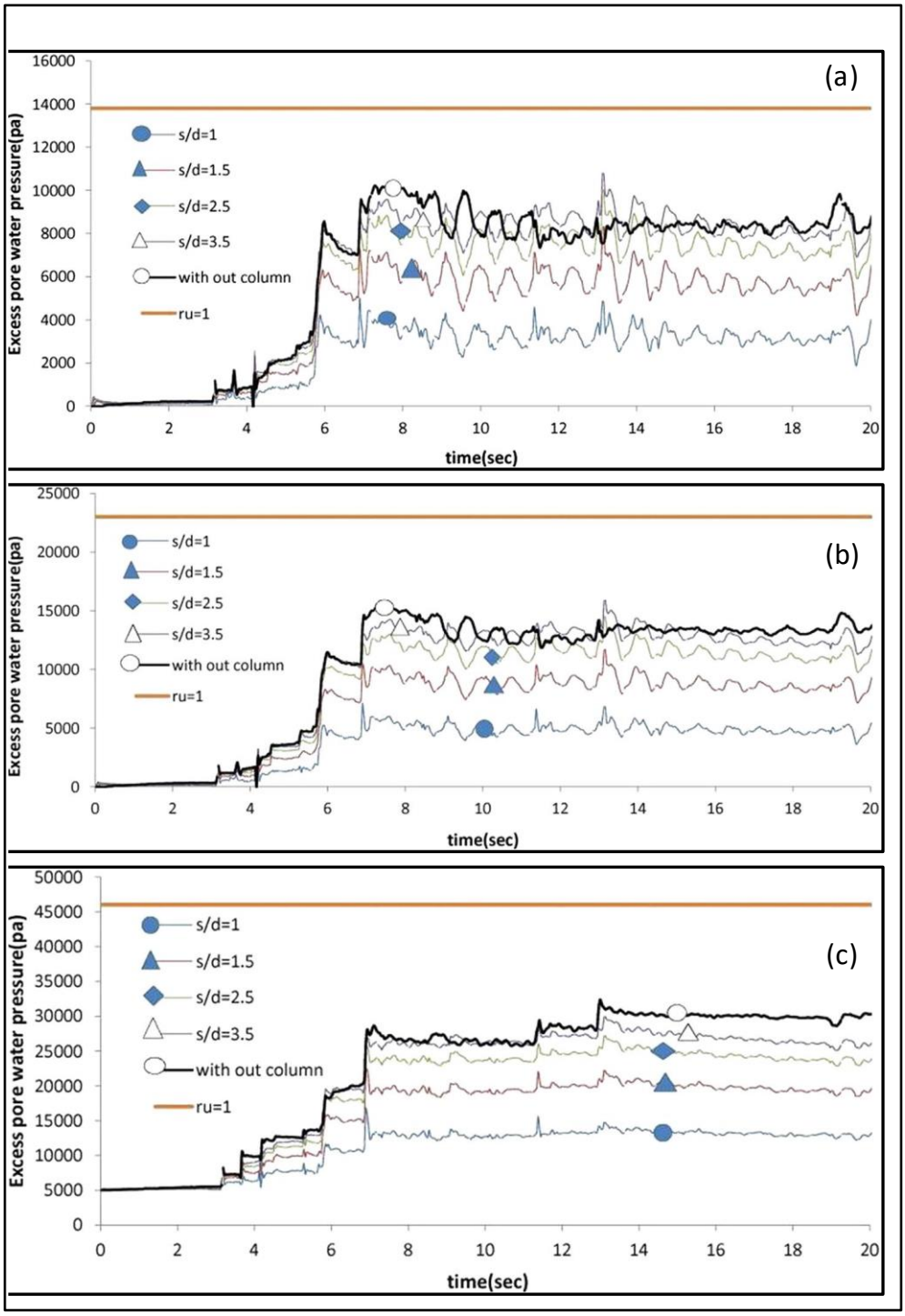

Figure 2.27 The excess pore pressure change s/d ratio with individual column diameter 1.0 m at a depth of (a) 1.5m, (b) 2.5m, and (c) 5.0m (Source: Meshkinghalam et al., 2017)

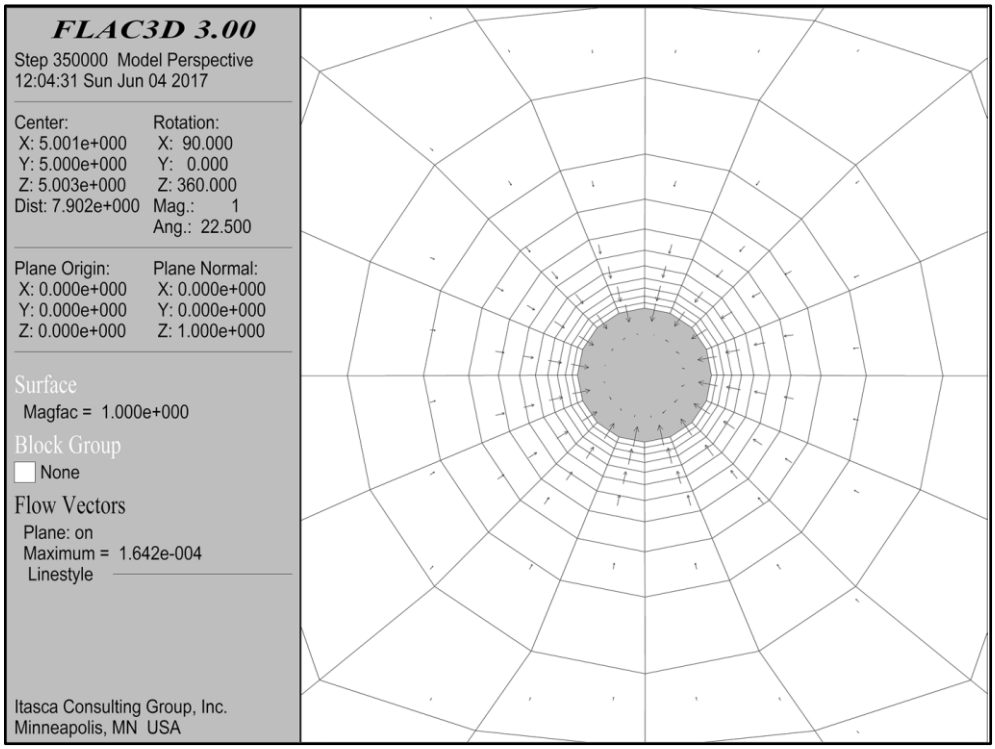

Figure 2.28 The flow vectors with radial drainage (Source: Meshkinghalam et al. 2017)

The final model was prepared by Meshkinghalam et al., (2017) for the three columns with a triangular arrangement (Figure 2.29) to control the drainage behavior of stone columns and the effect of settlement with different diameters as 0.6 m, 1.0 m, 1.2 m as shown in (Figure 2.30a,b,c) and (Figure 2.31a,b,c).

The study by Meshkinghalam et al., (2017) showed that stone columns cause drainage up to about 2.5 meters from the center of the columns, while drainage disappears at greater distances. However, it was determined that the increase in the diameter of the columns caused an increase in drainage at a distance of approximately 1.0-1.5 meters. In contrast, the increase in column diameter caused a decrease in drainage at greater distances. Another conclusion is that decreasing the distance between the stone columns causes the soil to heave. It was suggested that the column diameter should equal 2.5 to 3.5 times the diameter to prevent soil.

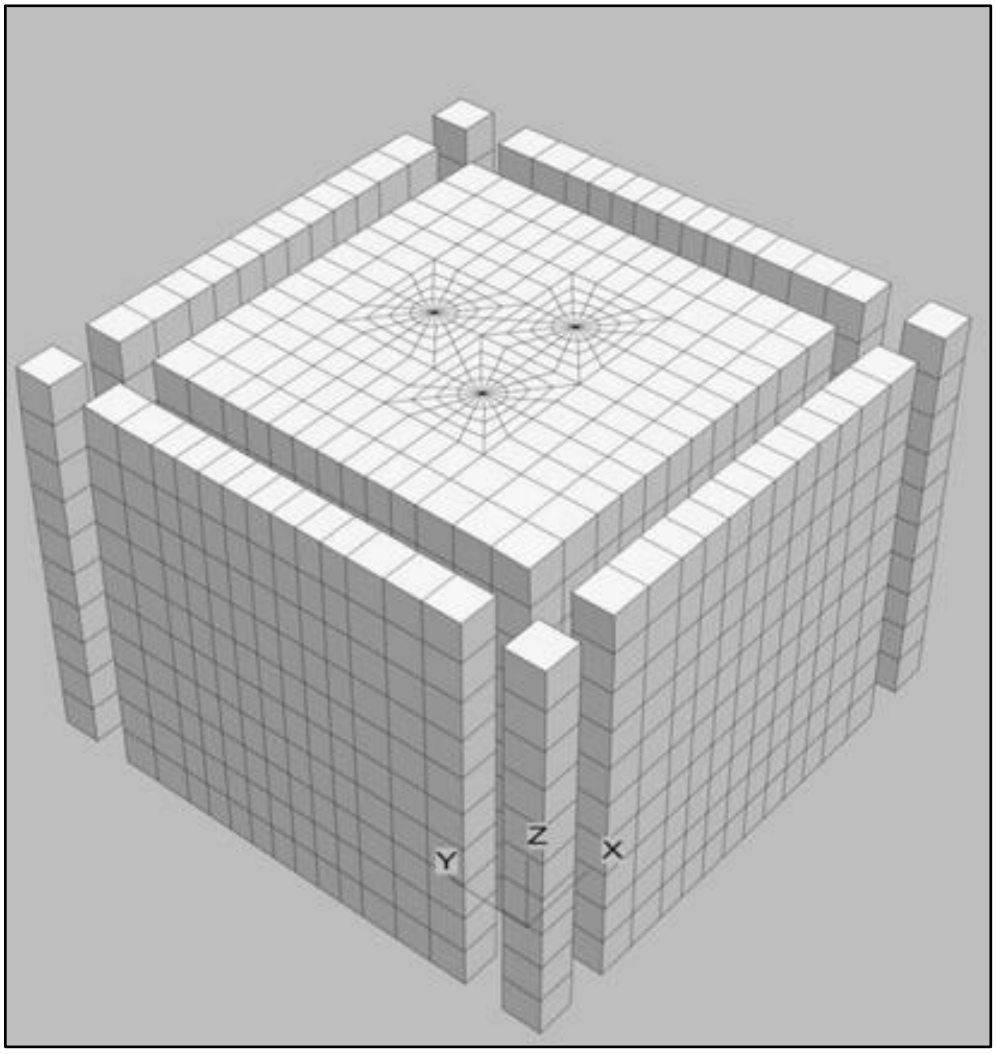

Figure 2.29 Finite difference mesh for the column group (Source: Meshkinghalam et al., 2017)

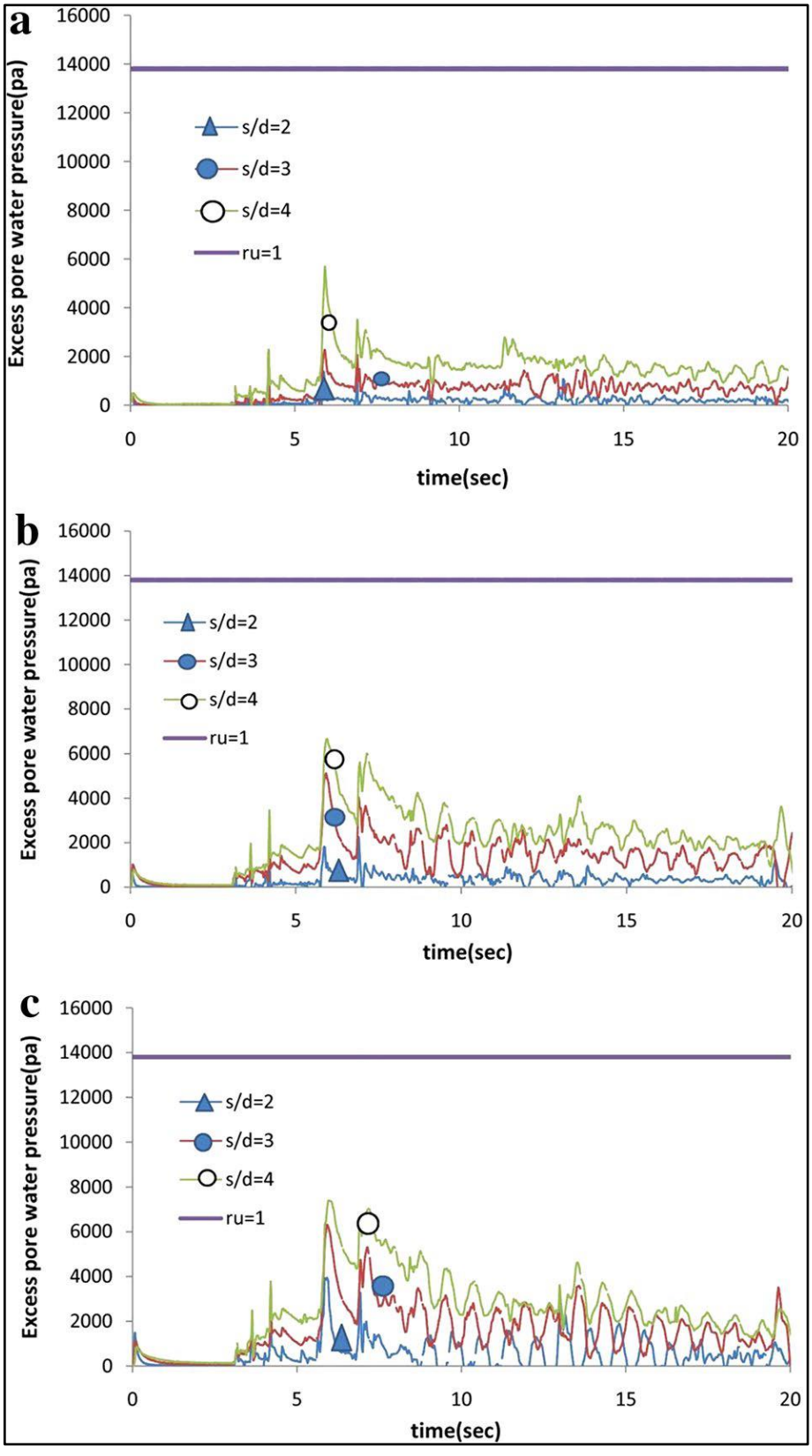

Figure 2.30 Variation of excess pore water pressure for stone columns that have s/d ratios = 2, 3, 4 with (a)d=0.6 m, (b) d= 1.0 m, (c) d= 1.2 m (Source:Meshkinghalam et al., 2017)

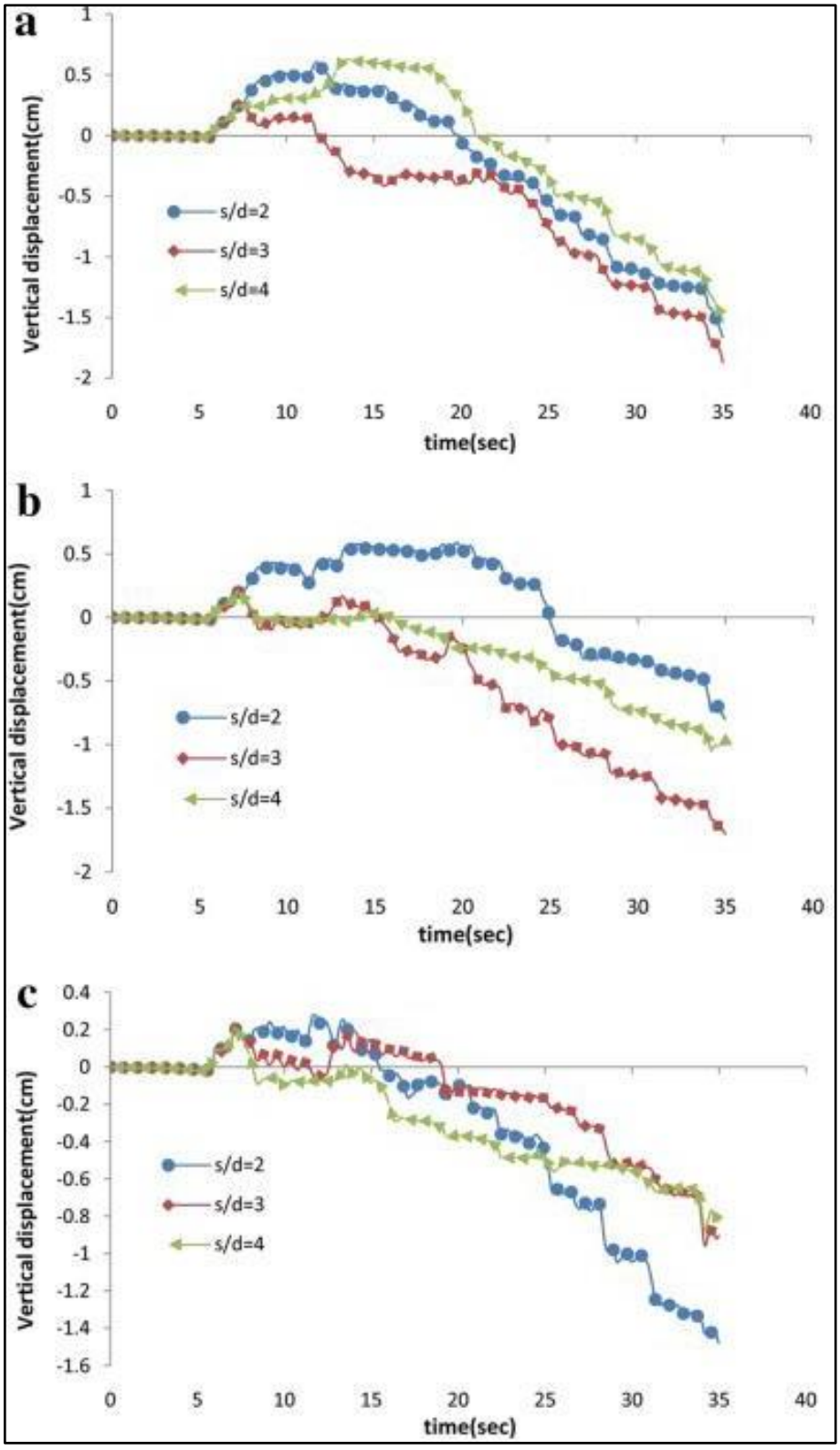

Figure 2.31 Changes in soil surface settlement for the group of columns with different s/d values. (a) diameter 0.6 m, (b) diameter 1.0 m, (c) diameter 1.2 m (Source:Meshkinghalam et al., 2017)

To investigate the behavior of partially saturated sands under cyclic loads, dynamic shear stresses were applied to two different relative density values of sand under repeated forces in a cyclic simple shear test (CSST). Based on the results of the research, the relative density significantly affects the seismic behavior of sands, when the relative density increase, resistance to liquefaction is increased (Beyaz et al., 2021)

Table 2.4 Some data obtained from the CSST liquefaction test of sand with a relative density (D_r) 40% and 70% (Source: Beyaz et al., 2021)

Relative Density (D_r)	Deformation Ratio	Vertical Stress	Pore Water Pressure	Cycle For Liquefaction	Maximum Excess Pore Water Pressure
(%)	γ – (%)	σ'_v – (kPa)	u-(kPa)		u_{max}-(kPa)
40	2.0	50.0	25.0	1	65.2
		100.0	50.0	1	101.4
		200.0	100.0	1	203.2
	3.5	300.0	150.0	2	300.0
		50.0	25.0	1	48.3
		100.0	50.0	1	101.1
		200.0	100.0	2	200.9
		300.0	150.0	3	302.5
	5.0	50.0	25.0	1	46.7
		100.0	50.0	3	99.9
		200.0	100.0	5	198.6
		300.0	150.0	7	294.7
70	2.0	50.0	25.0	1	23.9
		100.0	50.0	9	105.2
		200.0	100.0	11	203.4
	3.5	300.0	150.0	13	305.1
		50.0	25.0	1	55.1
		100.0	50.0	9	105.7
		200.0	100.0	12	212.8
		300.0	150.0	15	308.1
	5.0	50.0	25.0	1	51.0
		100.0	50.0	9	102.1
		200.0	100.0	15	212.8
		300.0	150.0	18	311.6

The relationship between pore water pressure and relative density in evaluating the potential for liquefaction under cyclic loads using shake table tests is investigated by Ecemiş, (2013). During the tests, piezocone penetration tests were conducted to measure

the excess pore water pressures. The test setup is illustrated in Figure 2.32a-b presented in the study.

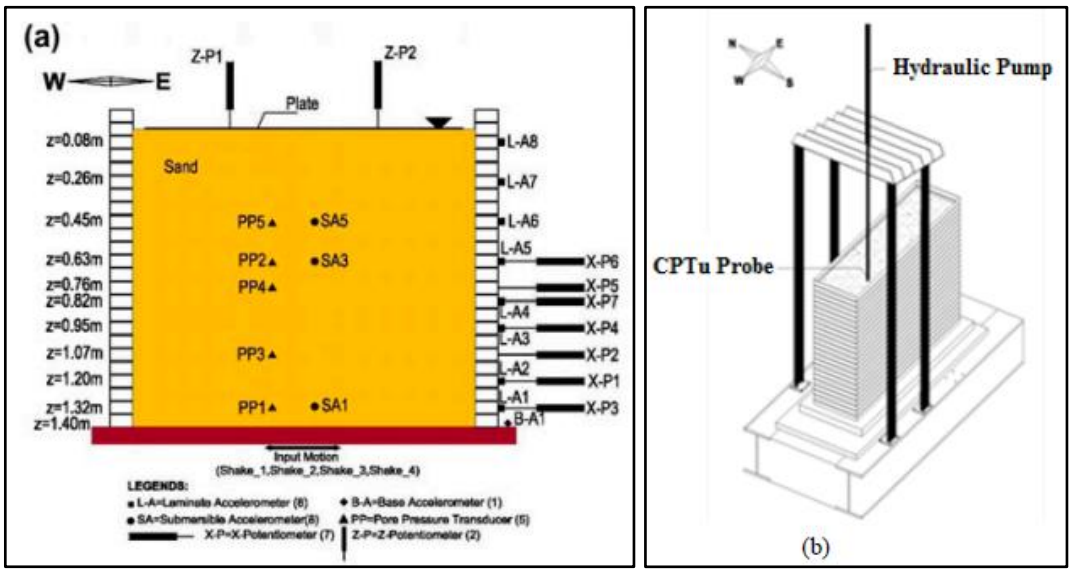

Figure 2.32 Schematic view of the (a) Shake Table Model (b) Cone Penetration System; (Source: Ecemiş, 2013)

The cone tip resistance measured from the piezocone penetration tests was corrected empirically to calculate the relative density. Then the relationship between pore water pressure and relative density by numerical analysis with the UBSSAND model. Cyclic loads with different acceleration values were applied to four different experimental setups within the scope of the shake table tests, and the changes in relative density (due to tip resistance) and excess pore water pressure values were recorded. Then, these relative density values determined during the test were used as soil parameters in numerical analyses. According to the analysis results, it was observed that the excess pore water pressure decreased as the relative density value increased (Figure 2.33).

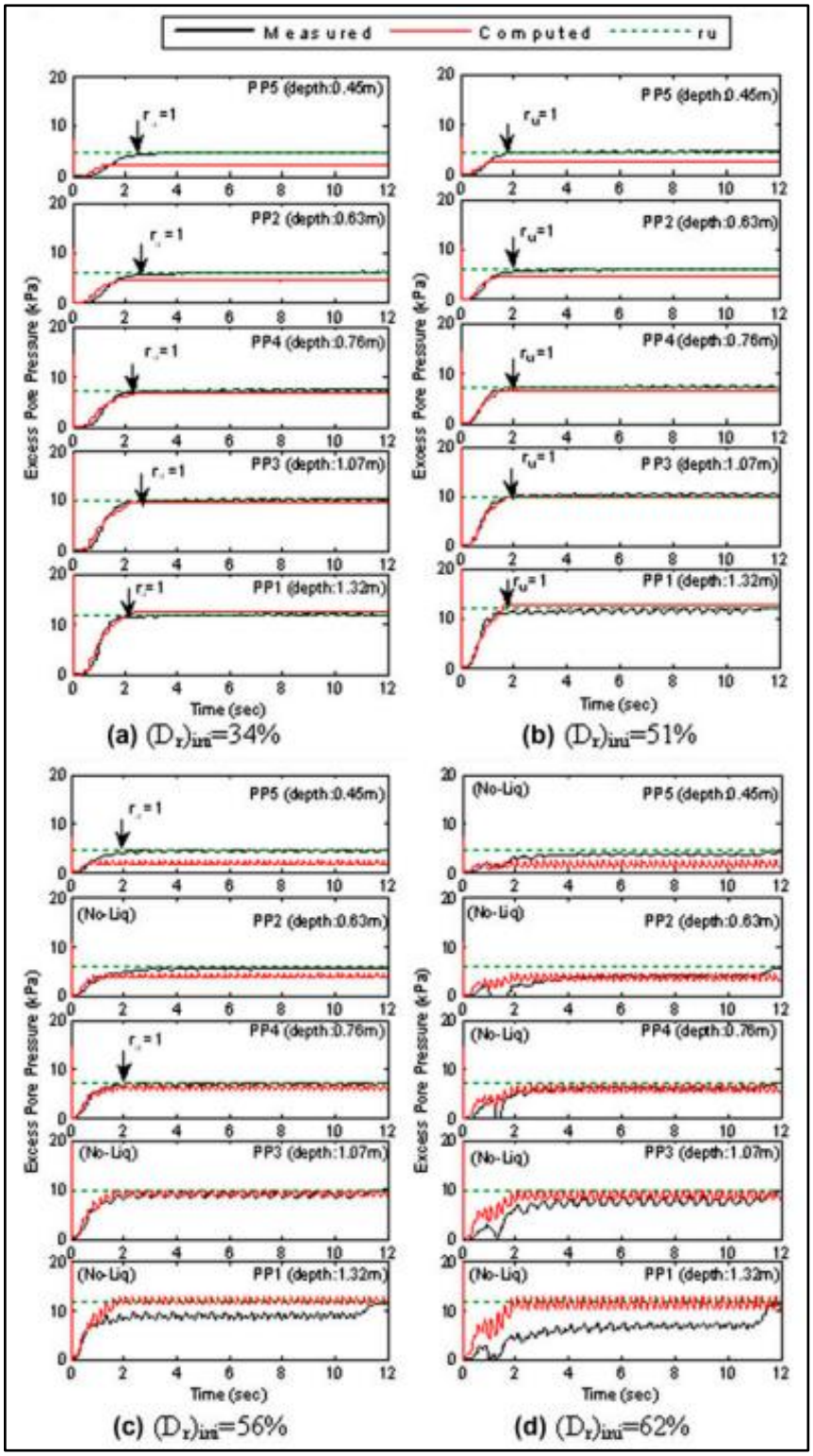

Figure 2.33 Measured and computed with numerical analysis excess pore pressure time histories during (a) first shake; (b) second shake; (c) third shake; and (d) fourth shake (Source: Ecemiş, 2013)

The study to investigate the relationship between relative density and pore water pressure was presented by Syed et al., (2009). The effect of increasing the relative density on the excess pore water pressure ratio is presented in Table 2.5 below. The results of the studies, similar to Ecemiş, (2016), show that as the relative density of the soil is increased, excess pore water generation decreases and thus, the liquefaction potential decreases.

Table 2.5 Relation of Excess Pore Pressure Ratio (r_u) and Relative Density (D_r) (Source: Ecemiş, 2016)

Depth	D_r=40%	D_r=58%	D_r=79%
1.5	1.00	0.9	0.64
2.5	1.00	0.75	0.55
3.5	1.00	0.63	0.5
4.5	0.95	0.56	0.47

2.4. Conclusion

This chapter summarizes the literature study on the dynamic behavior of stone columns and the reduction of liquefaction by stone columns using by analytical, experimental, and numerical simulations. Soil improvement with stone columns, especially in the case of sand and silt sand, has a significant advantage in seismic zones. The analysis of liquefaction potential reduction by stone columns has undergone considerable development.

In general, the drainage effect of the stone columns allows for the reduction of the liquefaction potential; this reduction is made for a limited depth and zone of influence; at the depth level, this dissipation by stone columns becomes secondary and negligible under the effect of the overload.

Numerical methods are effective for modeling soils improved with stone columns to understand the effects of excess pore water pressure on liquefaction mitigation by dissipation of excess pore water pressure into the stone columns.

Based on the different studies, stone column construction is suitable for sandy and silty soils to reduce liquefaction potential (Adalier et al.,2003; Syed et al., 2009; Esmaeili and Hakimpour, 2015; Tang et al., 2016 and Meshkinghalam et al., 2017). In particular, the stone columns constructed by the vibroflotation method increase the relative density of the surrounding soil (FHWA-RD-83-026, 1983). Increased relative density values enhance the resistance of the soil to liquefaction (Ecemiş, 2016 and Beyaz et al., 2021).

Various parameters, including stone column spacing, column and soil permeability, column diameter, and additional surcharge loading, the dissipation of excess pore water pressure and reduced liquefaction potential.

Stone columns designed as the group was more effective than single stone columns in increasing drainage and reducing mitigation the liquefaction. Applying structural loads as surcharge loading helped the stone columns decrease settlement.

CHAPTER 3

SITE STUDY / SOIL SURVEY

3.1. Site Properties

This chapter explains the project area, which is located within the borders of the Central District of Çanakkale Province. Çanakkale province is located in the Marmara Region, its location in Türkiye is shown in Figure 3.1 below.

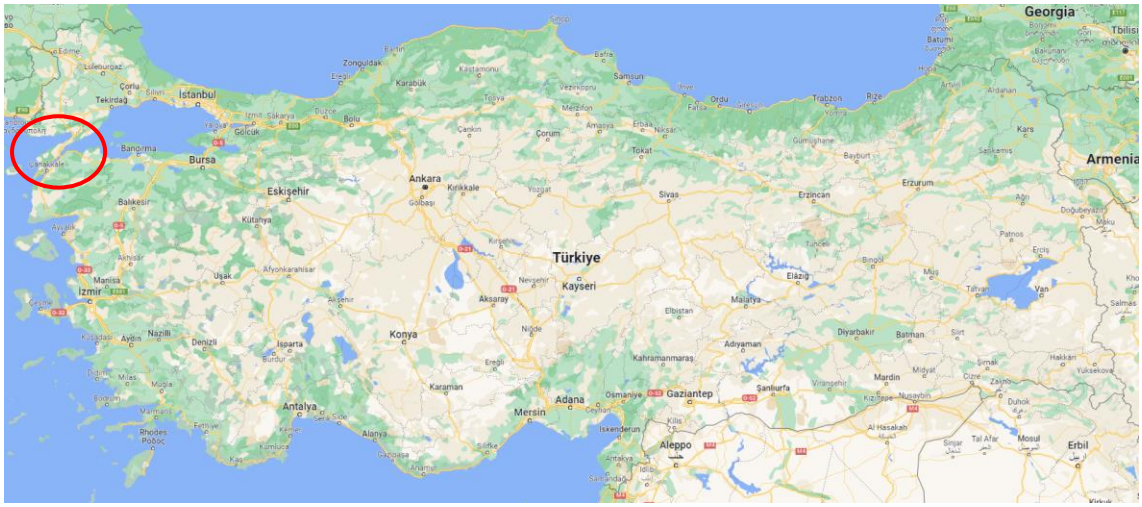

Figure 3.1 Çanakkale province location in Türkiye Map

The site is bordered by Barış Kordonu on the west and Atatürk Street on the east. The site has a rectangular area. The investigation area is shown in the Figure 3.2 below (Parsel Sorgu, 2023). The area elevations are generally between +0.90 m and +2.12 m. Due to the geological conditions of the study area, no significant topographic anomaly or mass movement (landslide, soil flow, rock fall, etc.) specific landforms were observed.

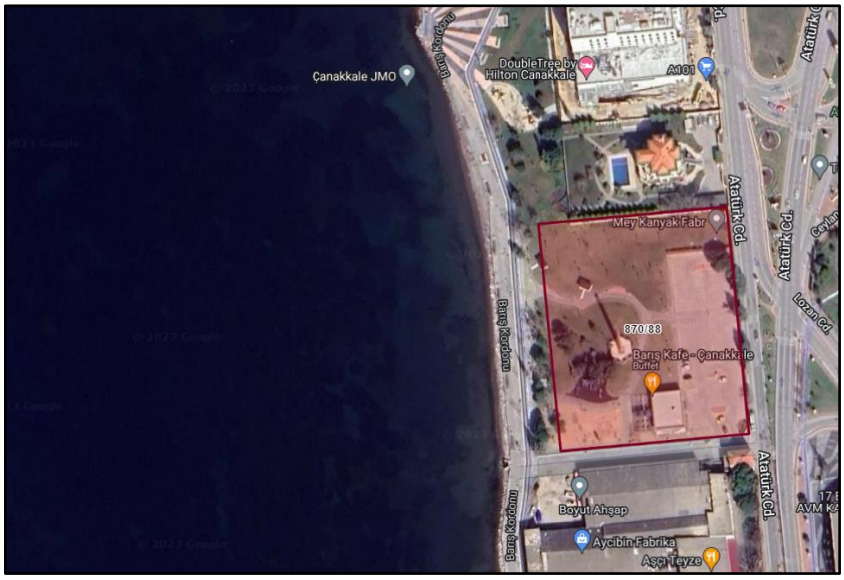

Figure 3.2 Plan view of investigation area (Source: https://parselsorgu.tkgm.gov.tr)

3.2. Geotechnical Evaluation of the Field

Field and laboratory tests were carried out to determine the behavior/strength parameters that will represent the geotechnical properties of the study area. The field tests: SPT and CPT were performed at the site, as shown in Figure 3.3. In this figure, BH represents borehole locations where SPT was performed, and the CPT abbreviation represents CPT locations.

Figure 3.3 CPT and SPT field test locations

Three boreholes with a depth of 20 m and four boreholes with a depth of 30 m were opened with a total depth of 180 m. Laboratory tests were conducted on disturbed and undisturbed soil samples collected from boreholes. Besides, 6 Standard Penetration Tests (SPT) and 7 Cone Penetration Tests (CPT) were performed in the investigation area.

3.3. Field Tests

3.3.1. Standard Penetration Test (SPT)

The Standard Penetration Test (SPT) is performed according to ASTM D1586 (2011) standard. Disturbed and undisturbed soil samples were taken by TS EN ISO 22475-1: Geotechnical investigation and testing - Sampling methods and groundwater measurements - Part 1: Technical principles for execution and other international standards. An automatic SPT hammer was used in the campaign. A split tube sampler is connected to the end of the SPT hammer, and the hammer is automatically dropped with a weight of 63.5kg to the ground.

$N_{1,60}$ value is calculated by using raw SPT-N data from the field (Turkish Building Earthquake Code, 2018).

Correction factors are defined below:

- Correction for groundwater level; If the test is performed below the groundwater table and if the soil type is fine sand or silty sand and SPT-N> 15, this factor is used (Terzaghi and Peck, 1948).
- The blow counts corrected for the fine grain content (IDI) are calculated by $N_{1,60f}$. According to TBDY 2018, fine-grained content corrections should be applied only in liquefaction analysis, which is not used in the table below.

$$N_{1,60f} = \alpha + \beta * N_{1,60} \quad (3.1)$$

α and β values corresponding to IDI percentages are given below table.

Table 3.1 α and β values corresponding to IDI percentages (Source: TDBY, 2018)

IDI percentage	α Values	β Values
IDI ≤ %5	α= 0	β= 1.0
%5 <IDI ≤ %35	A=exp (1.76-(190/IDI^2))	β= 0.99+IDI$^{1.5}$/1000
IDI ≥ %35	α= 5.0	β= 1.2

Depth correction factor (C_N); The effective vertical stress $\sigma_{vo'}$ (kN /m^2) at the depth where the Standard Penetration Test is performed is calculated. The factor is calculated by the formula (Liao and Whitman, 1986), (The C_N value should not exceed 1.7 by the Youd vd 2001);

$$C_N = 9.81 * (1/\sigma'_{vo}) * 0.5 \leq 1.70 \quad (3.2)$$

The energy correction factor (C_E), the rod length correction factor (C_R), the sample receiver type correction coefficient (C_S), and the drill hole diameter correction coefficient (C_B) are given in Table 3.2.

Table 3.2 SPT correction factors (Source: TDBY, 2018)

Correction Coefficient	Variation	Values
C_R	Between 3m and 4m	0.75
	Between 4m and 4m	0.85
	Between 6m and 10m	0.95
	Deeper than 10m	1.00
Cs	Standard Sample Receiver	1.00
	Sample receiver without an inner tube	1.10-1.30
C_B	Diameter between 65mm - 115mm	1.00
	Diameter 150 mm	1.05
	Diameter 200 mm	1.15
C_E	Safety Hammer	0.6 - 1.17
	Ringed Hammer	0.45 - 1.00
	Automatic pulsed Hammer	0.90 - 1.60

SPT-N correlations and uncorrected-corrected values for BH-1, BH-2, BH-3, BH-5, BH-6, and BH-7 are given in Table 3.3, respectively. Soil classifications are defined according to the laboratory test results.

Table 3.3 SPT-N values obtained from the SPT

Borehole	Depth (m)	SPT-N	N_{60}	$(N_1)_{60}$
BH-1	3.5	9	6	10
	5	16	12	19
	6.5	2	2	2
	8	14	12	15
	9.5	16	14	15
	11	16	14	15
	12.5	16	14	14
	14	23	21	19
	15.5	4	4	3
	17	4	4	3
	20	5	5	3
BH-2	3.5	2	1	2
	5	20	15	24
	6.5	18	15	21
	8	2	2	2
	9.5	24	21	23
	11	27	24	25
	14	15	14	12
	15.5	8	7	6
	18.5	19	17	14
	20	16	14	11
BH-3	3.5	34	23	39
	5	6	5	7
	6.5	20	17	23
	8	7	6	7
	9.5	2	2	2
	11	6	5	6
	12.5	2	2	2
	14	8	7	7
	15.5	2	2	2
	17	2	2	2
	18.5	9	8	7
	20	11	10	8
	24	43	39	27
	26	15	14	9
	28	4	4	2
	29	21	19	12
	30	48	43	27

(cont. on next page)

Table 3.3 (cont.)

Borehole	Depth (m)	SPT-N	N_{60}	$(N_1)_{60}$
BH-4	3.5	31	21	36
	5	16	12	19
	6.5	18	15	21
	8	2	2	2
	9.5	2	2	2
	11	2	2	2
	12.5	2	2	2
	14	18	16	15
	15.5	27	24	21
	17	3	3	2
	18.5	3	3	2
	20	13	12	9
	24	22	20	14
	26	14	13	9
	28	4	4	2
	29	22	20	13
	30	23	21	13
BH-5	3.5	5	3	6
	5	13	10	15
	6.5	2	2	2
	8	2	2	2
	9.5	3	3	3
	11	6	5	6
	12.5	2	2	2
	14	3	3	2
	15.5	15	14	12
	17	26	23	20
	18.5	3	3	2
	20	6	5	4
	24	16	14	10
	26	7	6	4
	28	31	28	18
	29	23	21	13
	30	22	20	12

(cont. on next page)

Table 3.3 (cont.)

Borehole	Depth (m)	SPT-N	N_{60}	$(N_1)_{60}$
BH-6	2	5	3	6
	3.5	7	5	8
	5	4	3	5
	6.5	2	2	2
	8	7	6	7
	9.5	21	18	20
	11	14	13	13
	12.5	6	5	5
	14	10	9	8
	15.5	8	7	6
	17	7	6	5
	18.5	11	10	8
	20	18	16	13
	24	20	18	13
	26	27	24	16
	28	15	14	9
	29	23	21	13
	30	20	18	11
BH-7	3.5	11	7	13
	5	13	10	15
	6.5	2	2	2
	8	4	3	4
	9.5	2	2	2
	11	2	2	2
	12.5	2	2	2
	14	2	2	2
	15.5	2	2	2
	17	15	14	11
	18.5	23	21	17

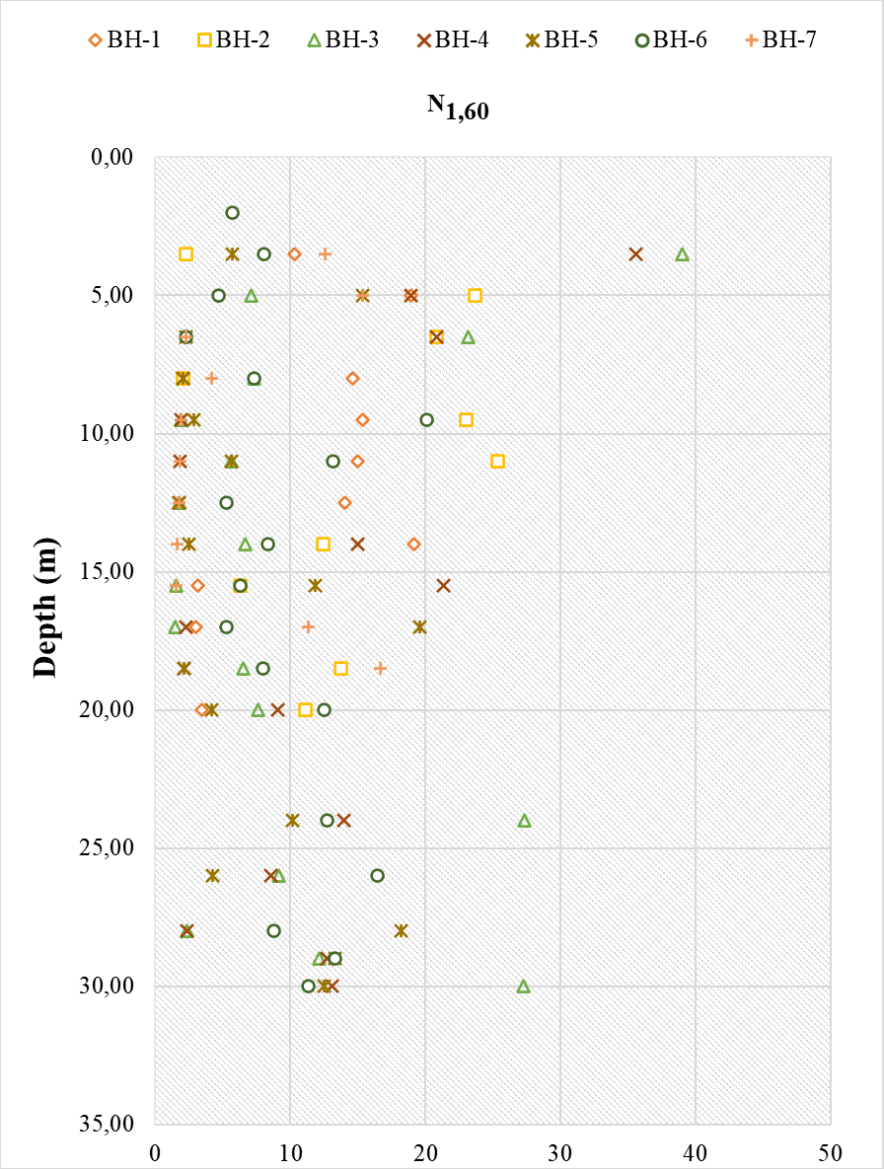

Figure 3.4 Variation of corrected SPT N ($(N_1)_{60}$) values with depth

3.3.2. Geophysical Studies

Within the scope of the geophysical surveys, a Multi-Channel Surface Analysis (MASW) study was carried out along three profiles to determine the shear wave velocity (V_s) from the bottom foundation elevation.

3.3.2.1. Multichannel Surface Analysis

MASW is a seismic method that provides shear wave velocity (V_S) information on near-surface materials. A sledgehammer was used as the source, and the location of

the exposures is shown in detail on the location map (Figure 3.4). The laying direction was chosen to reflect the study area best and to suit the surface conditions best. The geophone spacing was 3 m, and the offset distance was selected as 6 m. The total length of the grid was 42 m. Thus, the depth reached was ≈30 meters. The recording length was 1 s, and the sampling interval was 0.125 ms.

Geophysical measurements were taken at locations that best represent the area. Based on these measurements, stratigraphy, subsurface velocity structure, dynamic-elastic engineering parameters of soils, soil classes, soil dominant vibration periods, soil magnifications, and lateral and vertical discontinuities within the soil were determined according to the geophysical survey, and soil class defined (TBDY, 2018).

Figure 3.5 Geophysical surveys directions

Table 3.4 Soil class (TDBY, 2018)

Multichannel Analysis of Surface Waves	Depth (m)	Vs (m/s)	$(Vs)_{30}$ (m/s)	Soil Class
MASW-1	3.9	231	222	ZD
	8.8	195		
	-	228		
MASW-2	3.3	207	189	
	5.5	173		
	10.8	200		
	-	186		
MASW-3	7.2	144	212	
	10.7	209		
	-	258		

3.3.3. Cone Penetration Test (CPT)

In site investigations, six CPT tests were performed according to the "BS EN ISO 22476-12:2009- Geotechnical Investigation and Testing – Field Testing – Mechanical Cone Penetration Test (CPTM)" specifications. The CPT (Cone Penetration Test) includes a continuous measurement of the force required for a tip with a conical geometry to be pushed to the ground at a constant speed through hydraulic pressure by mounting a tip with a metal rod. CPT is a test to determine the cone tip resistance (q_c), lateral friction resistance (f_s), and pore pressure of the ground. It is aimed at determining the mechanical and physical properties of the soil. Figure 3.3 shows the CPT field test locations. A total of six CPTs were performed in the investigation area. Figure 3.6 and Figure 3.7 show the CPT's cone tip resistance and normalized cone tip resistance concerning depth. Since CPT-3 values give very high values compared to other CPTs, these values were not taken considered calculations as they would be misleading in the analysis. The parameters obtained aim to classify the layers in the field and determine their physical and mechanical properties.

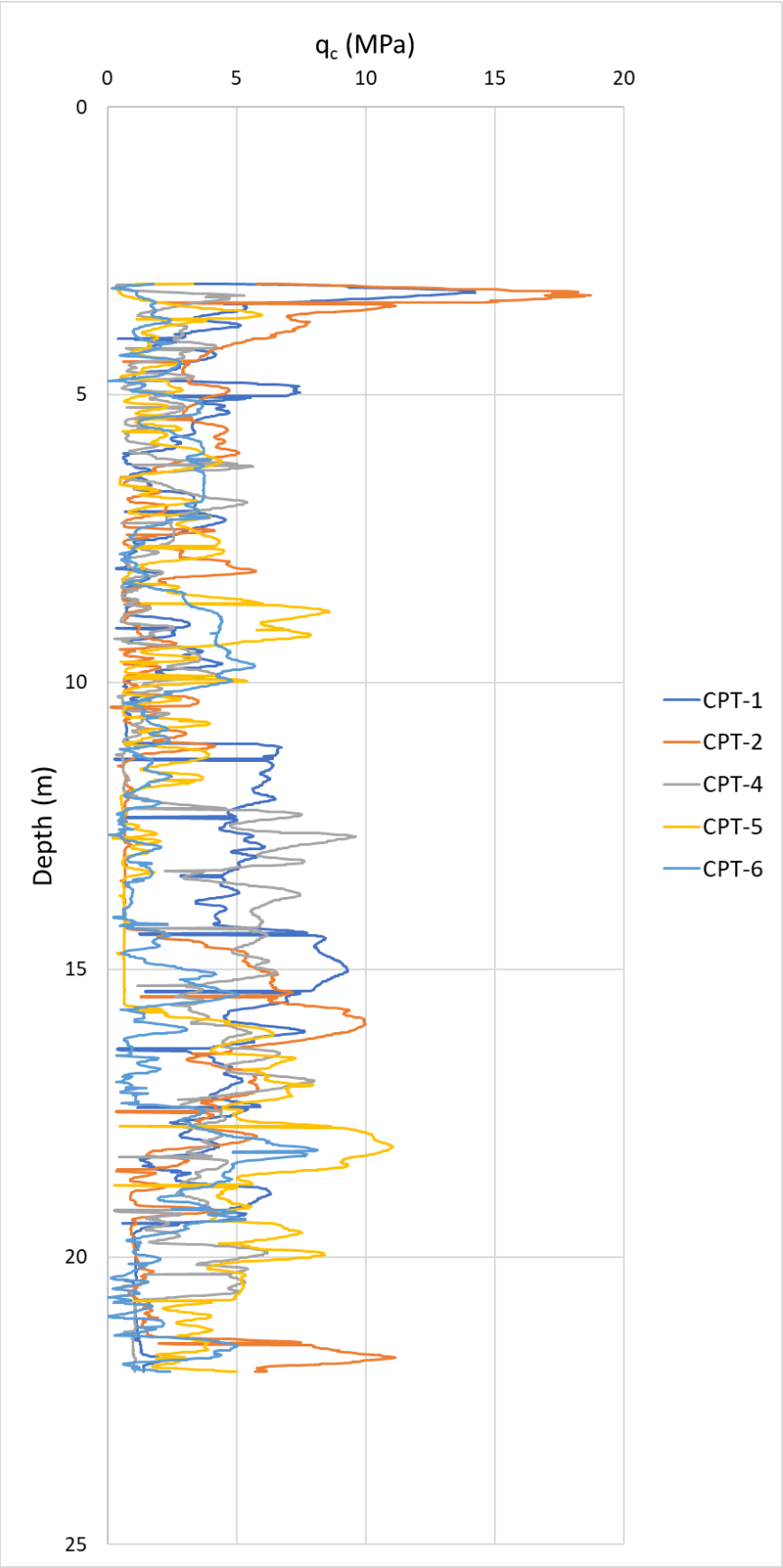

Figure 3.6 Variation of cone tip resistance with depth

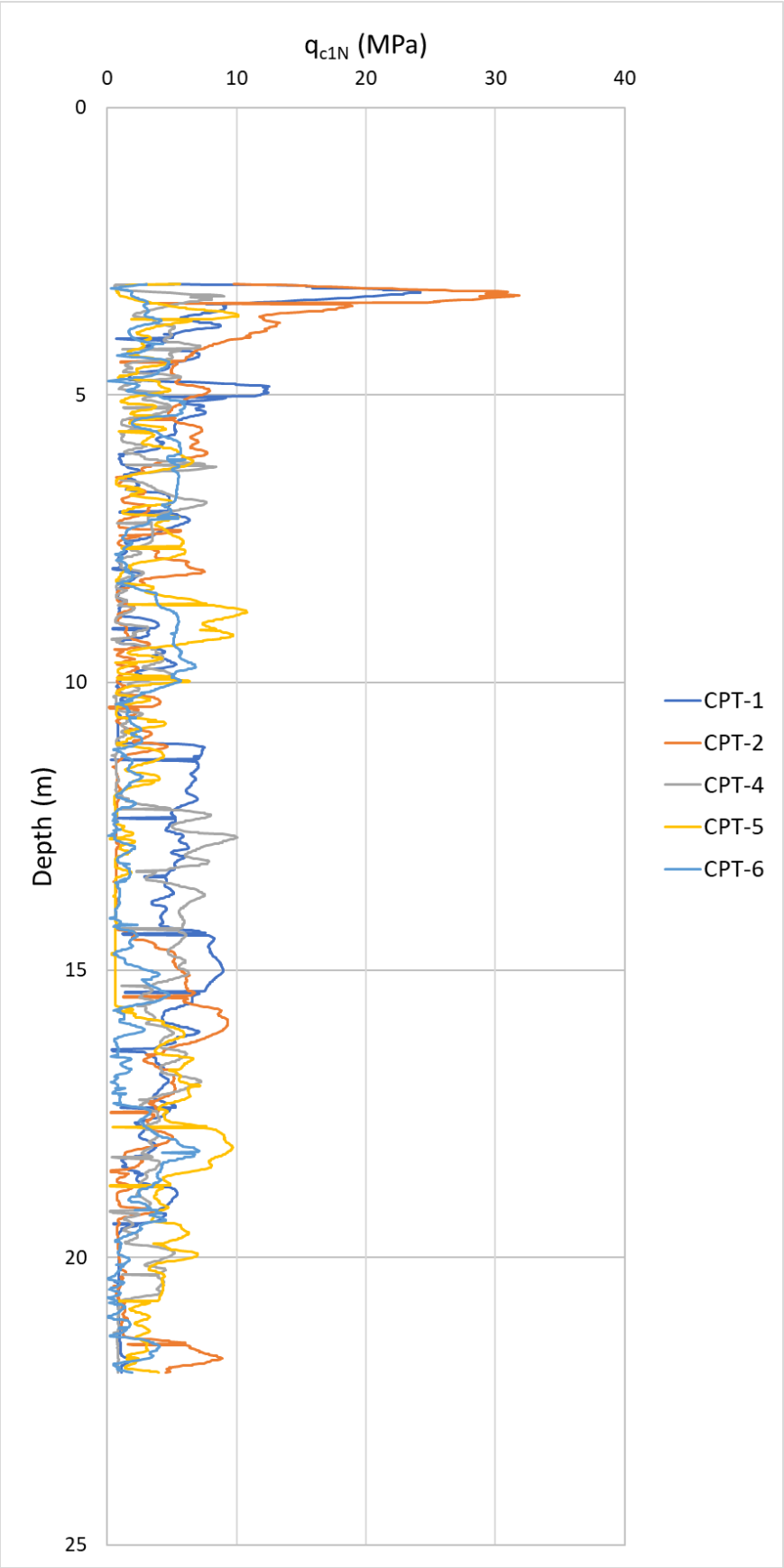

Figure 3.7 Variation of normalized cone tip resistance with depth

3.4. Laboratory Tests

To determine the physical and mechanical properties of the soil in the investigation area, laboratory tests were carried out on disturbed and undisturbed samples taken during drilling operations. The direct shear tests were carried out to determine the mechanical properties of the soil and the natural water content determination test, Atterberg Limits test, sieve analysis tests, hydrometric analysis, and specific gravity tests were carried out to determine the physical properties of the soil. The following tables summarize the results of the tests performed to determine the soil's physical properties (Table 3.7) and mechanical properties (Table 3.8). According to the laboratory results, the investigation area shows a non-plastic (NP) sand-like behavior.

Table 3.5 Physical properties of the soil in the investigation area

Sample		Classification	Classification Explanation	Water Content	Specific Gravity (Gs)	Sieve Analysis			Atterberg Limits		
No.	Depth					Gravel	Sand	Clay	LL	PL	PI
#	m	-	-	%	gr/cm^3	%	%	%	%	%	%
BH-1	3.00-3.45	SW-SM	Silty well-graded sand	23	-	6	83	10	-	NP	-
	6.00-6.45	SM	Silty sand	29	-	0	69	31	-	NP	-
	10.50-10.95	SW-SM	Silty well-graded sand	16	-	0	91	9	-	NP	-
	13.50-13.95	SP	Poorly graded sand	33	-	0	99	1	-	NP	-
	19.50-19.95	SP	Poorly graded sand	27	-	0	96	4	-	NP	-
BH-2	3.00-3.45	SM	Silty sand	36	-	0	68	32	-	NP	-
	4.50-4.95	SW-SM	Silty well-graded sand	22	-	7	88	5	-	NP	-
	6.00-6.45	ML	Silt	28	2.44	0	1	99	-	NP	-
	9.00-9.45	SW-SM	Silty well-graded sand	23	-	0	90	10	-	NP	-
	13.50-13.95	SP	Poorly graded sand	23	-	0	96	4	-	NP	-
	18.00-18.45	SM	Silty sand	28	-	0	82	18	-	NP	-
	19.50-19.95	SP	Poorly graded sand	15	-	26	74	0	-	NP	-

(cont. on next page)

Table 3.5 (cont.)

Sample		Classification	Classification Explanation	Water Content	Specific Gravity (Gs)	Sieve Analysis			Atterberg Limits		
No.	Depth					Gravel	Sand	Clay	LL	PL	PI
#	m	-	-	%	gr/cm^3	%	%	%	%	%	%
BH-3	3.00-3.45	SM	Silty sand	23	-	1	80	19	-	NP	-
	6.00-6.45	SM	Silty sand	30	-	0	86	14	-	NP	-
	7.50-7.95	ML	Silt	42	2.38	0	2	98	-	NP	-
	10.50-10.95	ML	Silt	38	2.51	0	4	96	-	NP	-
	13.50-13.95	SM	Silty sand	35	-	8	53	39	-	NP	-
	15.00-15.45	CL	Low Plasticity Clay	42	2.19	0	2	98	47	26	21
	19.50-19.95	ML	Silt	35	2.43	0	3	97		NP	-
	25.50-25.95	SW	Well graded sand	17	-	33	65	3	-	NP	-
	27.00-27.45	CL	Low Plasticity Clay	40	2.21	0	0	100	48	23	25
	30.00-30.45	SP-SM	Silty poorly graded sand	41	-	0	92	8	-	NP	-
BH-4	3.00-3.45	SW-SM	Silty well-graded sand	14	-	12	78	10	-	NP	-
	4.50-4.95	SP	Poorly graded sand	26	-	0	97	3	-	NP	-
	6.00-6.45	SM	Silty sand	36	-	0	76	24	-	NP	-
	9.00-9.45	ML	Silt	43	-	0	2	98	-	NP	-
	10.50-10.95	ML	Silt	46	2.61	0	4	96	-	NP	-
	13.50-13.95	SM	Silty sand	30		0	74	26	-	NP	-
	19.50-19.95	CL	Low Plasticity Clay	34	2.22	0	2	98	-	NP	-
	21.00-21.45	SM	Silty sand	18	-	19	63	18	-	NP	-
	25.50-25.95	CL	Low Plasticity Clay	42	2.16	0	2	98	47	20	27
	30.00-30.45	SM	Silty sand	35	-	0	86	14	-	NP	-
BH-5	1.50-1.95	SM	Silty sand	24	-	8	72	21	-	NP	-
	3.00-3.45	SM	Silty sand	28	-	0	85	15	-	NP	-
	4.50-4.95	SM	Silty sand	40	-	0	70	30	-	NP	-
	9.00-9.45	ML	Silt	45	-	0	33	67	-	NP	-
	12.00-12.45	CL	Low Plasticity Clay	45	-	0	2	98	47	26	22
	13.50-13.95	SM	Silty sand	29	-	0	86	14	-	NP	-
	19.50-19.95	ML	Silt	45	2.45	0	2	98	-	NP	-
	25.50-25.95	SM	Silty sand	29		0	86	14	-	NP	-
	27.00-27.95	CL	Low Plasticity Clay	44	2.19	0	4	96	48	26	22
	30.00-30.45	SW-SM	Silty well-graded sand	23		0	90	10	-	NP	-
BH-6	1.50-1.95	SP	Poorly graded sand	30	-	0	96	4	-	NP	-
	3.00-3.45	SP	Poorly graded sand	27	-	0	98	2	-	NP	-
	4.50-4.95	SM	Silty sand	37	-	0	82	18	-	NP	-
	6.00-6.45	SM	Silty sand	29	-	0	80	20	-	NP	-
	7.50-7.95	CL	Low Plasticity Clay	42	2.27	0	2	98	45	24	21
	9.00-9.45	SM	Silty sand	20	-	12	75	13	-	NP	-
	10.50-10.95	SW-SM	Silty well-graded sand	17	-	31	61	8	-	NP	-
	12.00-12.45	SP	Poorly graded sand	22	-	15	85	0	-	NP	-
	13.50-13.95	SP-SM	Silty poorly graded sand	36	-	0	94	6	-	NP	-
	16.50-16.95	SW-SM	Silty well-graded sand	18	-	21	70	9	-	NP	-
	19.50-19.95	SM	Silty sand	22	-	11	68	21	-	NP	-
	22.50-22.95	SM	Silty sand	23	-	9	65	26	-	NP	-
	30.00-30.45	SW-SM	Silty well-graded sand	22	-	2	92	6	-	NP	-

Table 3.6 Mechanical properties of the soil in the investigation area

Sample		Direct Shear Test	
Borehole No.	Depth	c	Ø
#	m	kPa	(˚)
BH-1	3.00-3.45	9.1	31
	6.00-6.45	10.8	20
	10.50-10.95	8.9	31
	13.50-13.95	4.8	30
	19.50-19.95	3.1	31
BH-2	3.00-3.45	12.3	20
	4.50-4.95	7.9	32
	6.00-6.45	35	11
	9.00-9.45	6.8	32
	13.50-13.95	9.2	31
	18.00-18.45	10.5	20
	19.50-19.95	11.3	33
BH-3	3.00-3.45	8.4	21
	6.00-6.45	14.7	19
	7.50-7.95	27.9	13
	10.50-10.95	28.6	12
	13.50-13.95	9.8	20
	15.00-15.45	41.8	8
	19.50-19.95	23.2	12
	25.50-25.95	2.8	32
	27.00-27.45	41.9	9
	30.00-30.45	13.3	29
BH-4	3.00-3.45	9.3	34
	4.50-4.95	4.2	30
	6.00-6.45	9.1	21
	9.00-9.45	29.7	12
	10.50-10.95	32.6	13
	13.50-13.95	7.6	20
	19.50-19.95	42.2	7
	21.00-21.45	11.8	22
	25.50-25.95	40.2	9
	30.00-30.45	7.9	21
BH-5	1.50-1.95	7.4	20
	3.00-3.45	10.8	20
	4.50-4.95	7.1	21
	9.00-9.45	32.3	12
	12.00-12.45	-	-
	13.50-13.95	9.1	21
	19.50-19.95	34.3	13
	25.50-25.95	9.8	20
	27.00-27.95	40.2	7
	30.00-30.45	6.7	31

(cont. on next page)

Table 3.6 (cont.)

Sample		Direct Shear Test	
Borehole No.	Depth	c	Ø
#	m	kPa	(˚)
BH-6	1.50-1.95	5.1	30
	3.00-3.45	-	-
	4.50-4.95	10.9	21
	6.00-6.45	-	-
	7.50-7.95	39.7	9
	9.00-9.45	10.2	21
	10.50-10.95	-	-
	12.00-12.45	-	-
	13.50-13.95	10.1	31
	16.50-16.95	9.1	32
	19.50-19.95	8.2	21
	22.50-22.95	6.4	21
	30.00-30.45	10.5	31

3.5. Idealized Soil Profile

According to the field and laboratory tests, the idealized soil profile is defined. The first layer of soil is defined as a silty clay depth of 10 m with a transient zone of sandy soil and continues up to 18 m as silty sand soil; the rest of the depth is silty clay and silty sand layer. Mechanical and physical soil properties were calculated from information collected from field and laboratory tests which were summarized in Section 3.3 and 3.4.

Table 3.7 Mechanical and physical properties of soil

Depth (m)			Soil	Unit Weight	Poisson Ratio	Cohesion	Friction Angle	Modulus of Elasticity
				γ (kg/m^3)	v	c (kPa)	ϕ	E (kPa)
0	-	3	Fill	1800	0.30	1	28	5000
3	-	10	Layer 1	1800	0.30	15	25	5000
10	-	14	Layer 2	1900	0.32	7	28	11000
14	-	18	Layer 3	1800	0.30	3	24	8000
18	-	30	Layer 4	1900	0.35	22	22	20000

3.6. Seismicity of the Site

For $M_w \geq 7.5$, maximum ground acceleration values (PGA) are expected to be 0.30 g in 475 years. The morphological structure of the investigation area shows that slope insensitivities are not likely in the future.

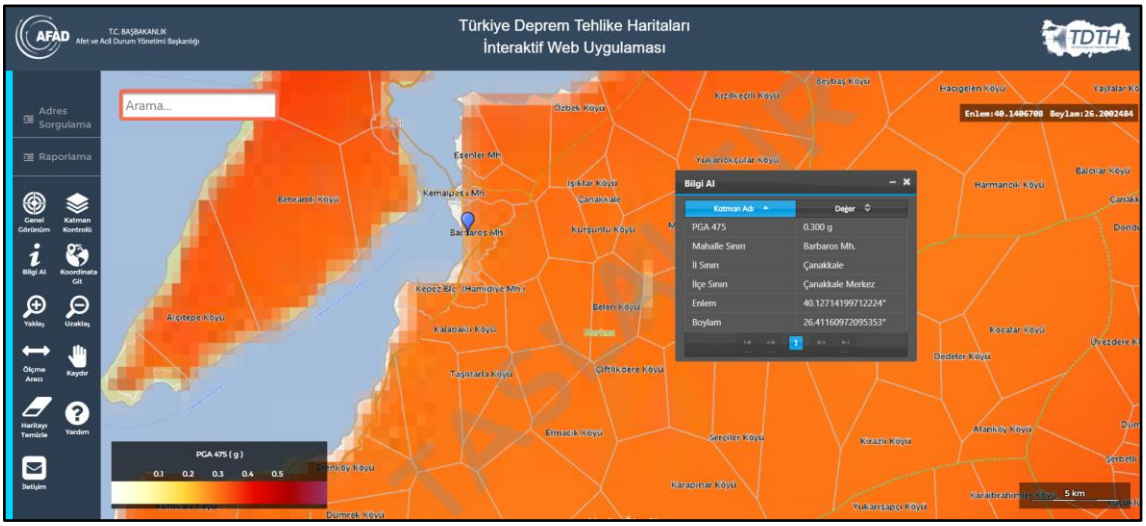

Figure 3.8 Türkiye Earthquake Hazard Map, determination of PGA (Source: https://tdth.afad.gov.tr, 2023)

3.6.1. Cone Penetration Test Based Liquefaction Assessment

Geotechnical engineering is increasingly utilizing the CPT due to its high accuracy and reproducibility. Unlike the SPT, the CPT offers continuous soil strength measurements, making it particularly useful for evaluating soil profiles that vary significantly in depth. However, this test is limited to non-gravelly soils and often requires a test pit since it does not allow sampling. The test involves determining soil resistance to the insertion of a cone, which is divided into two types: resistance at the tip (q_c) and lateral friction (f_s). The pressure applied on the rod's base calculates the tip resistance, while the lateral friction is measured along a mobile sleeve. To determine the CRR value, only the cone tip resistance is considered, and the value obtained must be normalized for a surcharge of 100 kPa and for clean sand using the relationships presented in Youd et al. (2001) to get the normalized peak resistance $(q_{c1N})_{cs}$.

Two equations can be used to calculate the resistance that the ground can provide during seismic shaking (CRR), according to Robertson and Wride (1998):

For $(q_{c1N})_{cs} < 50$:

$$CRR_{7.5} = 0.833 * \left(\frac{(q_{c1N})_{cs}}{1000}\right) + 0.05 \quad (3.3)$$

For $50 \leq (q_{c1N})_{cs} < 160$:

$$CRR_{7.5} = 93 * \left(\frac{(q_{c1N})_{cs}}{1000}\right)^{38} + 0.05 \quad (3.4)$$

CLiq software performs liquefaction calculation with CPT data using the method developed by Boulanger and Idriss (2014) and summarized in Figure 3.9. The liquefaction analysis results according to the CPT measurements made in the study area are given in Figure 3.10 below.

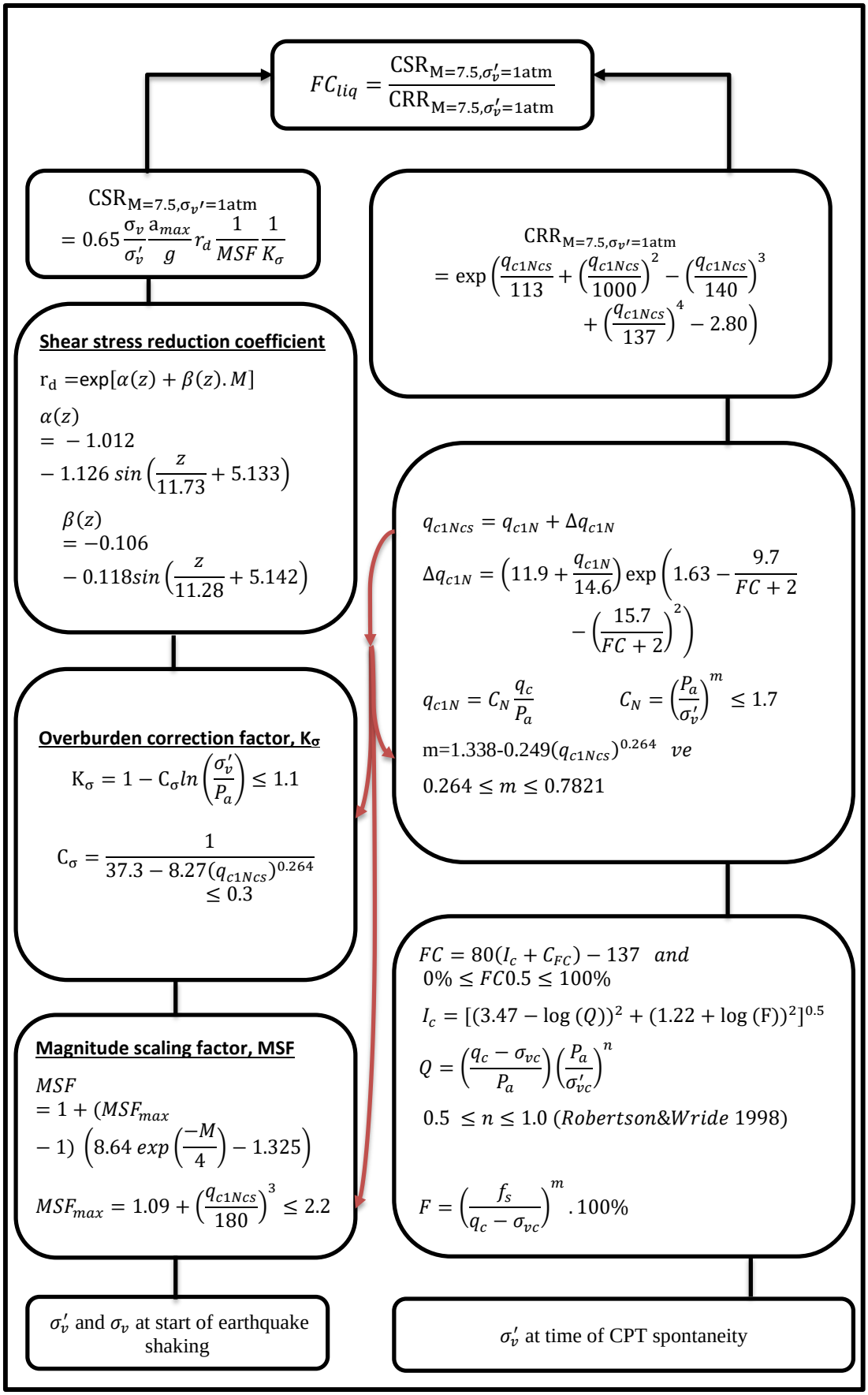

Figure 3.9 Scheme of liquefaction assessment (Source: Boulanger and Idriss, 2014)

The stress-based approach to determining liquefaction potential is based on the comparison of the earthquake-induced repetitive strain rate (CSR) with the soil's repetitive strain rate (CRR) (F.S.=CRR/CSR). The CRR is usually correlated with in-situ parameters of the soil obtained from field tests such as SPT number of hits, CPT penetration resistance, shear wave velocity, etc. The formulas used in this approach are given in Figure 3.9 as a flowchart, and the liquefaction analysis result graphs of the Cliq software that performs the analysis using this approach are shown in Figure 3.16.

The liquefaction analysis of cohesionless soils is based on four functions (r_d: stress reduction factor, C_N: geological load correction coefficient, K_σ geological load correction coefficient σ_v', and MSF: Earthquake Magnitude Scaling Factor). Of these, rd is a function of depth, ground motion properties, dynamic properties of the soil, C_N and K_σ effective geologic load (σ_v'), relative stiffness (D_r), fine grain fraction (FC), and MSF is a function of ground motion properties, D_r and FC.

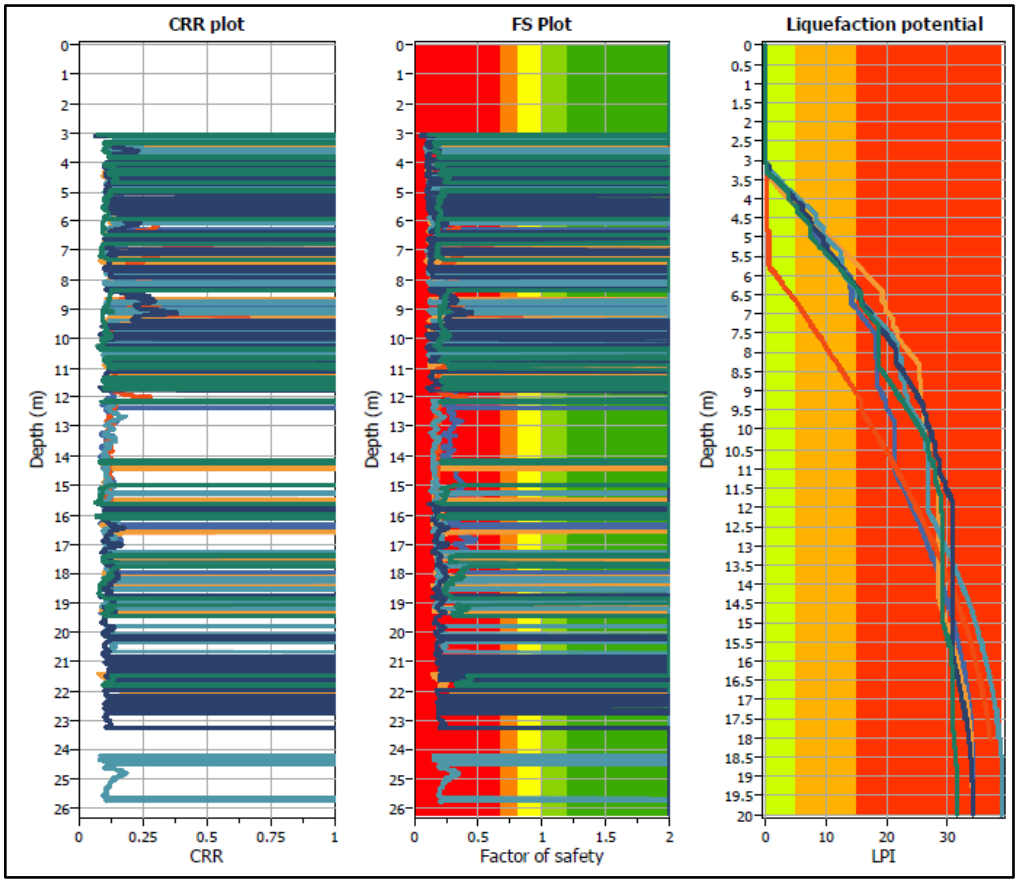

Figure 3.10 F.S and liquefaction potential according to CPT results

As seen in Figure 3.10, according to the CPT data factor of the safety number is less than 1,0, the liquefaction potential index of the area is high under the seismic loading.

3.6.2. Standard Penetration Test Based Liquefaction Assessment

The SPT has been the most widely used over the years and has built up a relatively large database. However, the results of this type of test must be qualified since it can rework certain soils differently. This test is based on the number of strokes required to drive a corner into the soil to a depth of thirty centimeters ($N_{1\text{-}60cs}$). The index "1" defines that the number of blows is normalized for a surcharge of 100 kPa. The subscript "60" implies that the value has been normalized for an efficiency of 60% of the total energy delivered by the hammer when driving the rod. On the other hand, the indis "cs" implies that the value is normalized for clean sand, i.e., without fine particles (Youd et al. 2001). Some relationships have been proposed to perform these normalizations (e.g., Youd et al., 2001; McCarthy, 2007), but they will be discussed elsewhere.

The liquefaction analysis for an earthquake magnitude of M_w=7.5 is performed according to the formulated version of the chart proposed by Seed et al. (1985) and revised by NCEER (1997):

$$CRR_{M7.5} = \frac{0.048 - 0.004721 * N_{1,60f} + 0.0006136 * N_{1,60f}^2 - 1.673 * 10^{-5} * N_{1,60f}^3}{1 - 0.1248 * N_{1,60f} + 0.009578 * N_{1,60f}^2 - 0.0003285 * N_{1,60f}^3 + 3.713 * 10^{-6} * N_{1,60f}^4} \quad (3.5)$$

Concerning fines content, Seed and Idriss (1997) recommend correcting SPT-$N_{1,60}$ values by multiplying them by the following coefficients.

$$N_{1,60f} = \alpha + \beta * N_{1,60} \quad (3.6)$$

$for\ FC \leq 5\%$:

$$\alpha = 0\ ;\ \beta = 1.0 \quad (3.7)$$

$for\ 5\% \leq FC \leq 35\%$:

$$\alpha = exp\left[1.76 + \left(\frac{190}{FC^2}\right)\right]; \beta = 0.99 + FC^{1.5}/1000 \quad (3.8)$$

$for\ FC \geq 35\%$:

$$\alpha = 5.0\ ;\ \beta = 1.2 \quad (3.9)$$

Table 3.8 SPT based liquefaction analysis

SPT Bases Liquefaction Analysis									
DD-2 SDS		0.97	0.4 SDS	0.39					
Magnitude of Earthquake		7.5	C_M	1					
Depth	$(N_1)_{60}$	IDC	$(N_1)_{60f}$	r_d	$t_{earthquake}$	$CRR_{7.5}$	t_r	Factor of Safety	Liquefaction Potential
m	-	(%)	-	-	kPa	-	kPa		
3.50	6	15	9	0.97	15	0.10	3	0.19	Liquefaction potential exist
5.00	15	30	22	0.96	22	0.24	10	0.44	Liquefaction potential exist
6.50	2	67	7	0.95	28	0.09	5	0.17	Liquefaction potential exist
8.00	2	15	5	0.94	34	0.07	4	0.13	Liquefaction potential exist
9.50	3	14	5	0.92	40	0.07	6	0.14	Liquefaction potential exist
11.00	6	14	8	0.88	44	0.10	9	0.20	Liquefaction potential exist
12.50	2	98	7	0.84	48	0.09	9	0.19	Liquefaction potential exist
14.00	2	14	4	0.80	51	0.07	7	0.15	Liquefaction potential exist
15.50	12	14	15	0.76	53	0.16	19	0.36	Liquefaction potential exist
17.00	20	14	23	0.72	56	0.26	35	0.63	Liquefaction potential exist
18.50	2	4	2	0.68	57	0.05	8	0.14	Liquefaction potential exist
20.00	4	7	4	0.64	58	0.07	11	0.18	Liquefaction potential exist

3.7. Conclusion

The results of the field tests and laboratory tests performed in the investigation area showed silt, sand, and silty sand layers as soil profiles. As a result of SPT and CPT-based liquefaction analysis, it was demonstrated that these soils are liquefiable. To eliminate the liquefaction problem, it was decided to carry out improvement works with stone columns. The center-to-center spacing is 1.6 m, and the diameter is 80 cm of stone columns applied. The fact that the soil profile consists of sandy silt soil allowed construction with the vibroflotation method.

CHAPTER 4

NUMERICAL MODELING OF STONE COLUMNS BY THE FDM

4.1. Introduction

In numerical modeling, according to whether the modeling is explicit or implicit, it is divided into two types: finite element method and finite difference method. In the first part of this chapter, numerical modeling methods FEM and FDM are mentioned. In order to understand the FLAC 3D solution concept, comparisons between these two modeling methods are necessary. The following sections explain the essential points of numerical modeling with FLAC 3D software.

4.2. Explicit and Implicit Solution

The Finite Element Method (FEM), which uses explicit methods, and Finite Difference Method (FDM), which uses implicit methods, are generally adopted for numerical analysis. A comparison of these two methods is given in Table 4.1 below.

Table 4.1 Comparison between explicit and implicit methods (Source: Cundall, 1980)

Explicit (FEM)	Implicit (FDM)
The time step must be less than a critical value to ensure stability.	No restriction on the time step, at least for some resolution schemes.
Few calculations per time step.	Numerous calculations per time step
No significant numerical damping was introduced for dynamic problems.	Time-dependent numerical damping for unconditionally stable schemes.
Consideration of nonlinear behavior laws without additional iterations.	Need for an iterative procedure to take into account nonlinear behaviors.
A nonlinear law is always followed correctly if the time step is less than its critical value.	It is always necessary to demonstrate that the procedure is: (a) stable; and (b) physically correct, i.e., follows a physically correct stress path.

(cont. on next page)

Table 4.1 (cont.)

Explicit (FEM)	Implicit (FDM)
No matrix is built. The memory required is minimal.	A stiffness matrix must be stored. The memory required is essential.
Since no matrix is built, large deformations and displacements can be considered with almost no additional calculation.	Additional calculations are required to track large deformations and displacements.

4.3. FLAC 3D Software

This part will discuss important points of FLAC 3D that will be used in numerical modeling for this thesis. The numerical analyses were performed using the FLAC 3D software. The software is based on the finite difference method: the variables are known at discrete locations in space, and storing a global stiffness matrix is unnecessary. Using time steps allowed FLAC 3D to solve the equations of motion explicitly and incorporate the nonlinear inelastic behavior of soil. The Finn soil model of pore pressure generation is used to model the phenomenon of liquefaction, but this does not prevent the use of other laws through programming either by the FISH language integrated with FLAC 3D or by the C++ language.

4.3.1. Mesh and time discretization

The code uses the mixed discretization technique proposed by Marti and Cundall (1982). From Figure 4.1, this technique starts with the dynamic equilibrium equations to calculate new velocities and displacements from the stresses or forces. Then, strain rates are deduced from the velocities, and further stresses are computed using the behavior law. Each cycle represents a time step Δt. Each box in this procedure updates the variables it must process from the known values that remain fixed during Δt.

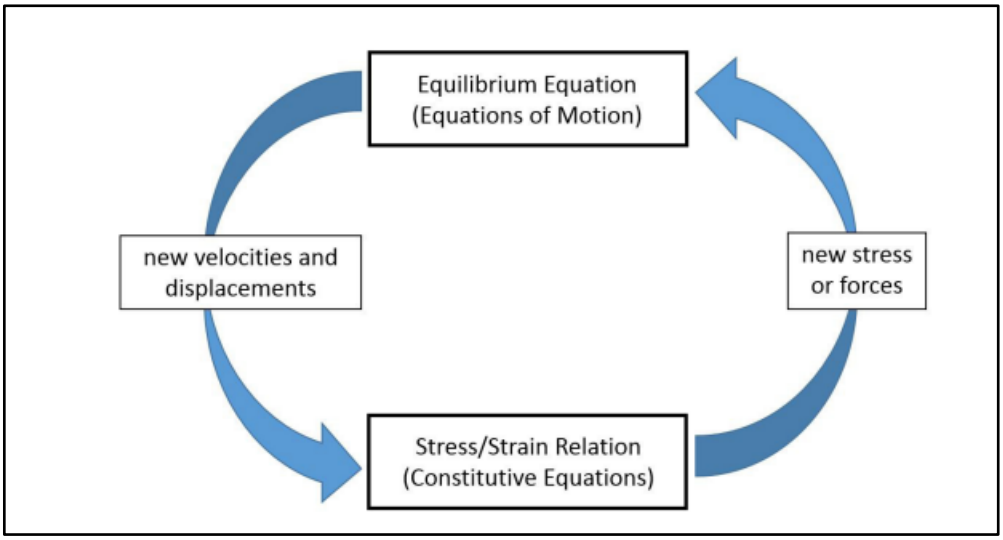

Figure 4.1 Solution procedure of FLAC 3D (Source: Billaux et Cundall, 1993)

Each area has two layers containing five tetrahedrons stacked for an 8-node area. The size of the mesh element must be small enough for the mesh to transmit the waves appropriately and without the digital distortion of these waves. This size depends on the frequencies involved and the speed of propagation of the waves:

$$f = \frac{V_S}{\lambda} \tag{4.1}$$

Where:

-V_S: propagation speed of compressional or shear waves as appropriate;

- λ: characteristic wavelength.

The mesh used can cause numerical distortion of wave propagation in a domain; to avoid this problem, it is necessary for the size of the element Δl to become smaller than one-eighth to one-tenth of the wavelength λ ($\Delta l \leq \lambda/10$ to $\lambda/8$) (Kuhlmeyer & Lysmer, 1973). Consequently, the maximum frequency that can be modeled correctly for a mesh is given by:

$$f = \frac{V_S}{10 * \Delta l} \tag{4.2}$$

4.3.2. Rayleigh Damping

Rayleigh damping was originally used to analyze structures and continuous elastic media. The damping matrix C is constructed by a combination of the stiffness matrix K and mass matrix M as:

$$C = \alpha * M + \beta * K \tag{4.3}$$

Where α is the mass contribution and β the stiffness contribution, both coefficients depend on the damping characteristics of the material.

For several degrees of freedom, the critical damping factor ζ_i for any angular frequency ω_i of the system is given by the following equation (Bathe & Wilson, 1976).

$$\alpha + \beta * \omega_i^2 = 2 * \omega_i * \xi_i \tag{4.4}$$

$$\xi_i = \frac{1}{2} * \left(\frac{\alpha}{\omega_i} + \beta * \omega_i\right) \tag{4.5}$$

ξi is the critical damping rate for mode i of vibration with frequency angular frequency ω_i.

Figure 4.2 gives the variation of the normalized damping rate with angular frequency. Three curves are shown:

- the mass component β = 0, the stiffness component α = 0, and a combination of both.

- the contribution of the mass to the damping is dominant for low frequencies, while the assistance of the stiffness is dominant for high frequencies.

- the curve representing total damping (mass and stiffness) reaches a minimum value at $f_{min} = \omega_{min}/2\pi$ for f_{min} only, the mass damping is equal to the stiffness damping.

In the dynamic analysis, the Rayleigh damping mechanism provides the energy absorption mechanism of the stone columns. Rayleigh damping is formed of two components: mass and stiffness. As the frequency of the cyclic motion increases, the contribution of the mass component tends to decrease. In contrast to the mass component, the stiffness component becomes more dominant than the mass component as the frequency increases (Figure 4.2). The goal is to reproduce the frequency-independent damping of materials at the correct level. Therefore, only the mass component is used in

this study, neglecting the stiffness component. The damping parameter used is 5% for the damping ratio.

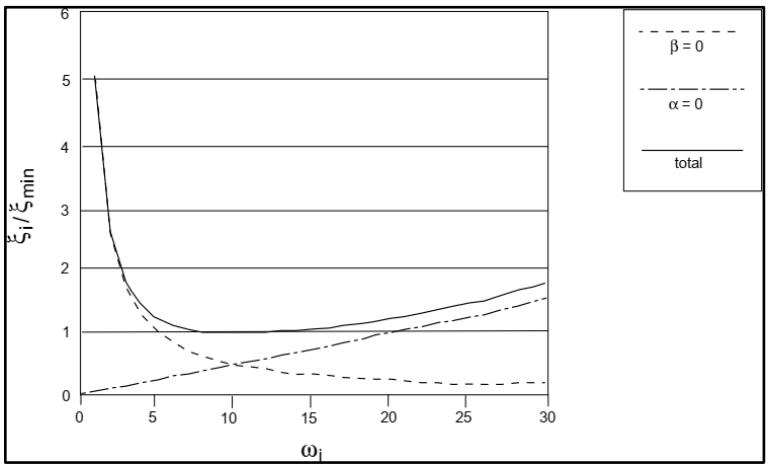

Figure 4.2 Variation of damping with frequency (Source: Itasca's FLAC 3D Documentation, 2019)

4.3.3. Dynamic Boundary Conditions

FLAC 3D software aims to model the material's behavior under dynamic boundary conditions. The loads acting on the model consist of internal and/or external dynamic loads applied from the boundaries or nodes. In the rigid base which is shown in Figure 4.3, an acceleration (or velocity or displacement) time history is applied for grid points along the base of the mesh. While simple to use, a potential disadvantage of the rigid base is that it acts as a fixed displacement boundary, reflecting downward propagating waves back into the model. A quiet boundary based on the viscous boundary conditions is specified along the base of the FLAC3D mesh to simulate a compliant base which is called the flexible base (Figure 4.4).

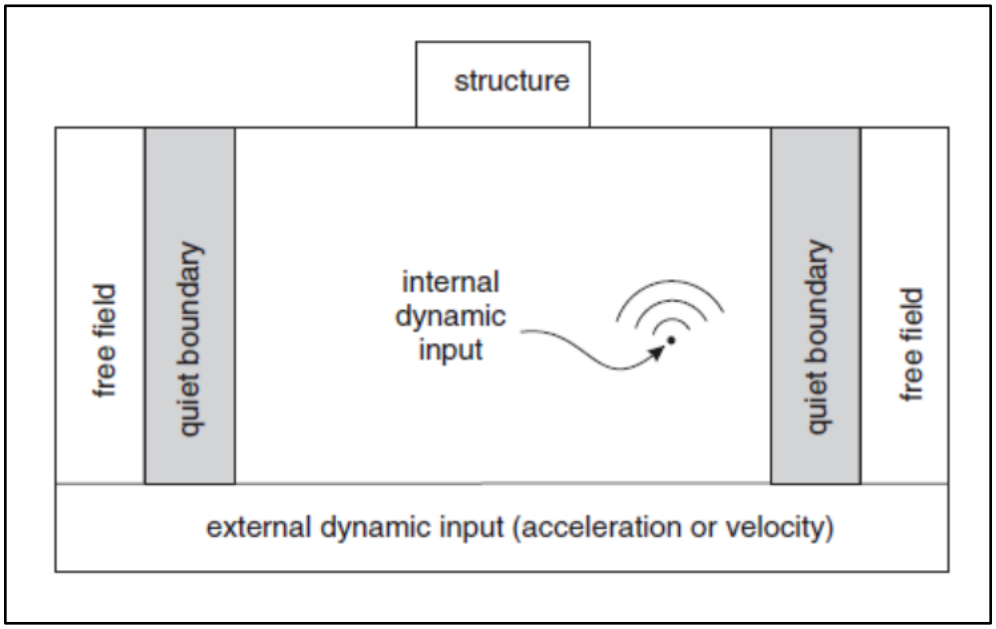

Figure 4.3 Rigid base boundary conditions (Source: Itasca's FLAC 3D Documentation, 2019)

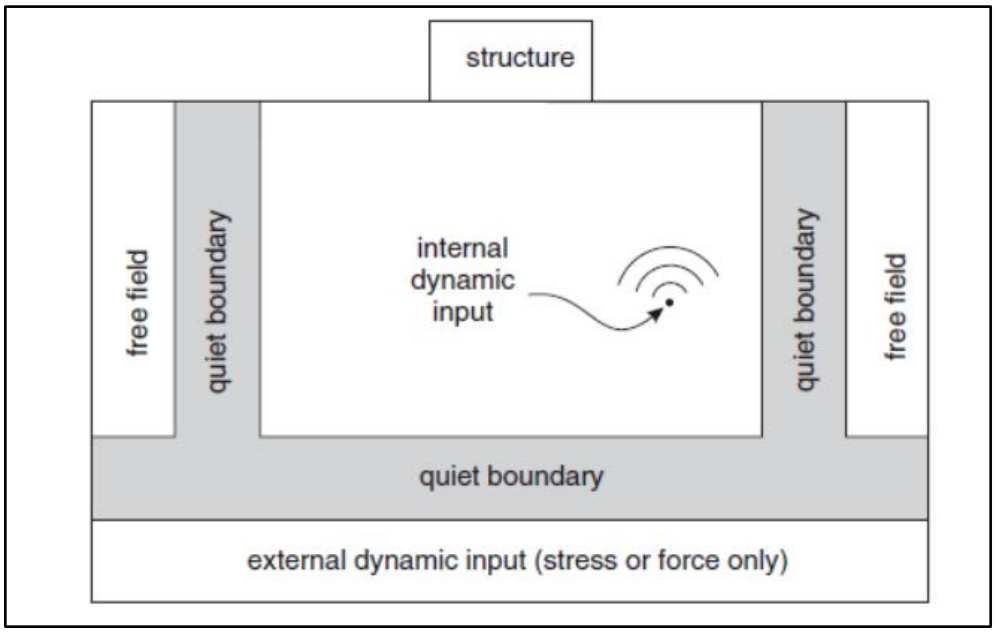

Figure 4.4 Flexible base boundary conditions (Source: Itasca's FLAC 3D Documentation, 2019)

These boundaries cause wave reflections in the dynamic case and prevent energy radiation. Using a large domain, however, reduces this effect because most of the energy dissipates in part. However, a large model increases the computation time. This difficulty can be overcome by using absorbing boundaries. The FLAC 3D code uses the viscous limits developed by (Kuhlmeyer & Lysmer, 1973).

The method uses a series of independent dampers attached to the boundaries in the normal and tangential directions. The dampers provide normal viscous and shear tractions given by:

$$t_n = -\rho * C_p * \upsilon_n \quad (4.6)$$

$$t_s = -\rho * C_p * \upsilon_s \quad (4.7)$$

Where:

- υ_n and υs: the normal and tangential components of the boundary velocity.
- ρ: the density of the soil.
- C_p and C_s: the normal and tangential velocity of the seismic wave.

These boundaries effectively absorb waves that arrive with an angle of incidence greater than 30°; the energy absorption is independent of frequencies. When modeling the dynamics of a structure, the boundaries must be placed far enough away from the structure to minimize wave reflection and create free field conditions. This distance is relatively small when the soil damping is huge (Seed et al., 1975). On the other hand, the small distance can lead to a large and unreasonable model in the case of low damping. The solution is, therefore, to force these boundaries to produce the free field motion by absorbing the waves coming from the structure. This approach has been used in the continuous finite difference code NESSI (Cundall, 1980)

The method is based on running a free field calculation in parallel to the one containing the structure. The free-field domain is coupled to the main domain by absorbing boundaries (Figure 4.4, Figure 4.3), and the unbalanced free-field forces are applied to the main domain. This type of boundary is used in the thesis model.

As a result of, wave reflections occurring at the model boundaries are reduced using "Quiet Boundary" or "Free-Field" boundary conditions.

4.3.4. Finn Soil Model

Finn's soil model has been used for liquefiable soil where the effective stress decreases and water pressure increases. The principle of this method is that the skeleton's behavior under cyclic loading is a volumetric stress to consider the pore water's excess pressure. The focus of this method is to consider that the skeletal behavior under cyclic loading is a volumetric stress to account for pore water pressure.

The Finn Model describes the relationship between increasing shear deformation and volumetric deformation under a simple shear load (Martin et al. 1975; Byrne 1991 and Itasca Consulting Group, Inc.).

$$\Delta\varepsilon_{vd} = C_1 * (\gamma - C_2 * \exp(-C_2 * \varepsilon_{vd}) + (\frac{C_3 * {\varepsilon_{vd}}^2}{\gamma + C_4 * \varepsilon_{vd}}) \quad (4.8)$$

C_1, C_2, C_3, and C_4 are constants relying on the relative density of the soil, the equation between these constants as (Itasca Consulting Group, Inc.):

$$C_1 * C_2 * C_4 = C_4 \text{ when } \Delta\varepsilon_{vd} = 0 \quad (4.9)$$

Byrne (1991) offered a more basic volume change model with C_1 and C_2 constants:

$$\frac{\varepsilon_{vd}}{\gamma} = C_1 * \exp(-C_2 * (\frac{\varepsilon_{vd}}{\gamma})) \quad (4.10)$$

Equation 4.8 and Equation 4.9 are coupled from the Mohr-Coulomb criterion, from which the Finn model can be derived.

The index form allows us to calculate the incremental volumetric deformation at each half cycle using Equation 4.11 (Carter et al. 2014).

$$(\Delta\varepsilon_{vd})_i = 0.5 * (|\gamma_i| - |\gamma_{thresh}|) * C_1 * \exp(-C_2 * \frac{(\varepsilon_v)_i}{(|\gamma_i| - |\gamma_{thresh}|)}) \quad (4.11)$$

Where $(\Delta\varepsilon_{vd})_i$ is the increasing volumetric deformation at each half cycle; γ_i is the amplitude of the i-th half cycle. γ_{thresh} is the threshold shear stress below which no volumetric stress will occur; $(\varepsilon_v)_i$ is the volumetric stress accumulated before the shear stress is applied.

The FLAC dynamic option study model incorporates the model of pore water pressure increase developed by Byrne. This model can calculate the volumetric unit deformations during dynamic loading by relating the dynamic shear unit deformation to the volumetric unit deformations. With this model, pore water pressures can be calculated from volumetric unit deformation values, and thus, pore water pressure and liquefaction problems during earthquakes can be modeled. According to this principle, Byrne

developed an SPT-dependent formula between volumetric deformation and stress-strain (ITASCA).

The parameter C_1 in Finn Model controls the volume change and is a function of the relative density (Byrne, 1991). Thus, it is expressed as:

$$C_1 = 7600 * (Dr)^{-2.5} \quad (4.12)$$

Where D_r values in percentage (%), the C_2 parameter in the Finn model controls the shape of the collected deformation curve with the number of cycles. Since the form is generally the same for identical densities, C_2 can become a function of C_1,

$$C_2 = 0.4/C_1 \quad (4.13)$$

4.3.4.1. Evaluation of Finn Soil Model Parameters

The relative density value is an essential input parameter for the Finn model in FLAC 3D. The Finn model is an empirical model that relates soil strength to relative density, and it requires a value for relative density to estimate the soil strength.

The relative density value is used to calculate the Finn parameters, C_1, and C_2, which are then used to estimate the soil strength. The Finn model assumes that soil strength increases with increasing relative density, so accurate estimation of relative density is important for accurate estimation of soil strength. The relative density value can be calculated using field test data. Relative density values can be calculated by empirical relationships using $(N_1)_{60}$ data obtained from SPT or cone tip resistance data obtained from CPT.

The relation between relative density and $(N_1)_{60}$ used by (Tokimatsu & Seed, 1987) can be approximated in the range $30 < D_r < 90$, using the relationship between the relative density (D_r) and the normalized SPT number of hits $(N_1)_{60}$, we find:

$$D_r = 15 * (N_1)_{60}{}^{0.5} \quad (4.14)$$

Several empirical relationships are proposed in the literature to correlate the cone resistance (q_c) obtained from the CPT and the soil's relative density (D_r). Here are a few examples:

The first attempt to correlate the density of sands with the tip cone tip resistance obtained from cone penetration tests date back to the work of (Schmertmann, 1978). Schmertmann presented the first comprehensive correlation between q_c and relative density (D_r) based on the Calibration Chamber (CC).

Jamiolkowski et al. (2003) proposed a correlation between cone tip resistance, relative density, and average effective stress as follows (Jamiolkowski, Ladd, & Germaine, 2003) :

$$D_r = \frac{1}{C_2} * ln\left(\frac{q_c*(\sigma'_{vo})^{C_1}}{C_0}\right) \quad (4.15)$$

where: C_0 C_1 and C_2 = empirical correlation factors.

According to the test results, provided that the soil is normally consolidated, having a K_0 constant with depth. In this case, non-dimensional correlation factors C_0, C_1, and C_2 can be taken as 17.68, 0.50 and 3.10 (case of tests on Ticino (TS), Hokksund (HS) and Toyoura sand (TOS)), respectively.

Lunne et al. (1997) suggested the relative density along the measurement depth can be determined indirectly using the relationship given empirically in the formula below.

$$D_r(\%) = -98 + 66 * log_{10}(\frac{q_c}{\sqrt{\sigma'_{vo}}}) \quad (4.16)$$

Where the σ_{vo}' is the effective initial vertical stress with the same units as measured cone penetration resistance, q_c.

Robertson & Campanella (1983) proposed an empirical relationship between cone tip resistance (q_c), effective overburden stress (σ'_{vo}), relative density (D_r), and two empirical parameters, C_1 and n. The relationship can be written as:

$$q_c = C_1 * (\sigma_v)_o{}' * D_r^n \quad (4.17)$$

Where q_c is the cone tip resistance, σ'_{vo} is the effective overburden stress, D_r is the relative density, C_1 and n are empirical parameters that depend on the soil type and testing conditions. This relationship is commonly used in geotechnical engineering practice to estimate soil strength and evaluate ground improvement techniques' effectiveness.

The other empirical relationship between cone tip resistance (q_c), relative density (D_r), and effective overburden stress (σ'_{vo}) is suggested by Liu & Byrne, (2002). There are two empirical parameters, C_1 and n, as well as an additional parameter, C_2. The relationship can be written as:

$$q_c = C_1 * \sigma'_{vo} * D_r^n * e^{-C_2 * \sigma'_{vo}} \quad (4.18)$$

Where q_c is the cone tip resistance, σ'_{vo} is the effective overburden stress, D_r is the relative density, and C_1, n, and C_2 are empirical parameters that depend on the soil type and testing conditions.

4.3.5. Model Geometry

Modeling the soil media in numerical modeling is imperative for a realistic result. The boundary surfaces of the soil zone should be selected at a sufficiently appropriate distance from the structure. The simplification of the layout model applied in the field and adapted to the analysis is usually performed in the following ways.

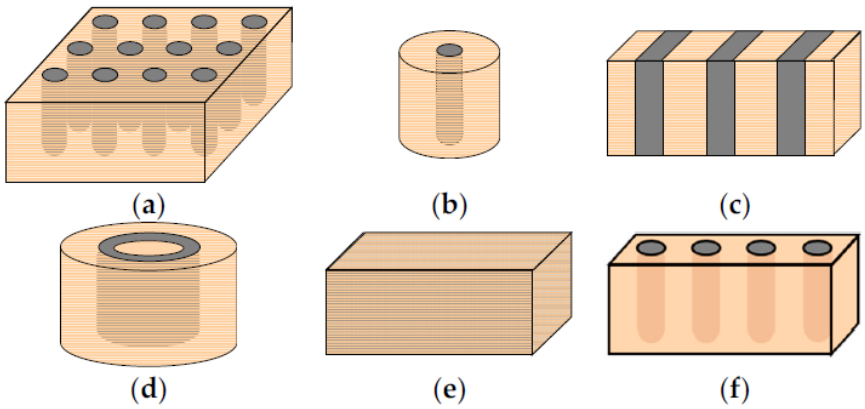

Figure 4.5 Modelling layout methods (a) whole layout, (b) unit cell, (c) longitudinal gravel trenches, (d) cylindrical rings of gravel, (f) small groups of stone columns (Source: Castro, 2017)

The layout models shown in the figure above (Figure 4.5) can be explained as follows; (a) is the whole layout, (b) is the unit cell method which is defined only one column and its corresponding surrounding soil studied. The (c) has been created with the stone columns transformed into longitudinal gravel trenches to study the problem in plane

strain conditions. In the model of (d), The columns are transformed into cylindrical rings of gravel to study the issue in axial symmetry cylindrical rings of gravel. (f) is represent geometrical models for small groups of stone columns.

When creating the numerical models, the subject of the diploma thesis, groups of four supports, were examined. The area outside these supports was generated by entering improved parameters for simplification.

4.3.6. Dynamic Loading

The Dynamic Wizard module of FLAC 3D software can process earthquake records. First, the velocity or acceleration file from the earthquake recording is imported as a table or PEER file. High-frequency ground motions can be filtered and removed. Then the processed data, such as acceleration, velocity, displacement, amplitude spectrum, response spectrum, or Arias intensity, can be exported as a FLAC 3D table. The data from the exported table is applied as acceleration or velocity to the dynamic model created in the analysis code.

4.4. Conclusion

The FLAC 3D Finn model is suitable for analyzing the dynamic liquefaction of the soil. One of the essential issues to be considered in transferring dynamic effects to the analysis model is boundary conditions. In FLAC 3D software, free field boundary conditions and damping boundaries are used to reflect the reality of the boundary conditions. In this way, the reflections of earthquake waves can be absorbed by viscous boundaries. In this way, time is saved by analyzing with a smaller model. Within the scope of this thesis, liquefaction and settlement analyses are performed under dynamic effects. Field data will be used in the analyses; therefore, the Finn Soil Model is selected as the material model. While creating the model geometry, the maximum grid width can be determined according to the dynamic frequency value so that convergence errors are not encountered during the analysis.

CHAPTER 5

ANALYSIS OF IMPROVEMENT OF LIQUEFACTION BY STONE COLUMN

5.1. Introduction

As seen in the literature review section (CHAPTER 2), numerical analyses have focused on the behavior of a single column or a group of columns, and the liquefaction of fully saturated soil under dynamic effects has been investigated. In this section, the Finn Model and FLAC 3D software will be used to investigate the change in pore water pressure in the soil between a group of stone columns under an earthquake load before and after the construction of the stone columns and to evaluate the liquefaction resistance of the soil before and after improvement. In addition, relative density values will be calculated using empirical equations from the measured cone tip resistance before and after the stone column construction.

5.2. Investigation Area by Pre-Post Survey Test Values

At the site investigation part of this thesis (CHAPTER 3) in Canakkale Region, stone columns were installed using the vibroflotation bottom feed wet method with 80 cm diameter and 1.6 m spacing. It is in principle similar to Figure 4.5a, provided that the boundary conditions are satisfied. In order to understand the effect of the stone columns on the soil, four control tests were carried out, two before and two after the improvement works. The drawing file exemplifying the test locations is presented below in Figure 5.1.

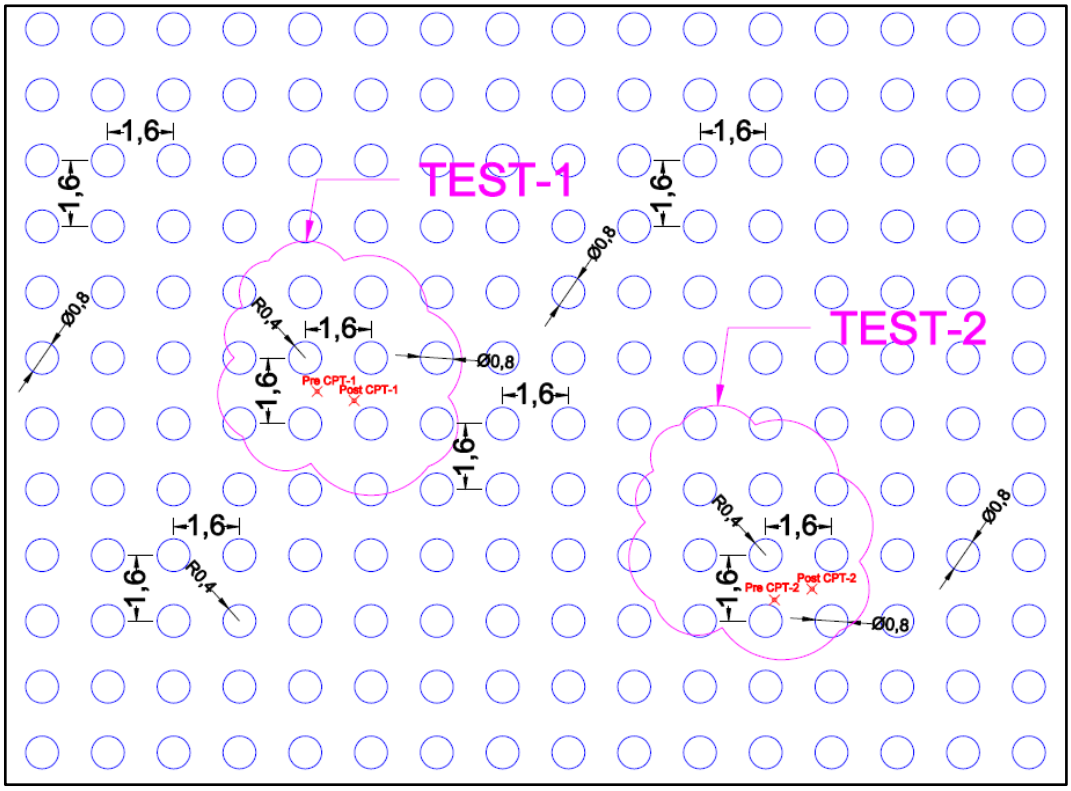

Figure 5.1 Illustrative locations of Pre and Post CPT

The changes in the cone tip resistance values obtained from the cone penetration tests before and after the construction of the stone columns are showed in Figure 5.2 and Figure 5.3 below.

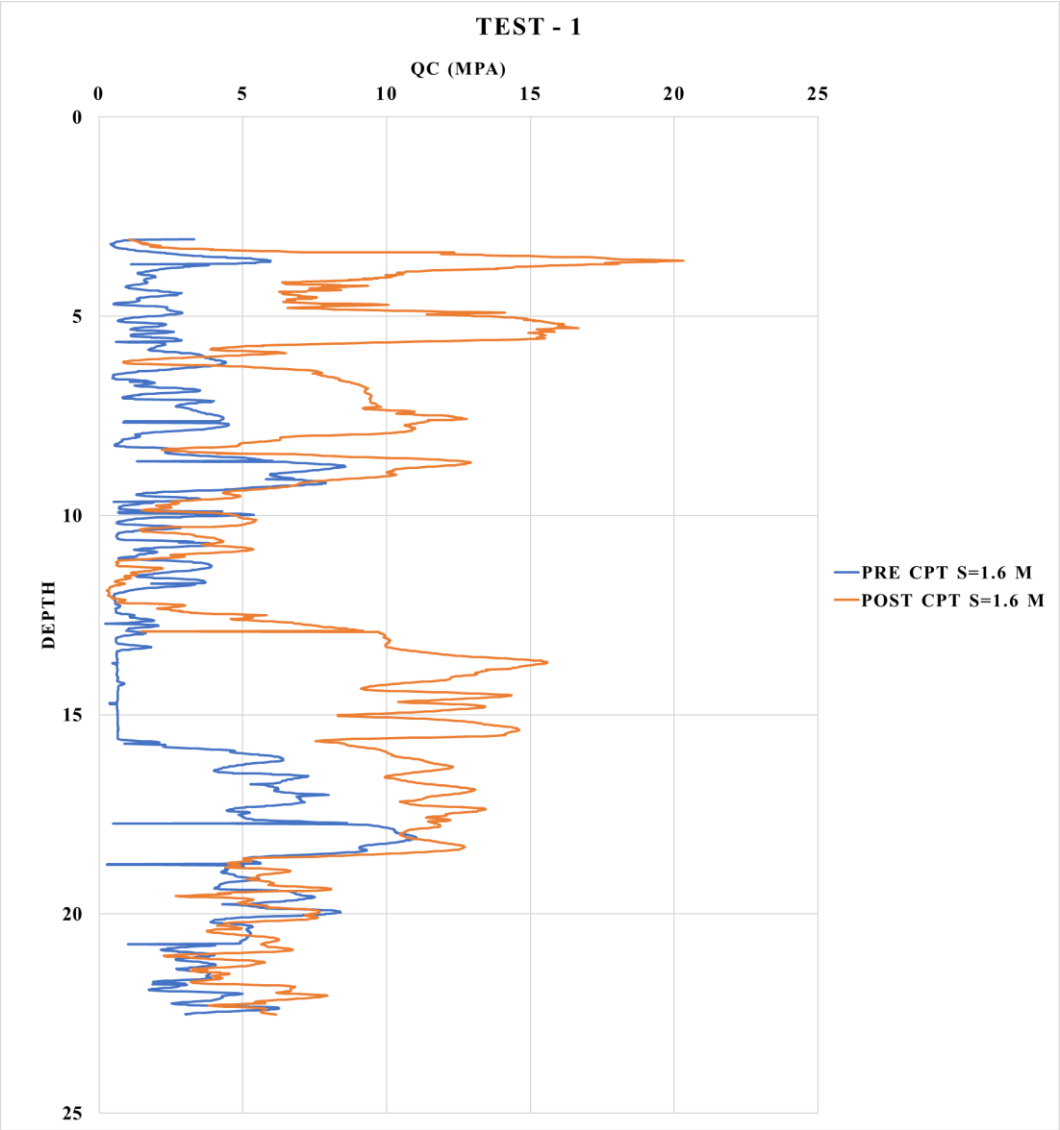

Figure 5.2 Pre and Post values of CPT (Test-1 for 1.6m spacing)

According to Test-1 results, the cone tip resistance values obtained from CPT are 3 MPa for the first 16 meters of depth and 5 MPa for the next 8 meters before improvement. After improvement, these values increased to an average of 9 MPa for the first 10 meters, remained at an average of 3 MPa for the next 3 meters, and increased to 13 MPa between the depths of 13 and 19 meters. At some depths, the cone tip resistance values before the stone column application are observed to be higher post values. It is thought that the reason for this may be clayey layer transitions.

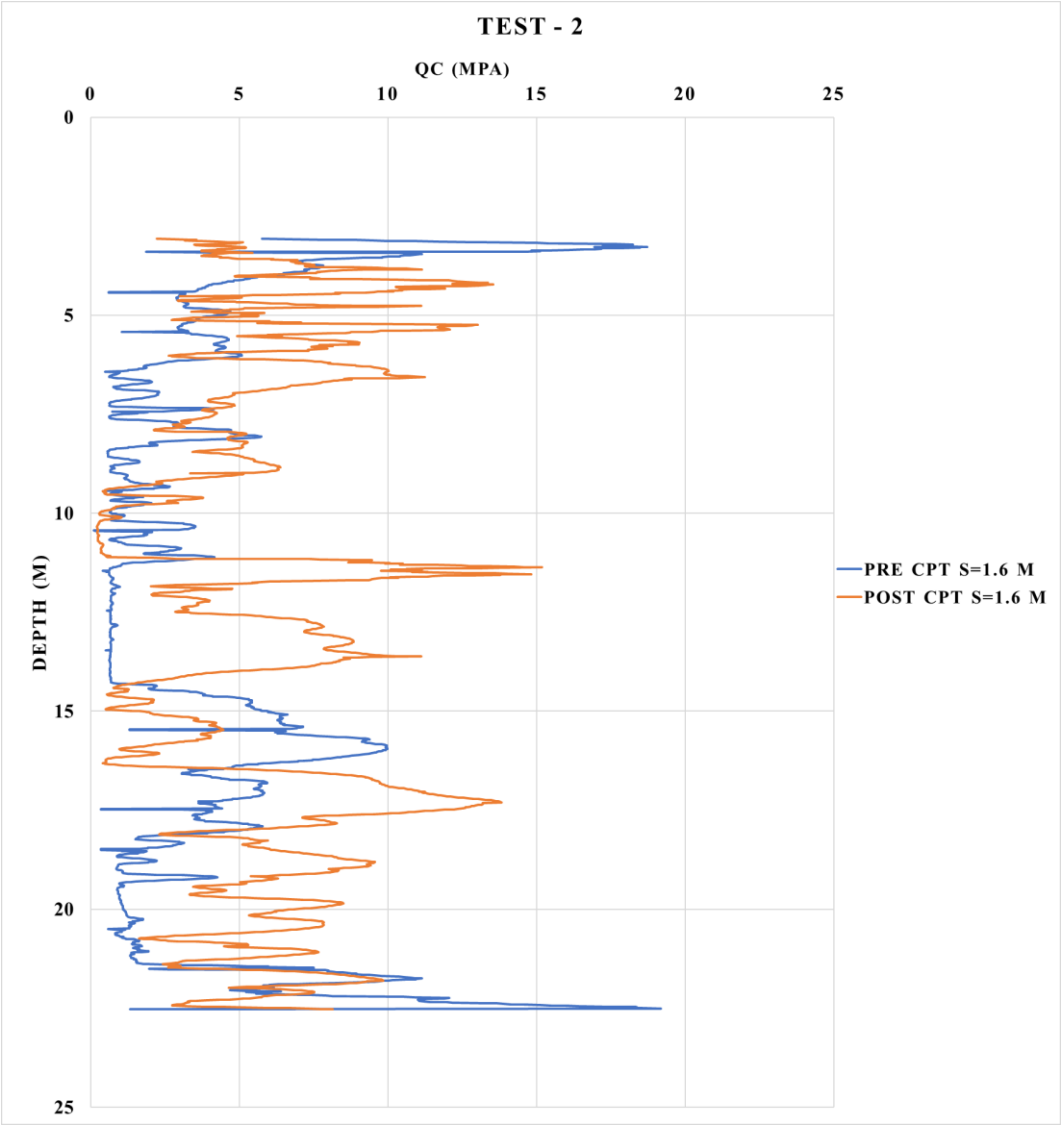

Figure 5.3 Pre and Post values of CPT (Test-2 for 1.6m spacing)

When the CPT test 2 cone tip resistances are evaluated, it is seen that the average values of 4 MPa between 3 m and 10 m increased to 7-8 MPa. Between 10 meters and 23 m depths, the cone tip resistance values increased from an average of 3 MPa to about 6-7 MPa.

A 1.1 to 4 times increase in cone tip resistance was observed before and after the improvement. The percentage increase in the cone tip resistance value provided an idea of the level of soil improvement. All the empirical methods representing the relationship between q_c and D_r investigated in the literature section (4.3.4.1) were examined with this information. The empirical approach to be used in calculating the soil stiffness values to be used in the analyses was chosen accordingly. In this context, the empirical method that is thought to express best the amount of increase in the cone tip resistance values was

used to calculate the values. Robertson & Campanella, (1983) proposed an empirical relationship between q_c, initial effective vertical stress (σ'_{vo}), relative density (D_r), and two empirical parameters, C_1, and n. The relationship can be written as:

$$q_c = C_1 * (\sigma_v)_o{}' * D_r^n \quad (5.1)$$

where q_c is the cone tip resistance, σ'_{vo} is the effective overburden stress, D_r is the relative density, C_1 and n are empirical parameters that depend on the soil type and testing conditions. This relationship is commonly used in geotechnical engineering practice to estimate soil strength and evaluate ground improvement techniques' effectiveness.

Relative density values calculated from q_c values obtained from CPT before and after the improvement with stone columns are presented in Figure 5.4 and Figure 5.5 below for Test-1 and Test-2. According to the relative density values obtained by the analytical method, an average increase of almost 4 times was observed for Test-1. These improvement values reached up to 9 times in the first 8 meters. For Test-2, the average relative density values increased about 3 times for the first 8 meters and about 0.2 times for the last 4 meters. The last 4 meters did not show the expected improvement percentage. However, the average improvement between 8 m and 16 m is around 5 times.

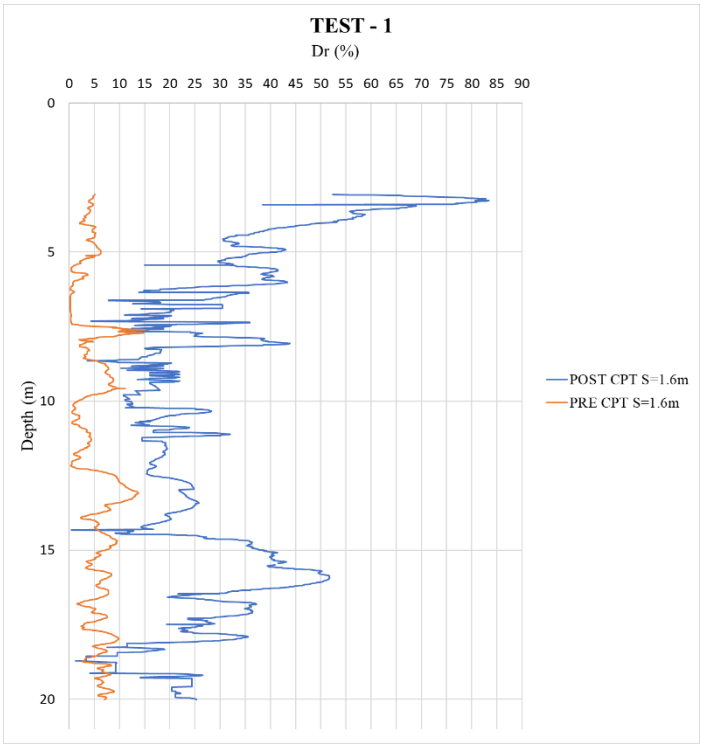

Figure 5.4 D_r values from CPT Test-1 cone tip resistance values

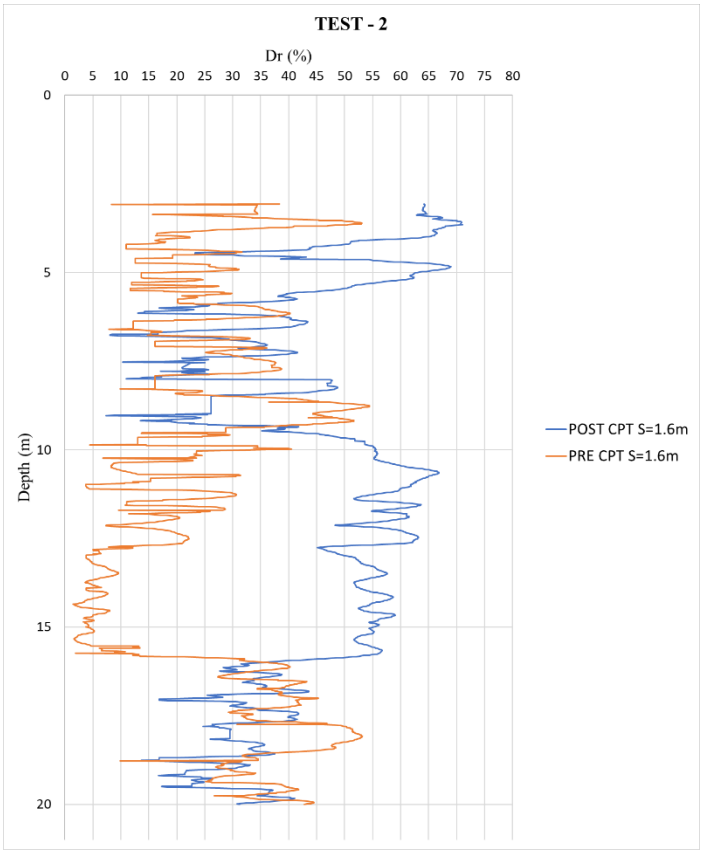

Figure 5.5 D_r values from CPT Test-2 cone tip resistance values

The following table has been used to assess the soil condition in saturated sand (Kirsch & Kirsch, 2010). According to this table, it is seen that the soil subject of this thesis has changed from very loose to medium dense.

Table 5.1 Values representing the physical properties of fully saturated sands (Source: Kirsch & Kirsch, 2010)

	Very Loose	Loose	Medium Dense	Stiff	Very Dense
D_r (%)	<15	15-35	35-65	65-85	85-100
CPT-q_c (MN/m^2)	<5	5-8	8-15	15-20	>20

5.3. Modeling of Stone Columns

The finite difference software FLAC 3D is used in this study for the analyses of liquefaction of a small group of stone columns (loose silty sand soil improved by four stone columns) and unimproved soil; these analyses are performed in the form of a nonlinear elastoplastic behavior fully coupled with a pore pressure accumulation

(effective stress) criterion; this behavior is summarized in the form of the Finn model in FLAC 3D software.

5.3.1. Meshing and Boundary Conditions

The FLAC 3D soil model has a total of 2246 mesh and 5304 solid elements. The boundary conditions are split into static calculation and dynamic calculation phases. In the static phase, the normal displacement around the model is constrained, and the base of the model is a fixed boundary. In the dynamic phase, the static computational boundary conditions of the model are removed. To avoid wave distortion, a free boundary is set around the model, and the base of the model is set as a viscous boundary.

5.3.2. Geometry

The numerical model is a square cross-section of 14.4 m and a depth of 25.0 m; there are four stone columns with a length of 20 m, center-to-center spacing is 1.6 m, and the diameter of the stone columns implanted in the loose soil layer is 0.8 m (Figure 5.6) the soil layer is defined homogeneous. In the numerical model, the mesh size needs to be reduced in order to avoid convergence problems (Section 5.3.3) depending on the diameter of the stone columns. For this reason, the mesh size of soils between the columns are densified.

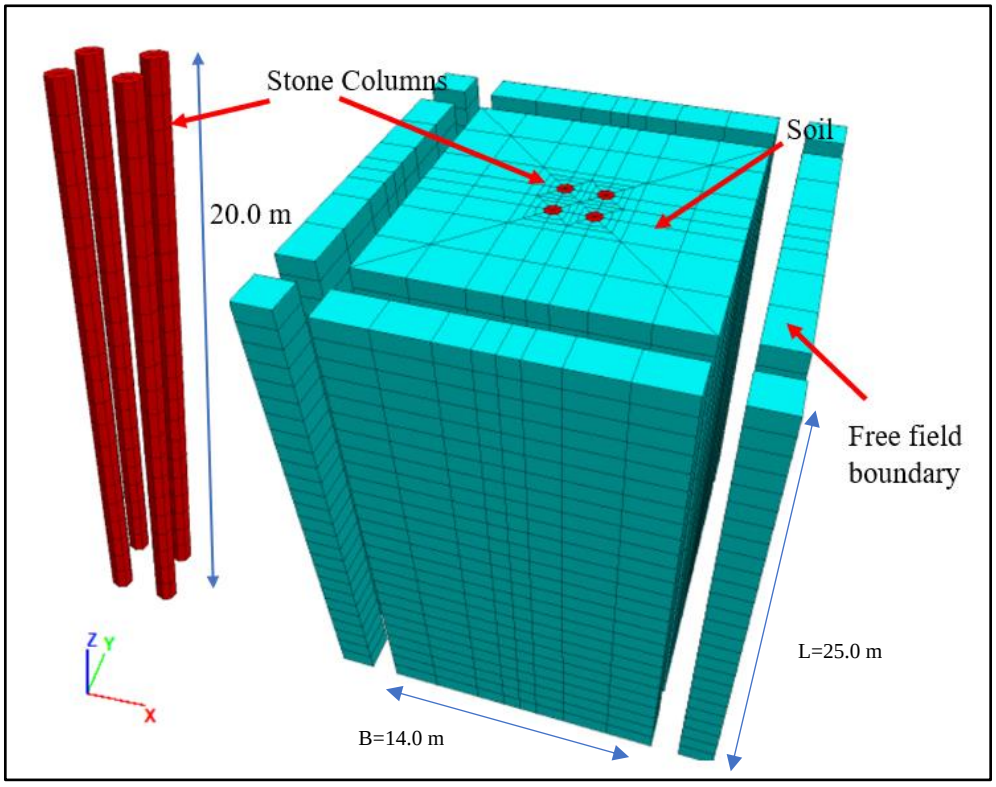

Figure 5.6 Soil and stone columns model and mesh system

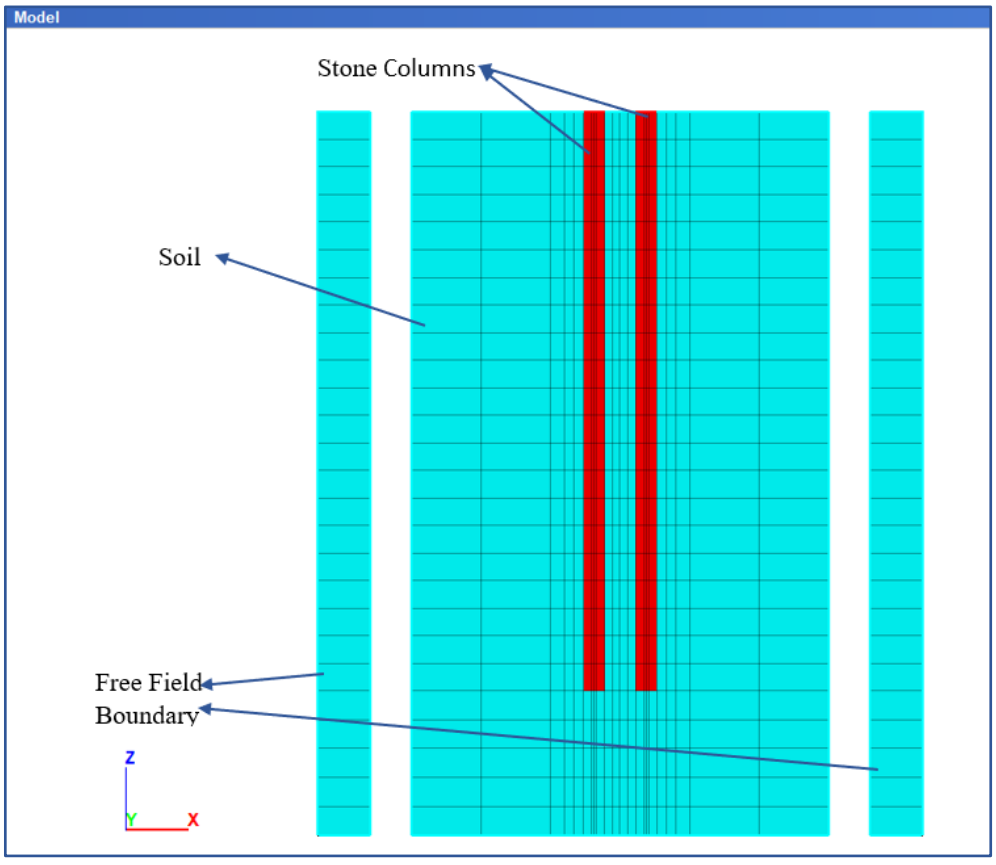

Figure 5.7 Analysis model section view

5.3.3. Mesh Convergence

Determining the mesh size is essential for numerical simulations' accuracy and fast convergence. Grids that are too fine can cause slower convergence than desired and may lead to erroneous results. The frequency content of the input wave and the wave velocity characteristics of the system affect the numerical accuracy of the wave transmission and may lead to numerical distortion of the transmitted wave. To address this issue, the size of the element is given in the equation below (Kuhlmeyer & Lysmer, 1973):

$$l = \lambda(1/8 \sim 1/10) \tag{5.2}$$

Where λ is the wavelength of the input excitation corresponding to the peak frequency. It is crucial to keep the relationship between the grid intervals within acceptable ranges in order to propagate the frequency correctly. In this context, according to the Equation 5.3 given below, the speed of s wave propagation through the soil medium (C_s) is calculated as 42 m/s.

$$C_s = \sqrt{G/\rho} = 42\ m/s \tag{5.3}$$

Depending on the frequency and speed of s wave propagation through the soil, the maximum mesh size that can be accurately modeled for the propagation of waves through the model is 2.1 m (Equation 5.4). Frequency is taken as 2 Hz and the speed of s wave propagation through the soil medium (C_s) is calculated as 42 m/s.

$$\mathrm{f} = \frac{C_s}{\lambda} = \frac{C_s}{10 * \Delta l} \tag{5.4}$$

5.3.4. Constitutive Model and Material Properties

The Finn constitutive model parameters C_1 and C_2 used in the liquefaction analyses are based on the plastic Mohr-Coulomb model (presented in CHAPTER 4-Section 4.3.4 as Equation 4.8 and Equation 4.10. For this reason, the mechanical and physical parameters of the soil and the stone column are selected on the Mohr Coulomb material model. Parameters of soil and stone columns are given in Table 5.2 below:

Table 5.2 Properties of soil and stone columns

Depth (m)			Soil Material	Unit Weight	Poisson Ratio	Friction Angle	Modulus of Elasticity
				γ (kg/m^3)	v	ϕ	E (kPa)
0.0	-	25.0	Liquefiable Silty Sand Soil	1800	0.30	24	8000
0.0	-	20.0	Stone column	1900	0.30	45	40000

For liquefaction analysis, Finn soil model parameters (C_1 and C_2) are defined as explained in Section 4.3.4, according to the D_r values of soil. D_r values are calculated from empirical relation proposed by Robertson & Campanella, (1983). An empirical relationship and idealized soil parameters are determined according to the Byrne calculations for finding C_1 and C_2 values (Table 5.3). The parameter C_1 in Finn Soil Model controls the volume change as a function of the relative density, and the C_2 parameter in the Finn model controls the shape of the accumulated deformation curve with the number of cycles as a function of the relative density (Byrne B., 1991).

The improvement of the soil when stone columns are constructed by the vibroflotation method has been discussed in the literature section. The cone tip resistance values measured in CPTs before and after the improvement work in the investigation area support the previous studies on this subject. While liquefaction analyses were performed using FLAC 3D and Finn Model, the increase in the relative soil density of the soil during construction was also taken into consideration.

Table 5.3 Finn Model parameters

Soil Material Condition	Dr (%) (mean)	C_1*	C_2*
Before Improvement	20	4.240	0.094
After Improvement	50	0.429	0.932

*C_1 and C_2 are Finn Soil Model parameters

5.3.5. Interface

The interface shear strength is defined by the Mohr-Coulomb failure criterion. Because of the difference between the stone column and surrounding soil stiffness, the interface is used. According to the Itasca Consulting Group, maximum interface stiffness

values indicated by the rule-of-thumb were adjusted to ten times its neighbor's equivalent stiffness zone according to the equation below:

$$k_s = k_n = max\left[10 * \frac{K + {}^{4}/_{3} * G}{\Delta z_{min}}\right] \quad (5.5)$$

Where K and G are the bulk and shear modulus of the soil zone, respectively, and are the smallest dimension of an adjoining zone in the normal direction. Stiffness values that are used in the model are calculated using the relation as 4 GPa. Bulk modulus of water was used as 2.0×10^9 Pa.

Analyses were performed for three different cases as defined as follows:

1. Investigation of the liquefaction condition of the site with the parameters obtained from field tests performed before ground improvement,
2. Investigation of the state of improvement with stone columns and determination of liquefaction potential with the parameters obtained from field tests performed after soil improvement.

5.4. Dynamic Loading

An earthquake that happened in Düzce, Türkiye, on November 12, 1999, was applied to the bottom of the model. The local depth of the earthquake was approximately 14 km. The recorded amplitude was given as a_{max}=1.49g by the Kandilli source station.

The earthquake duration was 31.27 seconds, and strong accelerations lasted in the range of 6 to 10 seconds.

Due to the lack of representative “rock” input motions, deconvolution of recorded surface motions is a suitable alternative to accurately characterize the earthquake wave down to the depth of the engineering bedrock. Deconvolution consists of inputting an outcropping motion at the surface of a 1D soil column and using an equivalent linear analysis to calculate the acceleration-time history at a point below the ground surface. Time-dependent acceleration-velocity displacement data are presented in Figure 5.8 obtained using many surface motions.

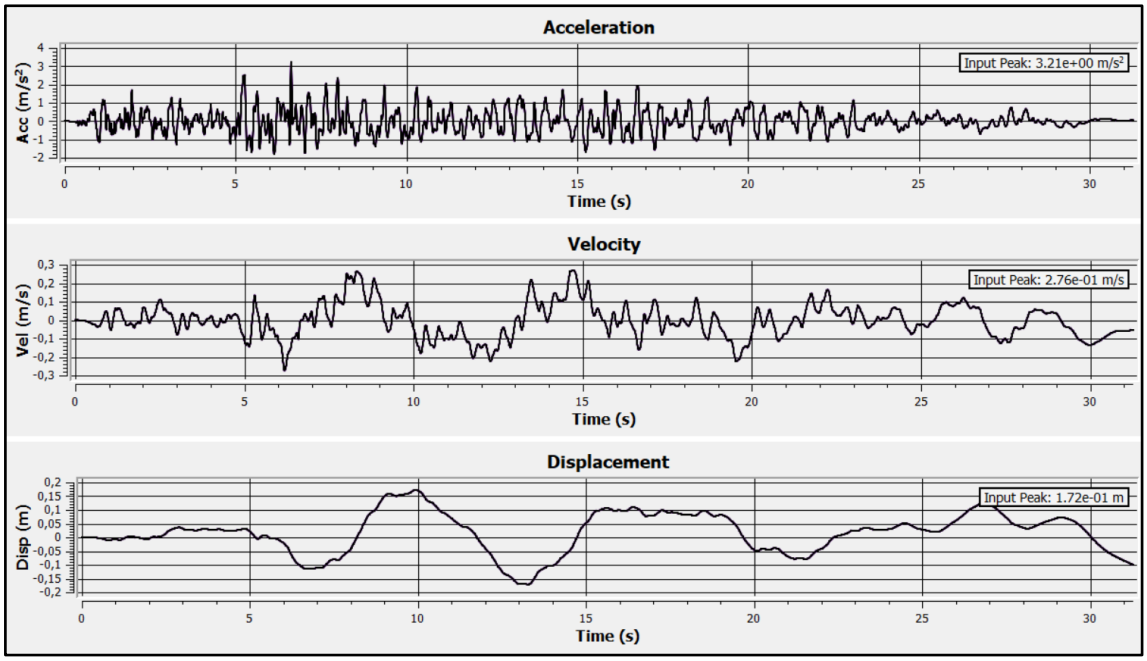

Figure 5.8 Time-dependent- acceleration-velocity and displacement graph of Düzce earthquake in Flac 3D dynamic input wizard

5.5. Results and Discussions

Liquefaction and settlement analyses were performed using the soil parameters obtained from the field data recorded in the field before the ground improvement works. Evaluations of the results obtained are given under the following headings.

5.5.1. Excess Pore Water Pressure (EPWP)

The numerical analysis results of excess pore pressure ratio (EPPR) of the unimproved site graph is shown in Figure 5.9. The calculation method of the excess pore pressure ratio is as shown in Equation 5.6.

$$r_u = \frac{\Delta u}{\sigma'_{vo}} \tag{5.7}$$

Where Δu is the EPWP, and σ'_{vo} is the initial vertical effective vertical stress.

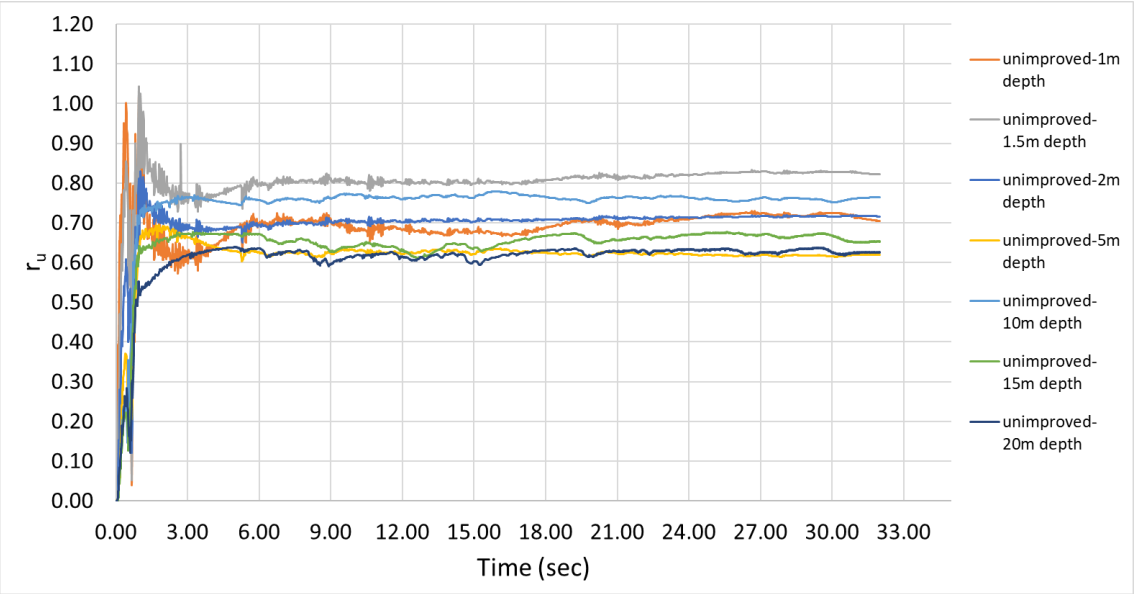

Figure 5.9 Excess pore water pressure ratio values concerning depth unimproved soil

The liquefaction process starts when the earthquake motion causes the grains in the soil to rearrange themselves, leading to a loss of contact between particles. As a result, the soil behaves like a fluid, and the excess pore water pressure increases rapidly within the soil. As shown in the graph above (Figure 5.9), the r_u value decreases after a while, which is thought to be due to the dissipation of excess water through the pores. The decrease in r_u value does not change the fact that the soil loses strength. Improvement works should be carried out in the investigation area with stone columns to dissipate the excess pore water pressure before the soil reaches the liquefaction state.

Excess pore water pressure is the pressure above and beyond the static groundwater pressure that exists within the soil pores. During an earthquake, shaking causes the water within the soil pores to become pressurized. When the excess pore water pressure equals the effective stress (the stress carried by the solid grains of the soil), the soil loses its strength and stiffness, leading to a loss of shear strength. At this point, the excess pore water pressure ratio reaches 1.0, and liquefaction occurs. As seen in the graph below (Figure 5.10), it is easier for the excess pore water pressure value to reach the liquefaction value because the effective stress of the soil has a smaller value in the first 2 meters from the ground level.

The sudden increase in pore water pressure in the first 0.8-0.9 seconds excess pore water pressure ratio exceeds 1.0. When the excess pore water pressure ratio exceeds 1.0,

it indicates that the soil's shear strength has been compromised due to the high pore water pressure (Figure 5.10).

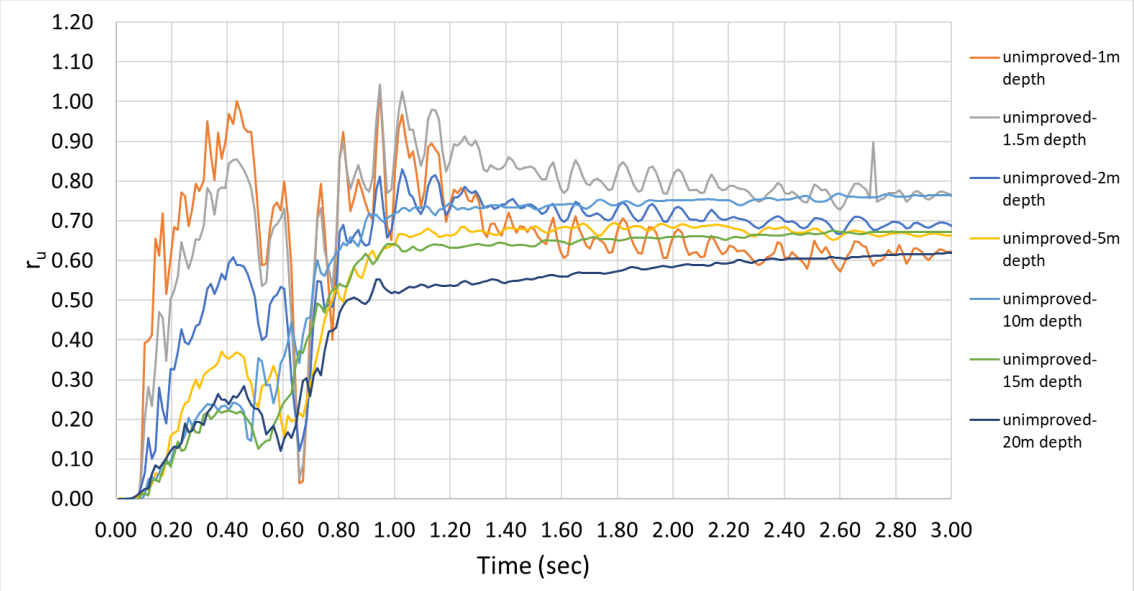

Figure 5.10 Sudden increment of pore water pressure ratio values in first 3 second concerning depth unimproved area for first 3 seconds

Improvement work was carried out with stone columns to reduce the r_u values by dissipating the excess pore water pressure. The pore pressure values recorded after numerical analysis under the center of the foundation at different depths (1.0 m, 1.5 m, 2.0 m, 2.0 m, 5.0 m, 10.0 m, 15.0 m, and 20.0 m from the ground), without and with stone columns, are presented in the following figures.

σ'_{vo} values are 7 kPa, 10.5 kPa and 14 kPa for 1.0 m, 1.5 m and 2.0 m depth, accordingly. For these depths, a decrease of approximately 4.0 kPa, 6.5 kPa, and 10.0 kPa in increasing excess pore water pressure (Δu) was observed for the case improved with stone columns, respectively. The liquefaction potential for the first 2 meters decreased by 78%, 82%, and 87%, correspondingly.

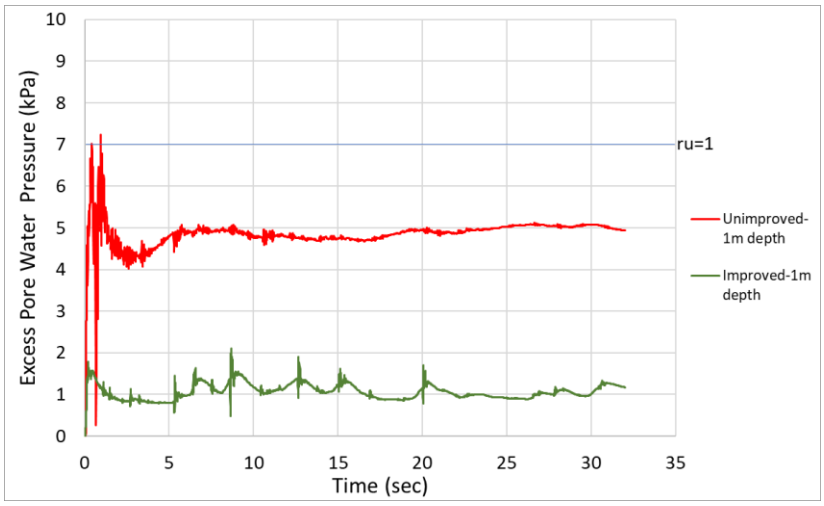

Figure 5.11 Change in excess porewater pressure by time at a depth of 1.0 m

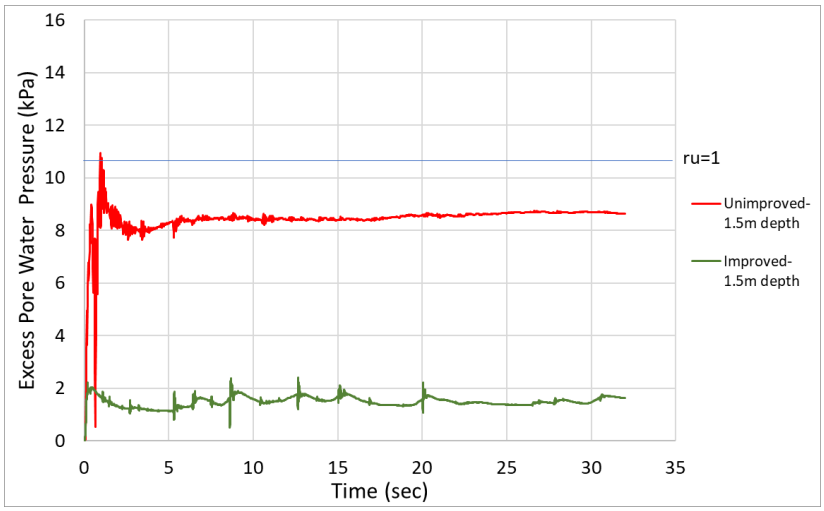

Figure 5.12 Change in excess porewater pressure by time at a depth of 1.5 m

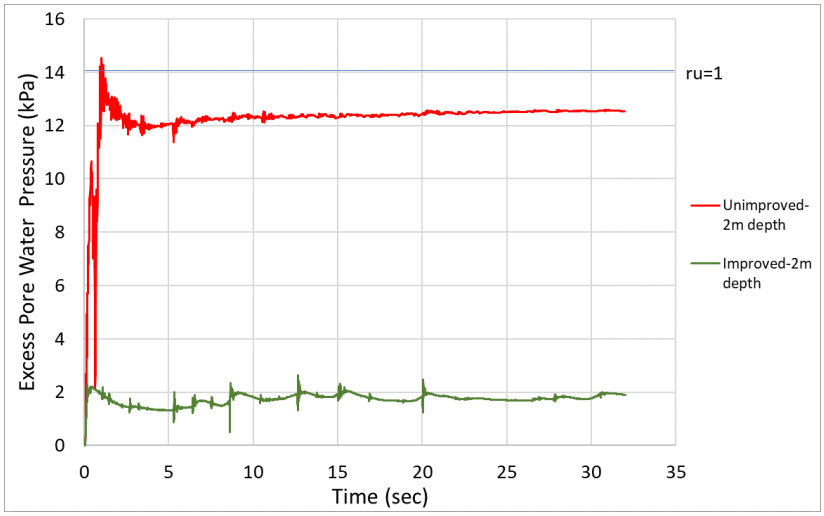

Figure 5.13 Change in excess porewater pressure by time at a depth of 2.0 m

σ'_{vo} values are 35 kPa, 70 kPa, 105 kPa and 140 kPa for 5.0 m, 10.0 m, 15.0 m and 20.0 m depth, accordingly. From the surface to the depths, the initial effective stress values increase, and the increases in excess pore water do not increase enough to cover this difference, that is why liquefaction becomes more difficult to observe. As shown in Figure 5.14, Figure 5.15, Figure 5.16, and Figure 5.17, the liquefaction potential decreased 88%, 91%, 95% and 96% between 5 m and 20 m depths. At the same time, it can be seen from the decrease in the increases in excess pore water pressure that the dissipation to the stone columns under the earthquake effect is more effective at the depths indicated.

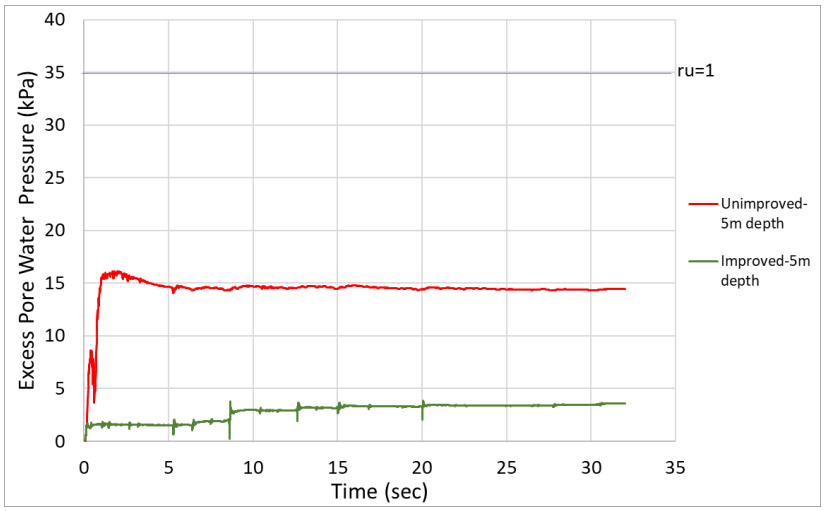

Figure 5.14 Change in excess porewater pressure by time at a depth of 5.0 m

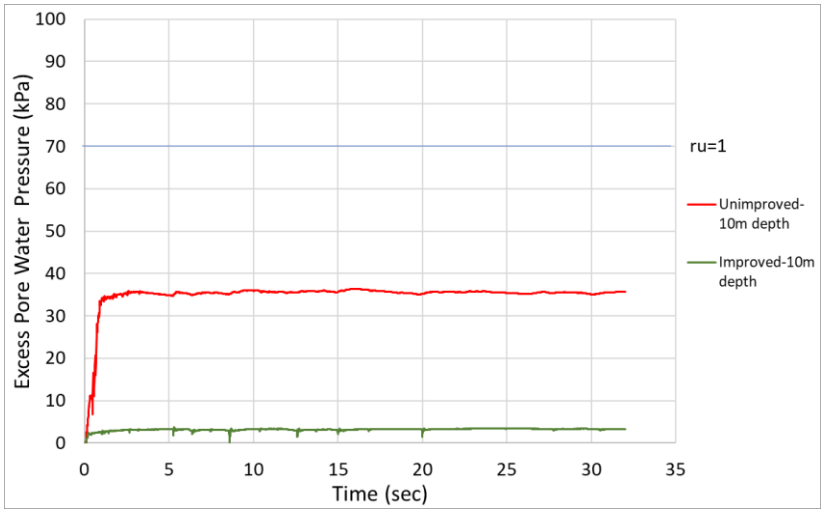

Figure 5.15 Change in excess porewater pressure by time at a depth of 10.0 m

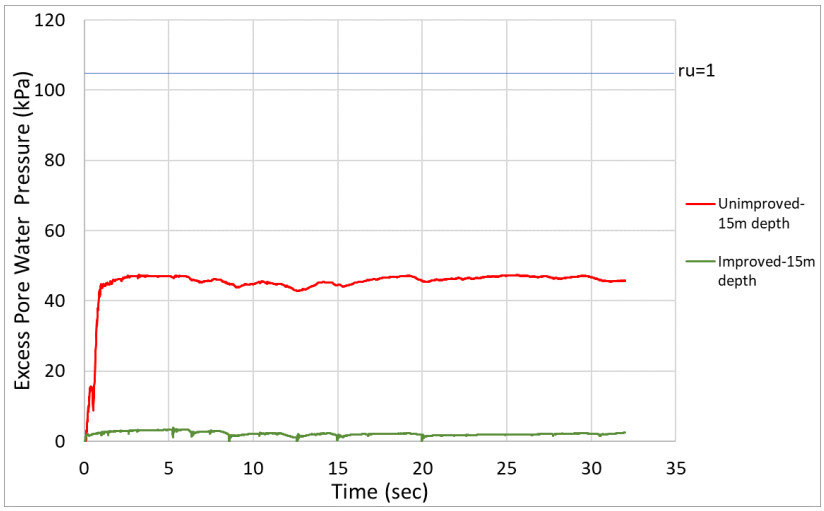

Figure 5.16 Change in excess porewater pressure by time at a depth of 15.0 m

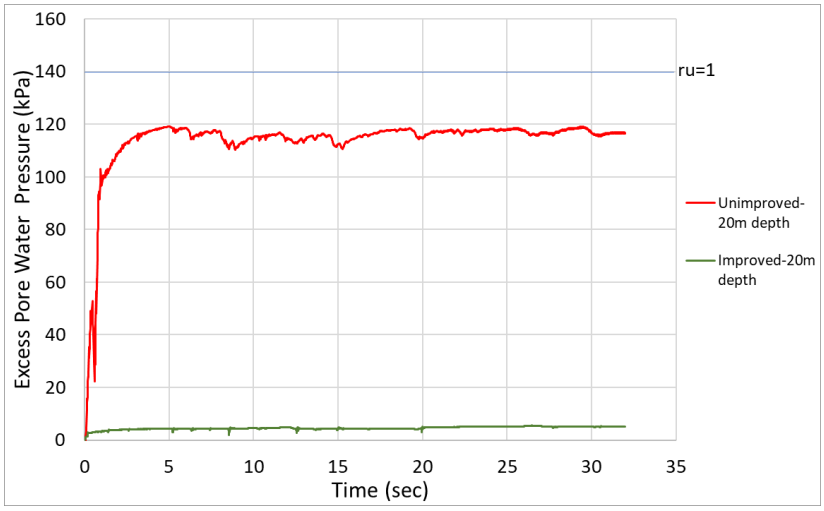

Figure 5.17 Change in excess porewater pressure by time at a depth of 20.0 m

Liquefaction typically occurs when the excess pore water pressure ratio to the effective vertical stress ($r_u = \Delta u / \sigma'_{vo}$) reaches 1.0. The analyses show that liquefaction of the soil is much easier to occur at shallow depths (e.g., the first 2 meters) due to the small effective stresses. This is because the effective stresses are much lower at these depths, and the increase in excess pore water pressure can easily reach the effective stress. In addition, in liquefaction analyses, especially in the first 1.5 meters, the r_u value exceeded 1.0. Some studies have shown that permanent changes in the total stress can occur due to dynamic effects, and the peak value of r_u can be considerably larger than 1.0 (Fiegel & Kutter, 1994). It is thought that the permanent increase in total stresses may be due to the rising water table elevation (Ecemis et al., 2015).

As a result of the analyses, the decrease in pore water pressures was recorded without and after the stone column construction. The construction of stone columns resulted in a decrease in liquefaction potential. Percent improvement of the soil was calculated using the excess pore water pressures obtained from the last second of the earthquake numerical analysis, and the results are presented in Table 5.4 and Figure 5.18.

Table 5.4 EPWP increment values varying depth under earthquake loading

Depth (m)	Unimproved Soil Δu Values (kPa)	Improved Soil Δu Values (kPa)	Percentage of Improvement (%)
1.0	5	1	77
1.5	9	2	81
2.0	13	2	87
5.0	14	2	87
10.0	36	3	91
15.0	46	2	95
20.0	116	5	96

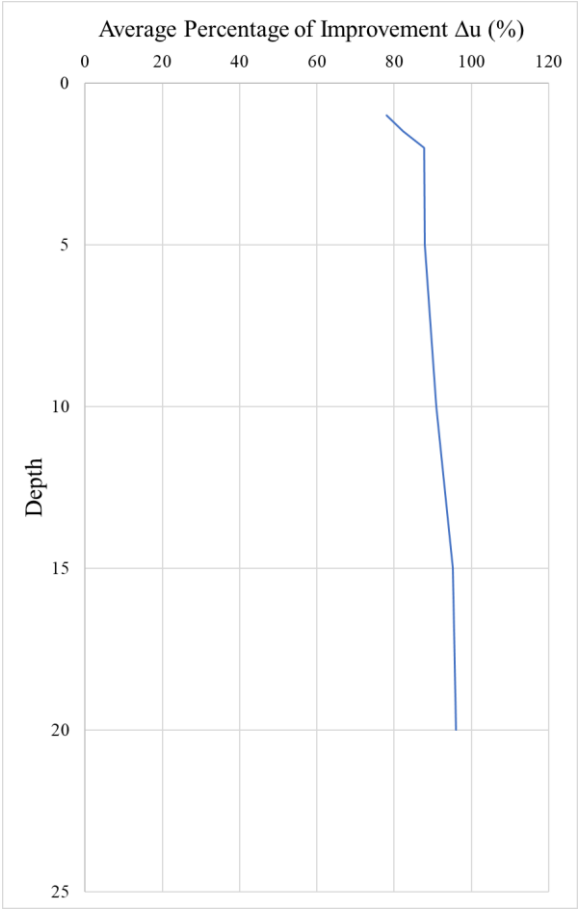

Figure 5.18 Percentage of EPWP increment before and after improvement by the depth at the end of earthquake loading

5.5.2. Settlement Analysis

Settlement analysis was made in the unimproved condition and the improved state with stone columns under the cyclic loading. Within the scope of the suitability investigations for the structure to be built on the site, the structure load was also included in the settlement analysis. The structural load was defined as 100 kPa in the analysis. As a result of the analyses, the time-dependent displacement graphs in the unimproved condition and the improved condition with stone columns are presented in the figures below.

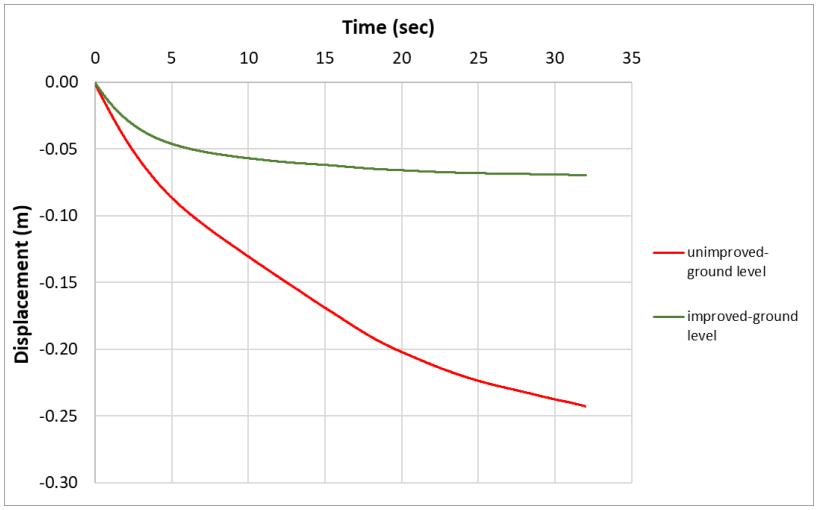

Figure 5.19 Displacement by time from the soil surface under earthquake loading and stress of 100 kPa

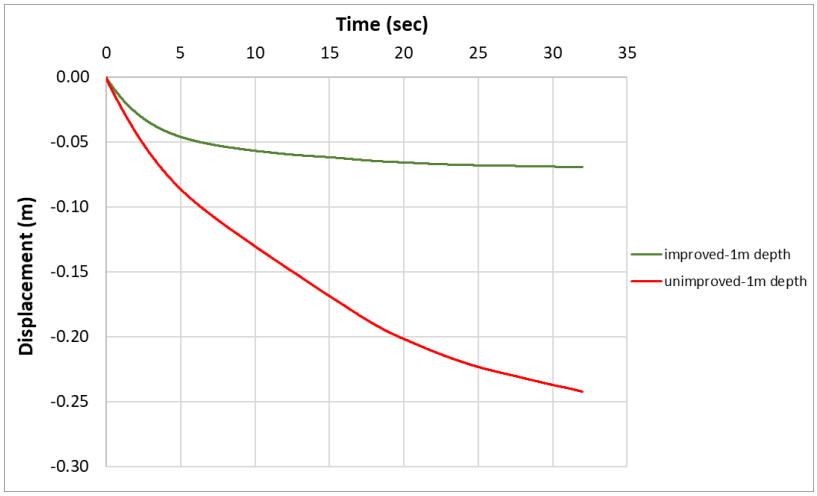

Figure 5.20 Displacement by time from 1.0 m depth under earthquake loading and stress of 100 kPa

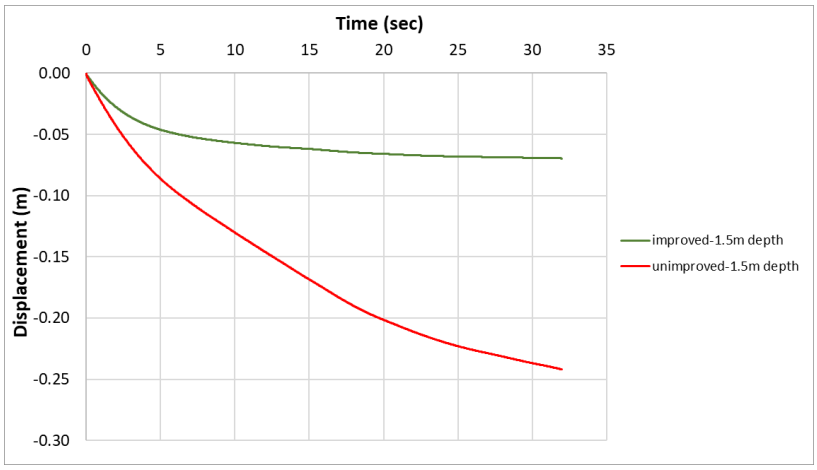

Figure 5.21 Displacement by time from 1.5 m depth under earthquake loading and stress of 100 kPa

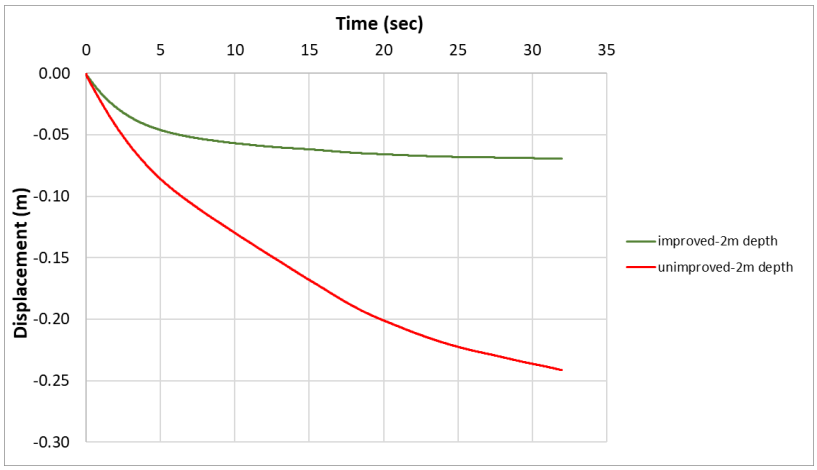

Figure 5.22 Displacement by time from 2.0 m depth under earthquake loading and stress of 100 kPa

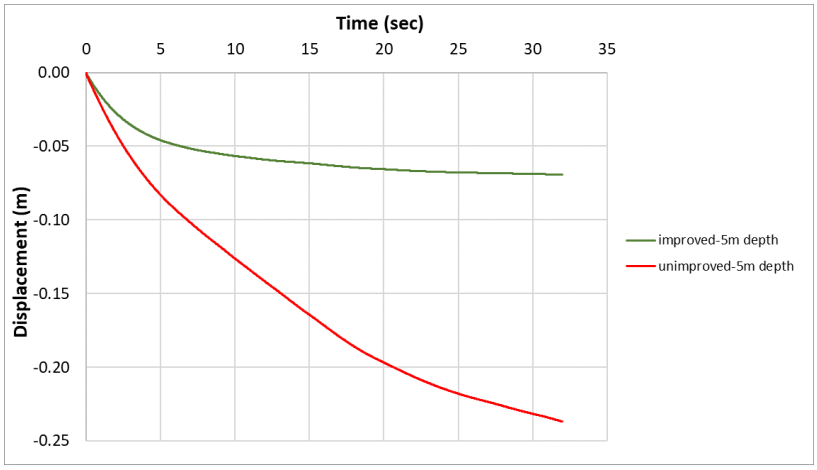

Figure 5.23 Displacement by time from 5.0 m depth under earthquake loading and stress of 100 kPa

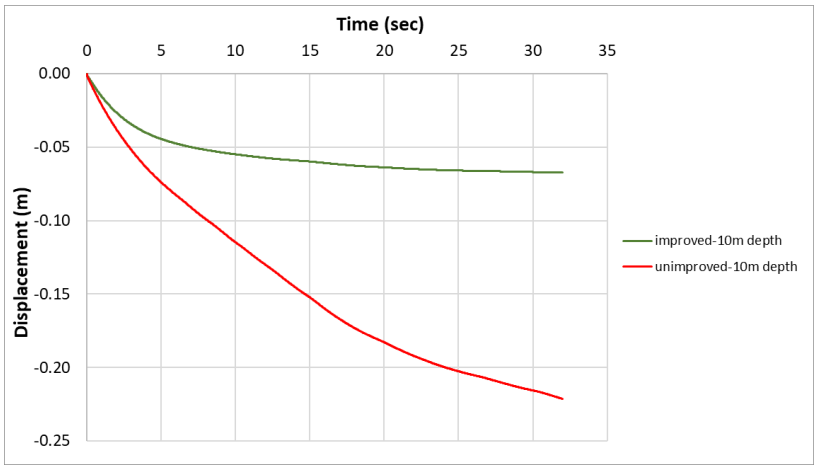

Figure 5.24 Displacement by time from 10.0 m depth under earthquake loading and stress of 100 kPa

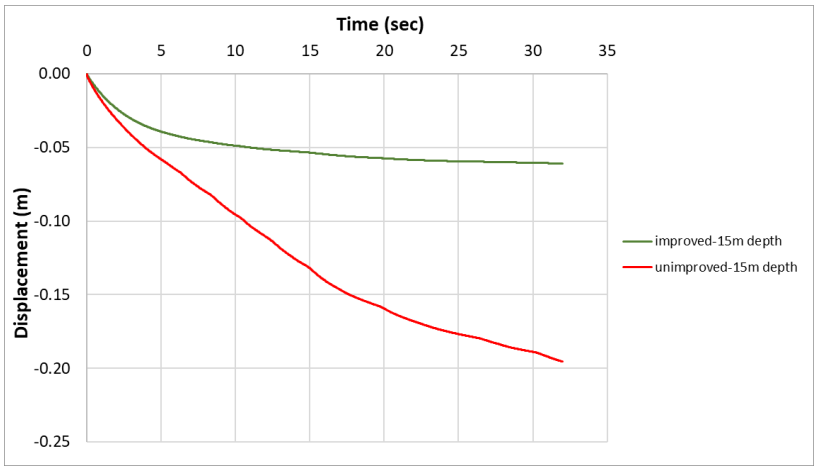

Figure 5.25 Displacement by time from 15.0 m depth under earthquake loading and stress of 100 kPa

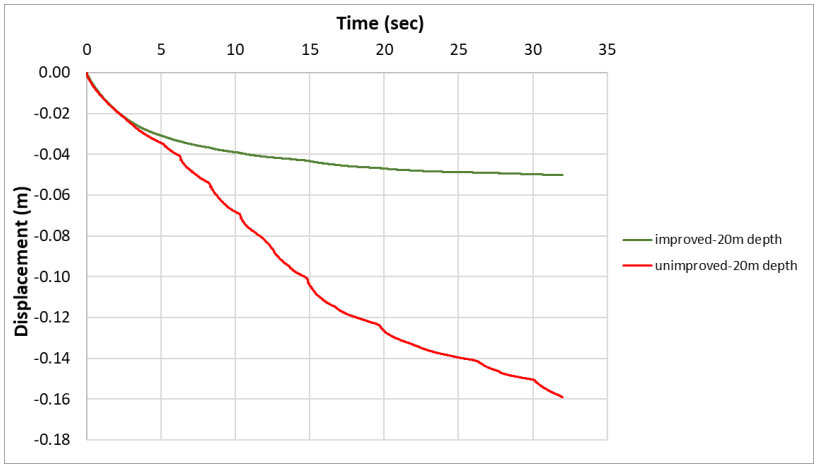

Figure 5.26 Displacement by time from 20.0 m depth under earthquake loading and stress of 100 kPa

Settlement analyses were performed for the structure, the free field under earthquake loads, and the soil improved with stone columns. As a result of the analyses, it was observed that the settlement values decreased significantly after the soil was improved with stone columns. The settlement values recorded at the last second of the earthquake effect and the percentage improvements obtained are summarized in Table 5.5 and Figure 5.27. Analyses performed during the earthquake force show that as the depths are more profound, the settlement improvements decrease. Earthquake loading, which affected the bottom of the model, caused soil movement and rearrangement. This resulted in less improvement in settlement with increasing depth.

Table 5.5 Settlement values under surcharge and earthquake loading

Depth (m)	Unimproved Soil Settlement Values (cm)	Improved Settlement Values (cm)	Percentage of Improvement (%)
0.00	24.30	6.96	71
1.00	24.20	6.96	71
1.50	24.20	6.94	71
2.00	24.10	6.93	71
5.00	23.70	6.92	71
10.00	22.10	6.74	70
15.00	19.50	6.09	69
20.00	15.90	5.02	68

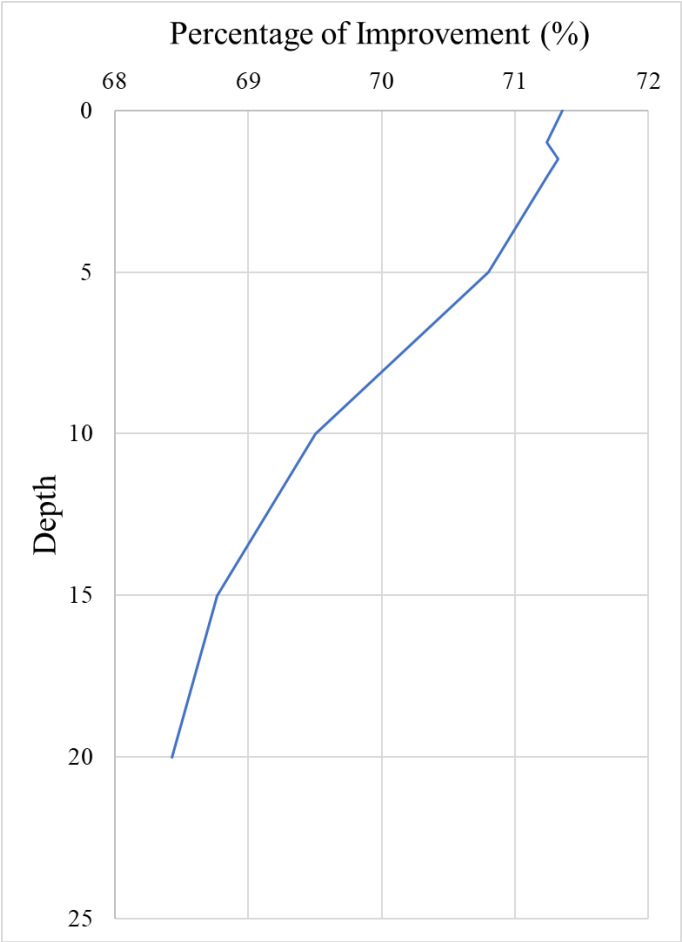

Figure 5.27 Percentage of settlement improvement by the depth at the end of earthquake loading

5.6. Conclusion

In this section, in first place, CPT data obtained pre and post-improvement of the stone columns are discussed. From the CPT data obtained, the relative density values of the soil were calculated with the correlation proposed by Robertson & Campanella, 1983. Liquefaction and settlement analyses were performed with FLAC 3D software by using the relative density of soil obtained from the correlation of the field data as a Finn Model parameter. Liquefaction evaluations were performed by controlling the excess pore water pressure ratio to the effective vertical stress ($r_u = \Delta u / \sigma'vo$). As a result of the analyses, it is concluded that the liquefaction potential of the soil is high in the first 5.0 meters in the unimproved area. This is because the initial effective stress values are very low up to this depth under the earthquake action, and excess pore water pressure can quickly rise to this level. In addition, it is observed that r_u instantly exceeds 1.0 in the first 2.0 meters in

depth. This is explained as a permanent increase in the groundwater level under the earthquake effect, causing a permanent change in the total stresses.

In the settlement analyses, the behavior of the unimproved soil and the soil improved with stone columns were investigated under structural load in addition to dynamic loads. It was observed that the settlement values of the soil improved with stone columns decreased by 70% compared to the settlement values of the unimproved soil.

As a result, it has been shown that during the construction of stone columns, drainage is provided by the vibroflotation method. Thus, the pore water pressure decreases, the relative soil density (D_r) increases, and therefore, the settlement values decrease Seed & Booker, (1977) and Ecemiş, (2013). Therefore, it provides an improvement in terms of settlement and liquefaction problems.

CHAPTER 6

CONCLUSION

Recent earthquakes and studies show that generating excess pore water pressures acting on soils under cyclic loading can lead to significant damage. In order to eliminate this effect and ensure the structure's safe construction, the soil should be improved with one of the improvement methods that can dissipate the excess pore water. Stone columns are an effective improvement method to increase liquefaction resistance and reduce excess pore water pressure (Seed and Booker, 1977; Priebe, 1998; Ishihara & Yamazaki, 1980 and Qu, 2005). It is mentioned in the literature review that stone columns constructed by the vibroflotation method improve the surrounding silty sandy soil (ex: Kirsch & Kirsch, 2010). These improvements were confirmed by the CPT data obtained before and after the stone column construction. The cone tip resistance values measured in the CPTs before and after the improvement works with stone columns in the investigation area, which were investigated within the scope of this thesis, support the previous studies on this subject.

Using the SPT and CPT data obtained from the site, the liquefaction of the site was determined by empirical methods developed by Seed and Idriss, (1997) and Boulanger and Idriss, (2014), respectively. At the same time, the relative density of the soil was calculated by the empirical method developed by Robertson & Campanella (1983) from the cone tip resistance values obtained from the field CPT data. In this way, the CPT data obtained from the field can be used as a Finn Material model parameter in FLAC 3D software. With the excess pore water pressure values obtained from the analyses, liquefaction is considered to occur when the initial state effective stress ratio ($ru = \Delta u / \sigma'_{vo}$) reaches 1.0. Three-dimensional liquefaction analyses performed with the soil parameters calculated for the pre-improvement condition showed that the liquefaction potential was very high in the first 5.0 meters depth. However, due to the permanent changes observed in the total stress under the earthquake effect, it was observed that the r_u value exceeded 1.0 instantaneously in the first 2.0 meters of depth (Fiegel & Kutter, 1994).

The improvement of the soil caused by the stone columns constructed by the vibroflotation method in sandy soil was determined by the cone tip resistance values

obtained from CPT after construction. The cone tip resistance increased between 150% and 300% before and after the improvement. Similar increases were obtained in the relative density values obtained from the cone tip resistance values correlated by Robertson & Campanella, (1983). After the improvement, the relative densities obtained by the correlation of the CPTs were defined as Finn model parameters to the soil around the stone column, and the analysis was performed again. The excess pore water pressures in the unimproved soil obtained from the three-dimensional dynamic analysis were compared with the excess pore water pressures in the soil improved with stone columns. Excess pore water pressure values decreased by 82% in the first 5 meters depth and decreased by about 92% for the next 15.0 meters. It was observed that the liquefaction potential of the soil improved with stone columns was eliminated due to the dissipation of excess pore water pressure by stone columns. Stone column design is a widely used method to eliminate the liquefaction potential of sandy soils. The results obtained within the scope of this study coincide with the studies presented in the literature (Pestana, (1998); Adalier et al., (2003); Sivakumar et al., (2004); Adalier & Elgamal, (2004); Bouassida & Frikha (2015); Esmaeili & Hakimpour, (2015); Ecemiş, (2013); Tang et al., (2016); Meshkinghalam et al., (2017) and Beyaz et al., 2021).

In order to calculate the settlements that will occur in the structure due to the earthquake loading effect, the surcharge load of 100 kPa was added to the analysis. As a result of the analyses, it demonstrates that the structure will settle at the level of 25.0 cm if it is constructed without the use of the improvement method. It is observed that the amount of settlement that may occur in the soil under earthquake load is not suitable for construction. The settlement analysis performed after the improvement with stone columns determined that the settlement value decreased to 7.0 cm and provided a 71% improvement at the ground surface under surcharge and earthquake loading. Analyses performed during the earthquake force show that as the depths are deeper, the settlement improvements decrease. Earthquake loading which affected the bottom of the model, caused the soil movement and rearrangement. This resulted in less improvement in settlement with increasing depth.

While designing stone columns in sandy soils, the increase in density of the soil during construction should be considered depending on the construction method, and the layout, spacing, diameter, and material properties to be used in the construction of stone columns should be determined accordingly. Within the scope of this study, the soil improvements according to the stone columns' construction method were calculated using

various variations, and data obtained from the field were projected in this way in the analyses.

6.1. Recommendation for Future Research

In this thesis, the numerical analyses are presented and discussed with respect to related previous studies and the results are summarized. The potential topics for future work are presented in the following order.

- The earthquake data used in this thesis was obtained from previously recorded earthquake records. If potential earthquake data that may occur in the study area is shared, control can be ensured.
- Finn Material Model was used for numerical modeling of the liquefaction condition. The results can be compared by re-solving the numerical analysis with different soil models, such as UBCSAND Constitutive Model.
- Artificial earthquakes can be generated in the study area and the liquefaction potential of the site improved with stone columns can be assessed again with the help of field tests such as CPT.

  In the numerical analysis, it had been assumed that the soil has homogeneous behavior, the analysis can be performed with layered soil.

REFERENCES

Afet ve Acil Durum Yönetimi Başkanlığı. (2018). TBDY – Türkiye Bina Deprem Yönetmeliği. Ankara: Türkiye Cumhuriyeti İçişleri.

Book of Standard Vol. 04.08. (2005). *Standard Test Method for Mechanical Cone Penetration Test of Soil.* ASTM.

Abbasi, B., Russell, D., & Taghavi, R. (2013). FLAC3D mesh and element quality. *Continuum and Distinct Element Numerical Modeling in Geomechanics*.

Adalier , K., & Elgamal, A. (2004). Mitigation of liquefaction and associated ground deformations by stone columns. *Engineering Geology*, 275-291.

Adalier, K., Elgamal, A., Meneses, J., & Baez, J. (2003). Stone columns as liquefaction countermeasure in non-plastic silty soils. *Soil Dynamics and Earthquake Engineering*, 571-584.

Ammari, K., & Clarke, B. (2018). Effect of Vibro Stone-Column Installation on the Performance of Reinforced Soil. *American Society of Civil Engineers (ASCE)*.

ASTM D5778-9. (2000). *Standard Test Method for Performing Electronic Friction Cone and Piezocone Penetration Testing of Soils.*

Balaam, N., & Booker, J. R. (1985). Effect of Stone Column Yield on Settlement of Rigid Foundation in Stabilized Clay. *International Journal For Numerical And Analytical Methods In Geomechanics,*, 331-351.

Barksdale, R., & Bachus, R. (1983). *A. Design and construction of stone columns.* Federal Highway Administration,.

Bathe, K., & Wilson, E. (1976). Numerical Methods in Finite Element Analysis. *Englewood Cliffs*.

Bergado, D., Anderson, L., Miura, N., & Balasubramaniam, A. (1996). *Soft ground improvement in lowland and other enviroment.* New York, USA: ASCE press.

Beyaz, T., Kayabali, K., & Sonmezer, Y. B. (2021). Investigation of the effect of the relative density and shear strain on liquefaction of sands. *Pamukkale University Journal of Engineering Sciences*, 436-438.

Bohn, C., & Lambert, S. (2013). CASE STUDIES OF STONE COLUMNS IMPROVEMENT IN SEISMIC AREAS.

Bouassida, M., & Frikha, W. (2015). Effect of Granular-Column Installation on Excess Pore Pressure Variation during. *International Journal of Geomechanics*.

Boulanger, R. W., & Idriss, I. M. (2008). Liquefaction Susceptibility Criteria for Silts and Clays. *Journal of Geotechnical and Geoenvironmental Engineering*, 1027–1028.

Boulanger, R., Idriss, I., Stewart, D., Hashash, Y., & Schmidt, B. (1998). Drainage capacity of stone columns or gravel drains for mitigating. *Geotechnical Special Publication No. 75 Geotechnical Earthquake Engineering and Soil Dynamics III* (s. 678-690). Seattle, Washington: American Society of Civil Engineers.

Brown, R. E. (1977). Vibroflotation Compaction Cohesionless Soils. *Journal of the Geotechnical Engineering Division*, 1437-1451.

BS EN 1097-2. (1998). *Tests for mechanical and physical properties of aggregates.* Standards Board.

BS EN ISO 22476-12. (2009). *BS-EN-Geotechnical Investigation and Testing – Field Testing – Mechanical Cone Penetration Test (CPTM).*

BS-EN-13450. (2013). *Aggregates for railway ballast.*

Byrne, B. (1991). The strength and dilatancy of sands. *Geotechnique*, 317-340.

Byrne, P. M. (1991). A Cyclic Shear-Volume Coupling and Pore Pressure Model for. *Second international conference on recent advances in geotechnical earthquake engineering and soil dynamics*, (s. 11–15). St. Louis-Missouri.

Castro, J. (2017). Modeling Stone Columns. *Materials*.

Castro, J., & Sagaseta, C. (2012). Pore Pressure During Stone Column Installation. *Proceedings of the Institution of Civil Engineers Ground Improvement*.

Cundall, P. A., Hansteen, H., Lacasse, S., & Selnes, P. (1980). *Soil Structure Interaction Program for Dynamic and Static Problems.* Norwegian Geotechnical Institute.

Das AK, D. K. (2014). Modeling of uniformly loaded circular raft resting on stone column-improved ground. *Soils and Foundations*, 54(6): 1212-1224.

Das, A. K., & Deb, K. (2017). Modeling of Stone Column-Supported Embankment Under Axi-Symmetric Condition. *Geotechnical and Geological Engineering*.

Deb, K. (2007). Modeling of granular bed-stone column-improved soft soil. *INTERNATIONAL JOURNAL FOR NUMERICAL AND ANALYTICAL METHODS IN GEOMECHANICS*, 1267-1288.

Deb, K., & Behera, A. (2017). Rate of consolidation of stone column–improved ground considering variable permeability and compressibility in smear zone. *International Journal of Geomechanics*.

DEMİR, S., & ÖZENER, P. (2019). Sıvılaşmanın UBC3D-PLM Model ile Tahmin Edilmesi: Santrifüj Deneyi Örneği. *Teknik Dergi*, 9421-9442.

Dhouib A, S. B. (2004). Méthode de Priebe: origine, développement et applications. *Actes de Symposium International sur l'Amélioration des Sols en Place (ASEP-GI)*, 131–146.

Ecemiş, N. (2013). Simulation of seismic liquefaction: 1-g model testing system and shaking table tests. *European Journal of Environmental and Civil Engineering*, 899–919.

Ecemiş, N., Demirci, H., & Karaman, M. (2014). Effects Of Relative Density And Coefficient Of Consolidation On Re-liquefaction Potential Of Sand. *Second European Conference On Earthquake Engineering and Seismology.* Istanbul.

Ecemis, N., Demirci, H., & Karaman, M. (2015). Influence of consolidation properties on the cyclic re-liquefaction potential of sands. *Bull Earthquake Eng 13*, 1655-1673.

EN-14731. (2005). *Execution of special geotechnical works - Ground treatment by deep vibration.*

Esmaeili, M., & Hakimpour, S. (2015). Three Dimensional Numerical Modelling of Stone Column to Mitigate Liquefaction Potential of Sands. *Journal of Seismologie and Earthquake Engineering, Vol. 17*, 127-140.

FHWA-RD-83-026. (1983). *Design and construction of stone columns, Vol. 1.* U.S. Department of Transportation.

Fiegel, G., & Kutter, B. (1994). Liquefaction mechanism for layered soils. *J Geotech Eng 120(4):737–755*, 737-755.

Geramian, A., Castro, J., Ghazavi, M., & Miranda, M. (2022). Installation of groups of stone columns in clay: 3D Coupled Eulerian Lagrangian analyses. *Computers and Geotechnics*.

Hazen, A. (1918). A Study of the Slip in the Calaveras Dam. *Engineering News Record*, 1158-1164.

Ishihara , K., & Yamazaki , F. (1980). Cyclic simple shear tests on saturated sand in multidirectional loading. *Soils and Foundations* , 45-59.

Itasca's FLAC3D Documentation. (2019). *Itasca's FLAC3D Documentation*. http://docs.itascacg.com/flac3d700/flac3d/docproject/source/flac3dhome.html adresinden alındı

Jamiolkowski, M., Ladd, C., & Germaine, J. (2003). New developments in field and laboratory testing of soils. *Journal of Geotechnical and Geoenvironmental Engineering*, 836-857.

Kirsch, F. (2006). Vibro stone column installation and its effect on ground improvement. *Proc. Num. Modelling Construction Processes Geotech. Eng. Urban Environment*, 115-124.

Kirsch, K., & Kirsch, F. (2010). *Ground Improvement by Deep Vibratory Methods.* Taylor & Francis Group.

Kuhlmeyer, R., & Lysmer, J. (1973). Finite element method accuracy for wave propagation problems. *Journal of Soil Mechanics and Foundations Division, ASCE*, 421-427.

Liu, C., & Byrne, P. (2002). Cone penetration test-based soil liquefaction evaluation. *Journal of geotechnical and geoenvironmental engineering*, 815-825.

Lunne, T., Robertson, P., & Powell, J. (1997). *Cone Penetration Testing in Geotechnical Practice.* Blackie Academic and Professional.

Marcuson, W. F. (1978). Definition of Terms Related to Liquefaction. *Journal of Geotechnical Engineering Division, ASCE*, 1197-1200.

McCabe, B., Nimmos, G., & Egan, D. (2009). *A review of field performance of stone columns in soft soils.* Proceedings of the Institution of Civil Engineers - Geotechnical Engineeering.

Mehrannia N, N. J. (2018). Experimental Investigation on the Bearing Capacity of Stone Columns with Granular Blankets. *Geotechnical and Geological Engineering* , 36(1): 209-222.

Meshkinghalam, H., Hajialilue-Bonab, M., & Azar, A. K. (2017). Numerical investigation of stone columns system for liquefaction and settlement diminution potential. *International Journal of Geo-Engineering*.

Millea, M. T. (1990). *Liquefaction mitigation technology.* Office of Naval Technology.

Mitigation of Liquefaction Potential of Silty Sands. (n.d.).

Pestana, J. M. (1998). Effect of storage capacity on vertical drain performance in liquefiable sand deposits. *2nd Int. Conf. on Ground Improvement Techniques* (s. 373–380). Boca Raton: Geosyntec Consultants.

Priebe, H. (1995). The Design of Vibro Replacement. *Journal of Ground Engineering*.

Priebe, H. (1998). Vibro-replacement to prevent earthquake induced liquefaction. *Proceedings of the Geotechnique-Colloquium*, 30-31.

Qu M, X. Q. (2016). Model test of stone columns as liquefaction countermeasure in sandy soils. *Frontiers of Structural and Civil Engineering* , 481-487.

Reddy, C. S., & Mohanty, S. (2017). Seismic Behavior of Stone Column on A Sloping Layered Soil. *Sixth Indian Young Geotechnical Engineers Conference.* NIT Trichy.

Robertson, P., & Campanella. , R. (1983). Cone penetration test evaluation of liquefaction and liquefaction-induced ground deformation. *Journal of geotechnical engineering*, 458-482.

Sadrekarimi , A., & Ghalandarzadah, A. (2005). Evaluation of gravel drains and compacted sand piles in mitigating liquefaction. *Ground Improvement*, 91-104.

Schlue, B. (tarih yok). Reconstruction in Haiti after Jenuary 12th 2010. *Seismic Design and Construction.* University of California.

Schmertmann, J. (1978). *Guidelines for cone penetration test (CPT) performance and design.* Washington, D.C.: FHWA-TS-78-209, U.S. Department of Transportation, Federal Highway Administration.

Seed , H., & Booker , J. (1977). Stabilization of potentially liquefiable sand deposits using gravel drain systems. *Journal of Engineering Mechanics Division*, 757-768.

Seed, H. B., Tokimatsu, K., Harder, L. F., & Chung, R. M. (1985). The Influence of SPT Procedures in Soil Liquefaction Resistance Evaluations. *Journal of Geotechnical Engineering, ASCE*, 1425-1445.

Selçuk, L., & Kayabalı, K. (2015). The design of stone column applications to protect against soil liquefaction. *International Journal of Geotechnical Engineering 9*, 279-288.

Shahu, J., Madhav, M., & Hayashi, S. (2000). Analysis of soft ground-granular pile-granular mat system. *Computers and Geotechnics*, 45-62.

Sivakumar, V., Bell, A., & McKelvey, D. (2004). Modelling vibrated stone columns in soft clay. *ICE Proceedings Geotechnical Engineering*, 137-149.

Syed, N. M., Maheshwari, B. K., & Kaynia, A. M. (2009). Numerical Modelling for Liquefaction using Simple Constitutive Models. *ACSGE*.

Tanahashi, H. (2007). Pasternak Model Formulation of Elastic Displacements. *Journal of Asian Architecture and Building Engineering*.

Tang, L., Zhang, X., & Ling, X. (2016). Numerical simulation of centrifuge experiments on liquefaction mitigation of silty soils using stone columns. *KSCE Journal of Civil Engineering*, 631-638.

Tapu ve Kadastro Genel Müdürlüğü. (2023). Parsel Sorgu Uygulaması: https://parselsorgu.tkgm.gov.tr/ adresinden alındı

Taube.G & Martin, P. (2002). Stone Columns for Industrial Fills.

Tokimatsu, K., & Seed, H. (1987). Evaluation of Settlements of Sands Using Field and Laboratory Data,. *Journal of Geotechnical Engineering, ASCE, Vol. 113, No. 8,*, 861-878.

Turkish Building Earthquake Code. (2018). Section 16. Ankara: Afet ve Acil Durum Yönetimi Başkanlığı.

Vikash Singh, A. K., Vikash, S., Anand, K. Y., & Samreen, B. (2019). A Theoretical Study of Liquefaction Process. *Journal of Civil Engineering and Environmental Technology* (pp. 32-36). Uttar Pradesh: Krishi Sanskriti Publications.

Zhan, Z., & Qi, S. (2017). Numerical Study on Dynamic Response of a Horizontal Layered-Structure Rock Slope under a Normally Incident Sv Wave. *Applied Science*.